THE UNIVERSITY
of EDINBURGH

The Regulation of Human M2 Pyruvate Kinase

A Thesis

Submitted for the Degree of

Doctor of Philosophy

by

Rosie Mitchell

2014

Abstract

Pyruvate kinase catalyses the final step in glycolysis and is responsible for net ATP production. There are four pyruvate kinase isoforms expressed in humans; LPYK, RPYK, M1PYK and M2PYK. The allosteric enzyme M2PYK plays an important role in cancer cell metabolism and is subject to complex regulation by numerous naturally occurring small-molecule metabolites. Post-translational modifications have also been found to play a key role in the regulation of M2PYK, among these cysteine oxidation. This thesis describes the production and characterisation of M2PYK cysteine point mutants in order to investigate the mechanism of regulation by cysteine modification.

From a total of ten cysteines present in M2PYK, five were chosen for mutation based on a combination of the results from the cysteine oxidation prediction program (COPP) web interface and published experimental evidence for cysteine modification of M2PYK. Eight point mutants of these five cysteines were produced and characterised. Low resolution gel filtration of all the mutants shows that mutation of these cysteines has an effect on tetramer:dimer:monomer equilibrium of M2PYK suggesting that cysteine modifications could regulate M2PYK activity by affecting oligomeric state. Activity assays show that none of the cysteine point mutations are sufficient to protect M2PYK from oxidation by H_2O_2 indicating that more than one cysteine is involved in the regulation of M2PYK by oxidation.

Nitric oxide (NO) imbalance has recently emerged as playing a key role in numerous diseases including cancer. NO regulates the function of target proteins through the addition of a nitroso moiety from NO-derived metabolites to a reactive cysteine, a process known as protein S-nitrosylation. M2PYK has been found to be S-nitrosylated *in*

vivo. Using the biotin-switch assay *in vitro* combined with mass spectrometry I have shown that a likely candidate for the target of S-nitrosylation of M2PYK is C326.

This thesis also describes the structures of two cysteine point mutants; M2PYK C424A and M2PYK C358S. The structures show that these mutations have very little effect on the overall conformation of M2PYK with only very subtle localised changes. The structure of the mutant M2PYK C358S shows some interesting features including varying occupation of the active site resulting in differing conformations of the B domains within the same tetramer, and an unusual B factor distribution which could be indicative of a perturbation in cooperativity within the tetramer caused by the mutation.

Declaration

The work presented in this thesis is the original work of the author. This thesis has been composed by the author and has not been submitted in whole or in part for any other degree.

Rosie Mitchell

Acknowledgements

First and foremost I would like to thank my supervisor, Professor Malcolm D. Walkinshaw, for his support and encouragement throughout my studies. His kindness, patience and understanding have played a large part in helping me to complete this degree.

In addition I would like to thank all members of the Structural Biochemistry Group, past and present, for their help and assistance throughout my period of study. I am especially grateful for the help, support and encouragement of Dr. Hugh Morgan, whose joy and enthusiasm for his research was contagious and hugely motivational during the earlier years of my studies. I also very grateful for the help I received from Sandra Bruce, Dr. Martin Weir, Dr. Liz Blackburn, Dr. Iain McNae, Dr. Jacqueline Doran, Dr. Paul Taylor, Dr. Linda Gilmore and Dr. Matthew Nowiki.

My thanks also go to Karen Traill who always made time for me in her busy schedule to offer friendly encouragement and guidance along with a lovely cup of tea and a biscuit.

I would also like to thank my mentor and friend Olga Degtyareva at Productivity for Scientists for her loving support and guidance over the past year and for helping me to find enjoyment in the writing process.

Finally I would like to extend my gratitude to my parents, without whom none of this would have been possible, and to my husband Fergus for his constant love, support, and encouragement over the years.

Abbreviation list

ABC ammonium bicarbonate

ACN acetonitrile

ADP/ATP adenosine diphosphate/adenosine triphosphate

COPA cysteine oxidation prediction algorithm

COPP cysteine oxidation prediction program

CRISPR clustered, regularly interspaced, short palindromic repeat

DLS Dynamic light scattering

DMSO Dimethyl sulfoxide

DTT Dithiothreitol

F-1,6-BP fructose-1,6-bisphosphate

GSH glutathione (reduced)

GSSG glutathione (oxidized)

HIF-1α Hypoxia-inducible factor 1α

HPLC High performance liquid chromatography

HPV human papilloma virus

HRP horse radish peroxidase

IMAC metal ion affinity chromatography

IPTG Isopropyl-β-D-thiogalactopyranoside

LB Luria-Bertani broth

LDH lactate dehydrogenase

LPYK liver pyruvate kinase

MALDI-TOF matrix-assisted laser desorption ionization-time of flight

MMTS methylmethanethiosulfonate

M1PYK muscle pyruvate kinase M1

M2PYK muscle pyruvate kinase M2

NADH nicotinamide adenine dinucleotide

NADPH nicotinamide adenine dinucleotide phosphate

NO nitric oxide

NOS nitric oxide synthase

PBS-CM phosphate buffered saline without calcium or magnesium

PDB	protein data bank
PEG	polyethylene glycol
PEP	phosphoenolpyruvate
PFK	phosphofructokinase
PPP	pentose phosphate pathway
PTMs	post-translational modifications
PYK	pyruvate kinase
ROS	reactive oxygen species
RPYK	erythrocyte pyruvate kinase
SDS-PAGE	sodium dodecyl sulfate – polyacrylamide gel electrophoresis
SNP	single nucleotide polymorphism
VEGF	vascular endothelial growth factor

Table of Contents

Table of Figures

Chapter 1: Pyruvate Kinase

1.1: Structure and function of pyruvate kinase

1.1.1 The role of pyruvate kinase in cellular metabolism

Pyruvate kinase (PYK) catalyses the final step of glycolysis, the conversion of phosphoenolpyruvate (PEP) and ADP into pyruvate and ATP (Figure 1.1). The product pyruvate is used by several metabolic pathways, thus placing PYK at an important metabolic intersection [1] (Figure 1.1). Additionally PYK is responsible for net ATP production in the glycolytic pathway which, in contrast to mitochondrial respiration, is independent of oxygen supply thus allowing for cell survival under hypoxic conditions [2].

Historically it has been stated that PYK is a key regulatory enzyme of glycolysis that, together with phosphofructokinase (PFK) and hexokinase, controls the flux through the glycolytic pathway in almost every cell type [3]. This statement is based on the belief that the steps of a biochemical pathway that control the flux are those that catalyse the reactions with large negative ΔG° values (thermodynamic approach) and have the lowest maximal rates (kinetic approach) [4]. However, these approaches yield qualitative results and assume that the "key" steps have full control of the pathway. In reality, the situation appears to be much more complex. It was hypothesized that over-expression of one or a few key glycolytic enzymes should increase the flux through the glycolytic pathway of *Saccharomyces cerevisiae*. However, when advances in genetic engineering allowed for this hypothesis to be tested experimentally it was discovered that the presumed limiting enzymes, when over-expressed individually or in combination, had very little to no effect on the steady state flux through the pathway in *S. cerevisiae* [5]–[9](reviewed in [4]).

This has also been shown to be the case in other organisms including *Escherichia coli* [10], [11], *Lactococcus lactis* [12], *Aspergillus niger* [13], and Chinese hamster ovary [14] (reviewed in [4]).

In addition, computational modeling based on kinetics data obtained for individual enzymes has been used to study the control of glycolysis in *Trypanosoma brucei*. It was found that control appeared to shift between the glucose transporter on the one hand, and aldolase, glyceraldehyde-3-phosphate dehydrogenase, phosphoglycerate kinase and glycerol-3-phosphate dehydrogenase combined on the other, depending on the exact experimental parameters [15].

In summary, it is no longer valid to assume that PYK is one of the few key regulatory enzymes that control the flux through the glycolytic pathway. In reality it is likely that its role in controlling flux is more subtle and is combined with the regulatory effects of many or all of the other glycolytic enzymes, including the glucose transporter.

1.1.2 Pyruvate kinase isoforms in humans

There are four pyruvate kinase isoforms expressed in humans; LPYK, RPYK, M1PYK and M2PYK. LPYK is found in tissues where gluconeogenesis is carried out, primarily in liver, but also in kidney and intestine [16]. Its expression is regulated by diet; a carbohydrate-rich diet increases LPYK expression whereas hunger reduces it [2]. LPYK provides key regulation for maintaining the balance between gluconeogenesis and glycolysis in the liver and is therefore under investigation as an antihyperglycemic target in diabetics. RPYK is exclusively found in erythrocytes and is very similar to LPYK, both enzymes being expressed by the same gene under the control of different tissue-specific promoters [17]. Erythrocytes rely exclusively on glycolysis for their ATP production and are thus heavily dependent on RPYK for survival. Deficiency of RPYK

leads to ATP depletion and ultimately hemolysis and it is one of the most common causes of nonspherocytic hemolytic anaemia in humans. M1PYK is a highly active, non allosteric isoform that is expressed in tissues where large amounts of energy need to be produced rapidly, such as brain and muscle [2]. M2PYK is expressed in all proliferating cells and is a tightly controlled allosteric enzyme. M1PYK and M2PYK are splice variants of the same gene, the alternatively spliced exon consisting of 56 residues of which 22 are different [18].

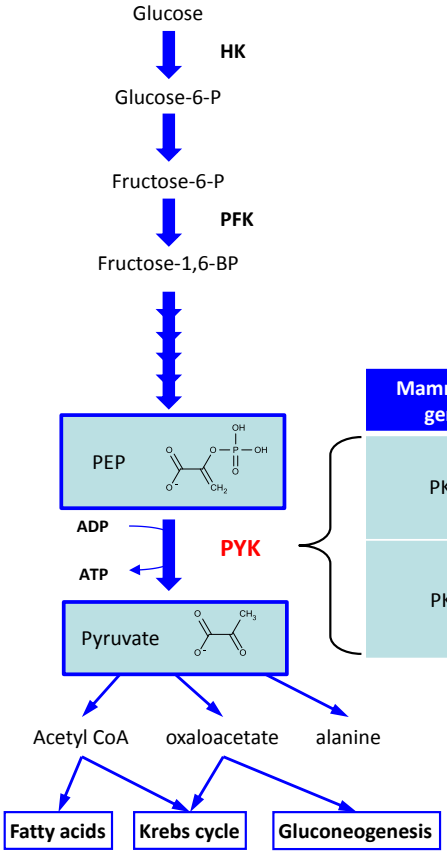

Mammalian genes	Gene products	Physiological location	Allostery
PKLR	LPYK	Liver	Yes
	RPYK	Red blood cells	Yes
PKM	M1PYK	Skeletal muscle, heart, brain	No
	M2PYK	Increased in proliferating cells including cancer	Yes

Figure 1.1 Pyruvate kinase (PYK) catalyses the final step of the glycolytic pathway.

PYK catalyses the reaction between PEP and ADP producing ATP and pyruvate. Pyruvate feeds in to multiple metabolic pathways so PYK is at an important metabolic intersection. There are two PYK genes found in mammals, *PKLR* and *PKM*, from which four isozymes can be produced.

1.1.3 Regulation of pyruvate kinase isoform expression

Human pyruvate kinase is encoded by two genes, *PKLR* and *PKM*, which result in expression of 4 protein products (Figure 1.1). The *PKLR* gene produces LPYK and RPYK by way of alternative promoters; in liver, kidney and intestine transcription starts from the second exon, whereas in erythrocytes it is initiated from the first exon with the second exon being spliced out as an intron [19](Figure 1.2). The *PKM* gene produces M1PYK and M2PYK by mutually exclusive alternative splicing; exons 9 and 10 are specific to M1- and M2PYK respectively while all other exons are common to both isoforms [18](Figure 1.2). It has been found that, in cancer cells, expression of heterogeneous nuclear ribonucleoproteins (hNRP1 and hNRP2) and polypyrimidine tract binding protein (PTB) is upregulated by c-Myc, and that these proteins bind to sequences flanking exon 9 to hinder its transcription, resulting in inclusion of exon 10 [20][21].

1.1.4 The architecture of human pyruvate kinases

Human pyruvate kinase is generally a homotetrameric enzyme which is made up of monomers of 58-62 kDa, depending upon the isoform (Figure 1.5). The PYK monomer is made up four domains: the N-terminal domain, A-, B-, and C-domains (Figure 1.4). The effector site is situated within the C-domain and is about 40 Å from the active site, which is located in the A-domain (Figure 1.5). The tetramer is held together by reciprocal hydrogen bonds across the C-C or ‘small’ interface, between neighbouring C-domains, and A-A or ‘large’ interface, between neighbouring A-domains (Figure 1.5).

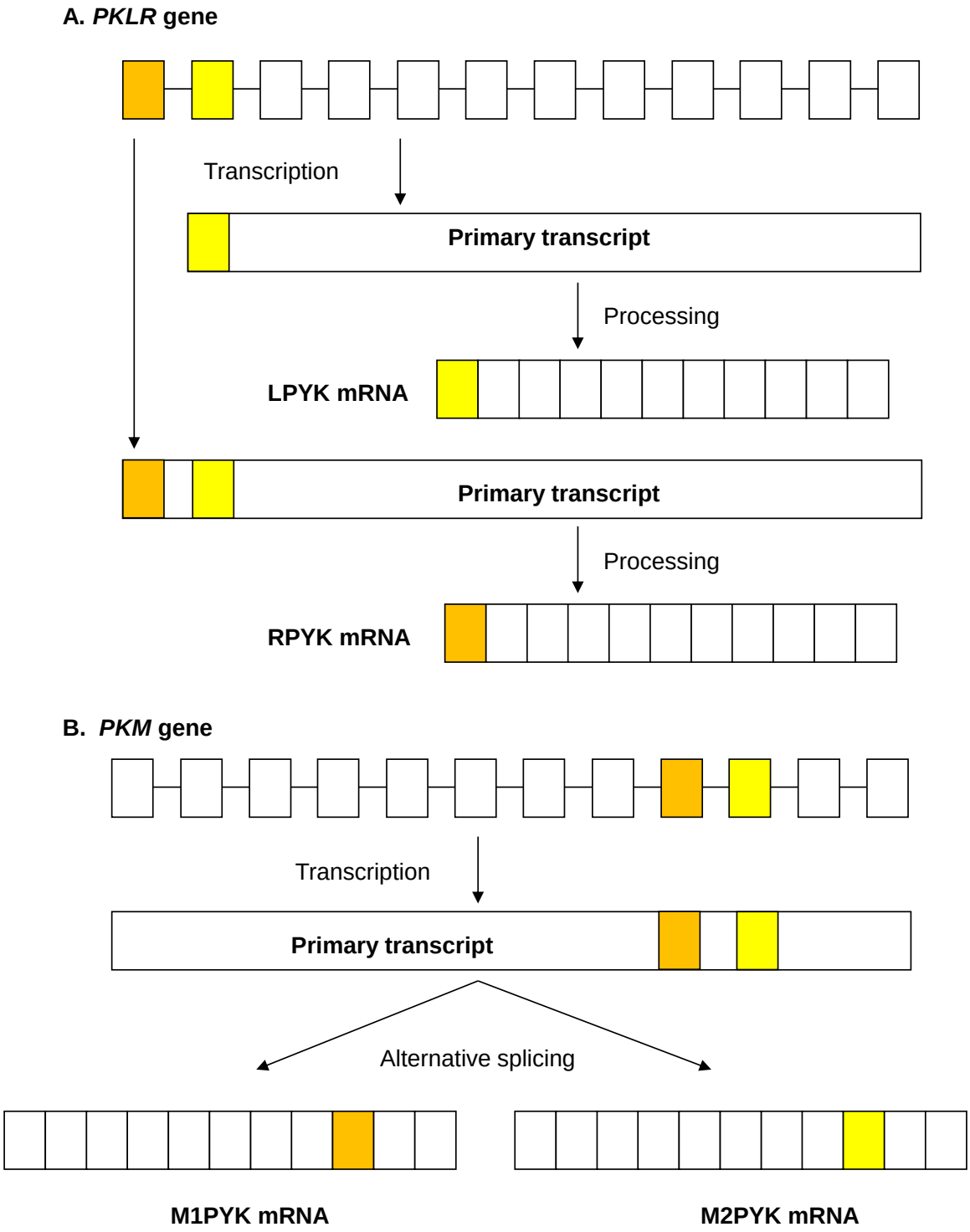

Figure 1.2 Illustration of the expression of the mammalian pyruvate kinase isoforms (Diagram from [19]**).**

A. LPYK and RPYK are produced from the same gene by use of tissue-specific promotors. **B.** M1PYK and M2PYK are produced by alternative splicing of the *PKM* primary transcript

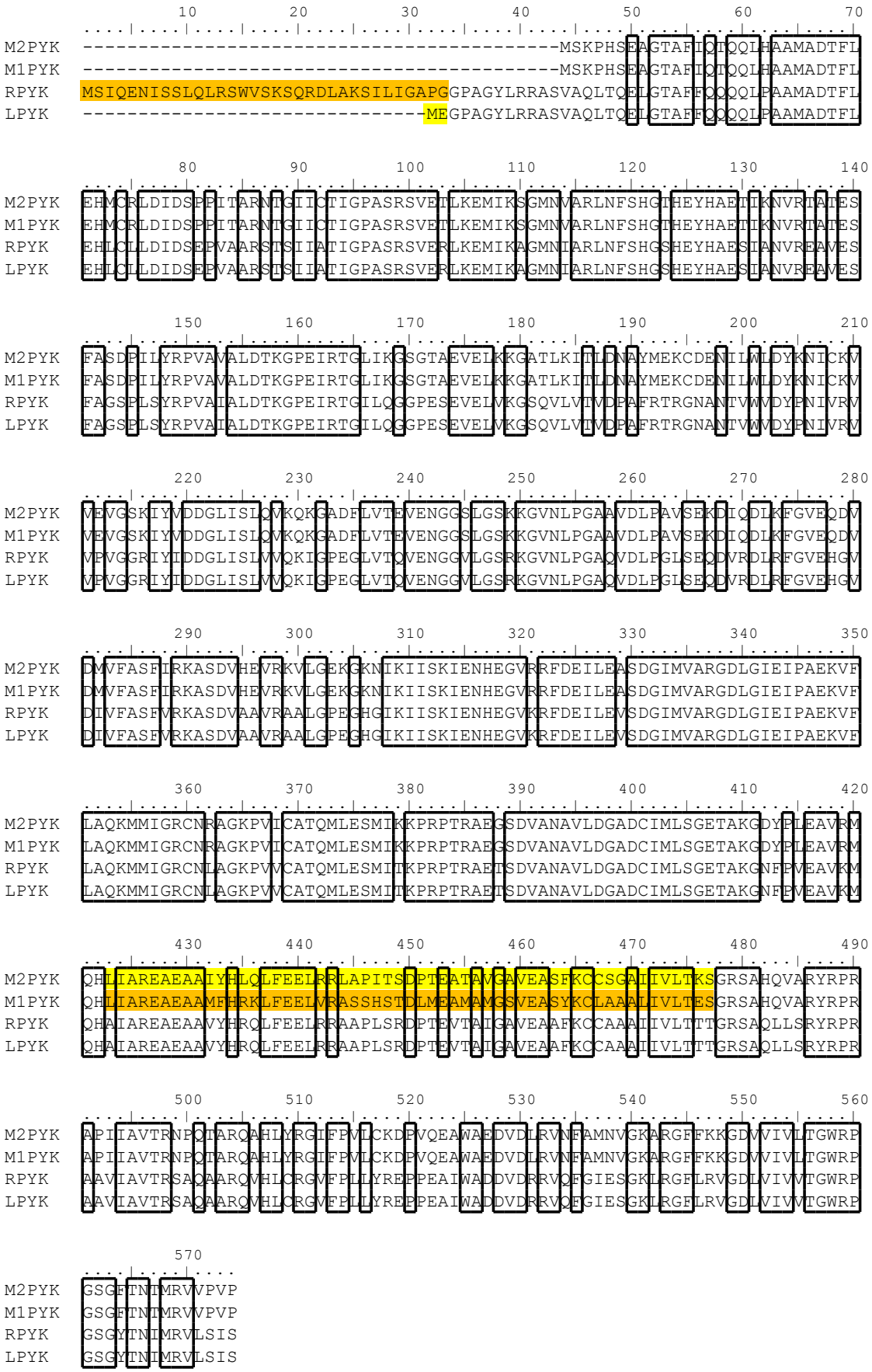
M2PYK
M1PYK
RPYK
LPYK

Figure 1.3 Multiple sequence alignment of human pyruvate kinase isoforms.

Regions resulting from the different exons included are highlighted. Colour scheme has been chosen to correspond to Figure 1.2. *PKL* exon 1 product = yellow, *PKL* exon 2 product = orange, *PKM* exon 10 product = yellow, *PKM* exon 9 product = orange.

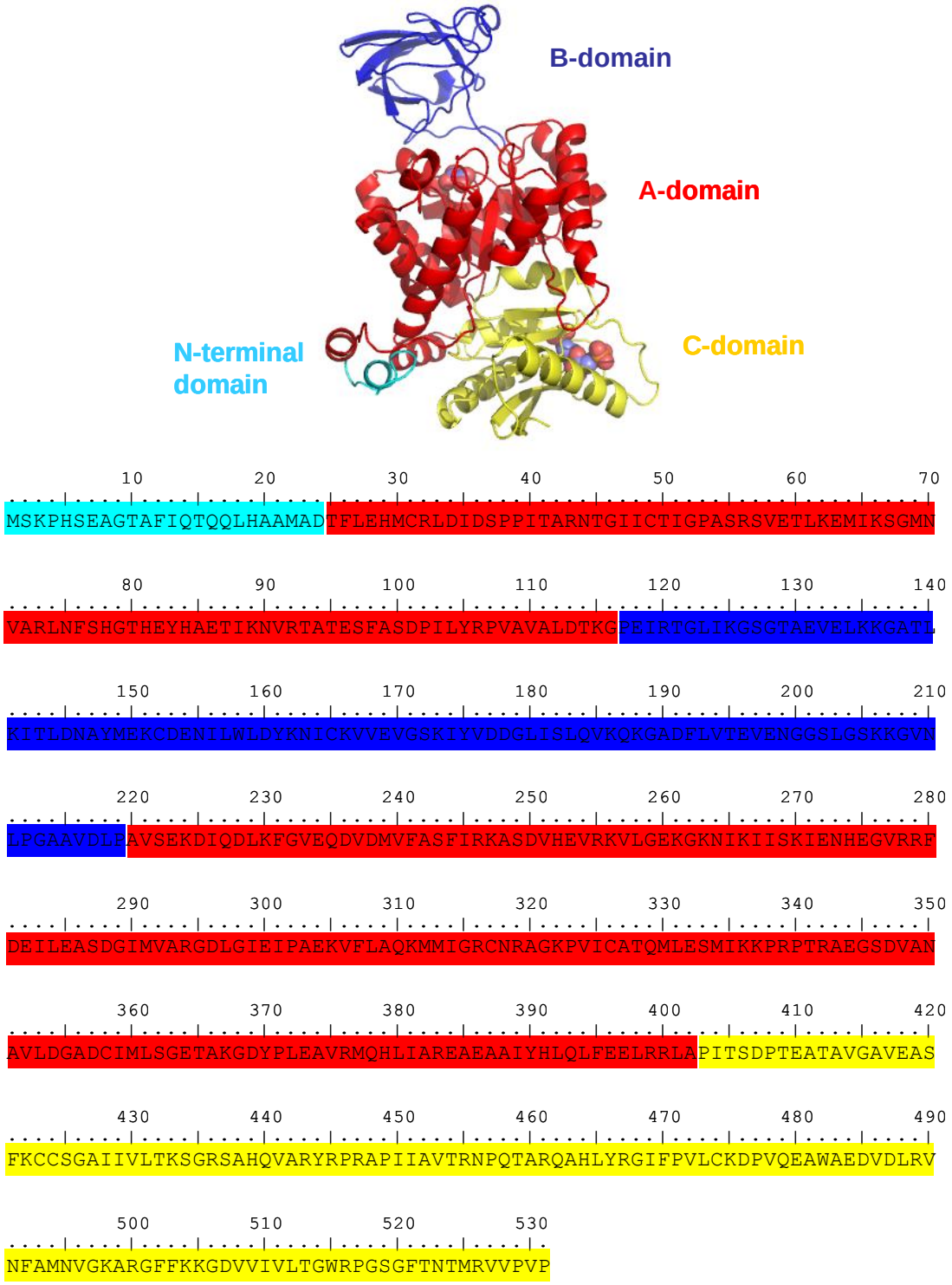

Figure 1.4 Architecture of M2PYK monomer.

Structural representation of M2PYK monomer with protein sequence below coloured to help identify the different domains; A=red, B=blue, C=yellow, N=cyan.

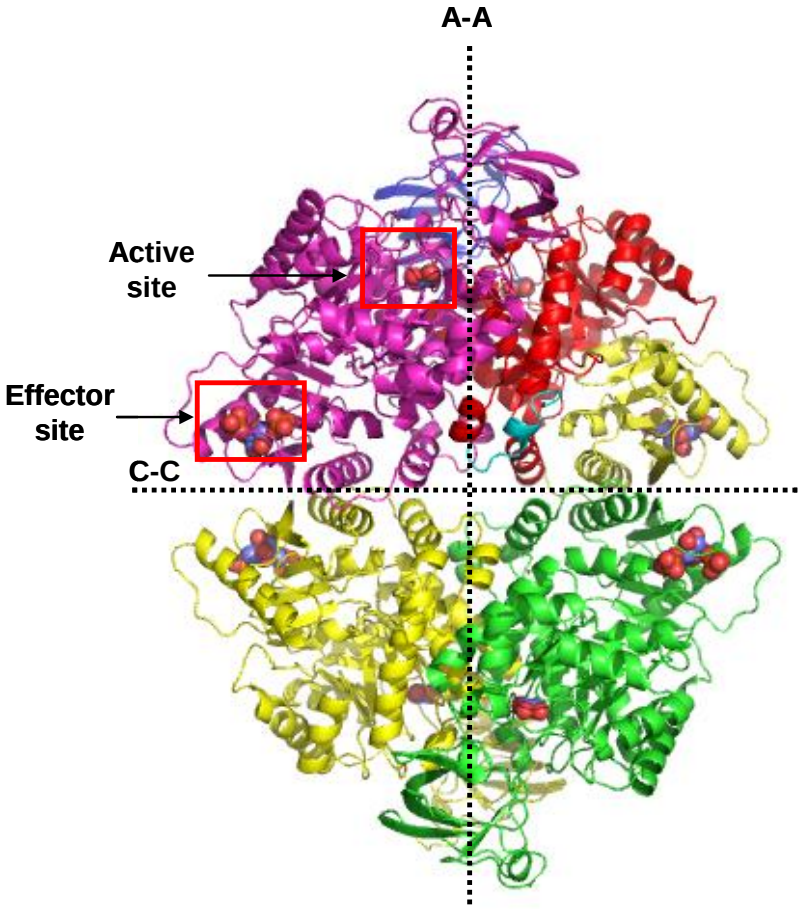

Figure 1.5 Architecture of the M2 pyruvate kinase tetramer.

Chain A has been coloured to help to identify the different domains; N (cyan = residues 1-25), A (red = residues 25-116 and 220-402), B (blue = blue = residues 117-219), and C (yellow = residues 403-531).. The large (A-A) and small (C-C) interfaces are indicated by the dashed lines. The active site and effector site have been highlighted by red boxes.

1.2: Allosteric regulation of pyruvate kinase

1.2.1 Differences between M1- and M2PYK

The result of mutually exclusive splicing of the *PKM* gene is that M1- and M2PYK differ in 22 residues within a 56 residue region situated at the C-C interface close to the F-1,6-BP binding site (Figure 1.6)[18]. These differences alone allow for M2PYK to be in an allosterically regulated tetramer:dimer:monomer equilibrium while M1PYK is held in a constitutively active tetrameric state [22][23][24]. Comparison of the crystal structures of M1PYK and M2PYK bound to ATP, oxalate and F-1,6-BP shows an overall r.m.s fit of ~0.5 Å with the only significant difference being seen in the splice variant region [22]. Specifically there are important differences in the hydrogen bonding involving Lys422 (Figure 1.6). In M1PYK a tight clasp is formed the Cα1 and Cα2 helices around Lys422, which interacts with Glu409 via a salt bridge and forms hydrogen bonds with Ser402, Ser405 and Tyr444 [22]. In M2PYK, the Cα1 and Cα2 helices are pushed further apart by 2.5 Å due to a difference in the backbone of the linker between the two helices thus resulting in relaxation of the tight "peg-in-hole" conformation observed in M1PYK [22]. This model has been validated using M2PYK point mutants and double mutants in which the M2PYK residues have been mutated to the M1PYK equivalent residues in the splice variant region. Specifically, work carried out during my MSc project showed that the three residues P403, P408 and T409 play an important role in determining the ability of M2PYK to dissociate. The double mutants P403S/P408L and P408L/T409M result in M2PYK that is tetrameric even in the absence of effector and substrates (unpublished data). This supports a model in which P403 and P408 play a role in holding the two α-helices apart thereby relaxing the "clamp" around K422 from the neighbouring chain.

In addition, a point mutation of K422 to glutamate in M2PYK was also studied in order to investigate the importance of this residue in the oligomerisation of M2PYK. It was found that this mutation almost completely prevented tetramerisation (unpublished data). This was the expected outcome based on the model because the change in charge would prevent the formation of the salt bridges that hold the tetramer together across the C-C interface (Figure 1.6).

1.2.2 The relationship between M2PYK oligomeric state and activity

M2PYK exists in a concentration-dependent tetramer:dimer:monomer equilibrium with a K_d for tetramer dissociation of around 8 μM [22]. The tetramer:dimer:monomer equilibrium requires a long time to stabilize and M2PYK dissociates into monomers that are inactive at sub K_d concentrations [22]. In the presence of F-1,6-BP M2PYK monomers re-associate into active tetramers, a characteristic of V-type allosteric regulation [22]. M2PYK can also exist as an inactive T-state tetramer when bound to the allosteric inhibitor phenylalanine [22].

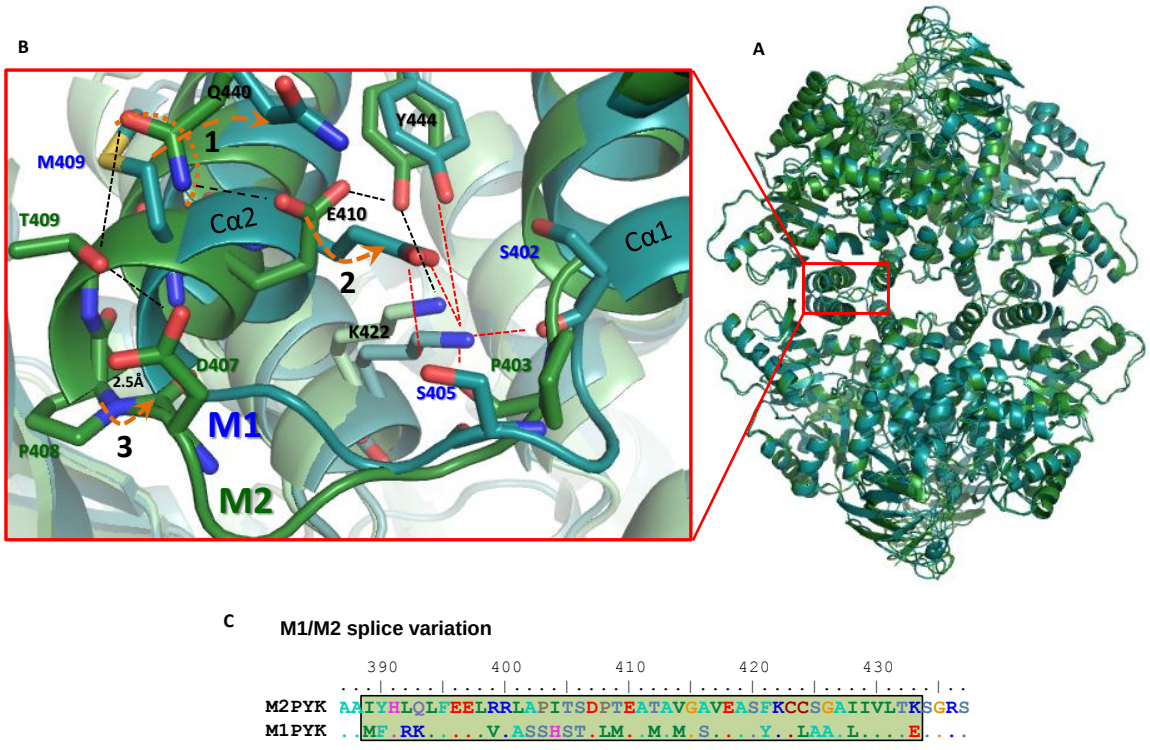

Figure 1.6 Differences between M1- and M2PYK (adapted from [22]**).**

A. M1PYK and M2PYK tetramers superimposed; M1PYK = blue, M2PYK = green **B.** Enlarged view of the splice variant region indicated in **A** showing an alignment of M1- and M2PYK structures with important side-chains shown. Significant differences are shown with numbered orange arrows: (1)In M1PYK, M409 repels Q440 which is no longer able to form a hydrogen bond with E410. (2) E410 is able to form a salt bridge with K422 from the neighbouring chain in M1PYK stabilising the dimer interface. (3) Cα2 of M2PYK is 2.5Å further from K422 than Cα2 of M1PYK due to the presence of two proline residues (P403 and P408) that act like a clamp to hold Cα1 and Cα2 apart in M2PYK. **C.** Sequence alignment of M1- and M2PYK sequences in splice variant region.

1.2.3 The regulation of M2PYK by small molecules

M2PYK activity has been found to be influenced by more than 30 naturally occurring metabolites including amino acids, nucleotides, and intermediates of the glycolytic pathway, tricarboxylic acid cycle and pentose phosphate pathway [22]. This study was the first of its kind to test the effects of such a large number of naturally occurring small molecules on pyruvate kinase activity. The activities of M1PYK and M2PYK were measured in the presence of 58 naturally occurring metabolites selected from the glycolytic, tricarboxylic acid cycle and pentose phosphate pathways as well as other potential PYK modulators (amino acids, oxalic acid, tartaric acid and triiodo-L-thyronine (T3)) [22]. After expressing activity as a percentage deviation from that of the WT enzyme in the absence of modulator, ligands were defined as inhibiting if activity was less than 75% and activating if activity was more than 125% of that of WT enzyme in the absence of modulator [22]. Seventeen inhibitors were identified for M2PYK including the previously described inhibitors phenylalanine and thyroid hormone triiodo-L-threonine (T3), but also tryptophan, alanine, oxalic acid, and ribose-5-phosphate [22]. Phenylalanine and alanine have also been identified as inhibitors of M2PYK in rat and mouse [25][26][27]. In addition, tryptophan has been found to be an inhibitor of rat M2PYK [27]. Only phenylalanine, oxalic acid and oxaloacetic acid were identified as weak inhibitors of M1PYK [22]. M2PYK was also found to have fourteen activators with F-1,6-BP, histidine and serine being the strongest, whereas no activators were identified for M1PYK [22]. F-1,6-BP is a well known allosteric activator of pyruvate kinase in many organisms from bacteria to mammals [28][29][25][30]. Histidine and serine have thus far only been identified as pyruvate kinase activators in human. Complex regulation by a wide range of naturally occurring small molecules allows M2PYK to act as a

nutrient sensor for the proliferating cell, a role that is discussed in more detail in section **1.3.2**.

1.2.4 The regulation of M2PYK by post-translational modifications

M2PYK has been found to be regulated by acetylation [31], phosphorylation [32], proline hydroxylation [33], and cysteine oxidation [34]. Protein acetylation involves the reversible addition of an acetyl group (CH_3CO) to the terminal amine of lysine residues. It was first studied in relation to histone acetylation decades ago but recently there has been increased interest in enzymatic acetylation of other proteins as it is emerging as a widely used post-translational modification involved in regulating diverse cellular processes [35]. It has been found that the majority of metabolic proteins are acetylated and that this modification affects enzyme activity [36]. An interesting observation was that the concentration of extracellular nutrients had an influence on the acetylation of metabolic proteins indicating that acetylation could be involved in regulating metabolism based on extracellular cues [36]. M2PYK has been reported to be acetylated on lysine K305 leading to inhibition of enzyme activity and promoting lysosome-dependent degradation of M2PYK [37].

Protein phosphorylation is catalysed by protein kinases which covalently attach a phosphate group to serine, threonine, or tyrosine residues of proteins. This form of post-translational modification has been studied in detail as it is a commonly used modification in cell signalling pathways. In particular, tyrosine kinase signalling is often increased in tumours due to overexpression of cell surface growth factor receptors with tyrosine kinase activity within their cytoplasmic domains [38]. Furthermore, there is believed to be a link between tyrosine kinase signalling and cellular metabolism [38]. M2PYK has been reported to be phosphorylated on tyrosine Y105 by the oncogenic

tyrosine kinase FGFR1 (Fibroblast growth factor receptor 1) resulting in inhibition of M2PYK activity [39].

Proline hydroxylation is the most frequent post-translational modification found in humans and results in the formation of (2S,4R)-4-hydroxyproline (Hyp), an irreversible modification [40]. Hyp is well known for its role in stabilising the collagen triple helix [41] but has been found to be involved in a wide range of cellular processes [40]. It has recently been demonstrated that M2PYK can be hydroxylated on prolines P403 and P408 and that this modification enhances its binding to and activation of HIF-1α (Hypoxia Inducible Factor 1α [33].

More recently it has been discovered that cysteine oxidation also plays a role in regulating M2PYK activity [34]. Although an M2PYK monomer contains 10 cysteines, it was found that mutation of one cysteine (C358) to serine was enough to protect M2PYK from the effects of oxidation [34]. The regulation of M2PYK by cysteine oxidation is the main focus of this thesis and is discussed in more detail in section **1.3.5** and chapters 3 and 4.

1.2.5 The regulation of M2PYK by protein-protein interactions

The role of protein-protein interactions in the regulation of M2PYK is very poorly characterised due to the difficulty in studying these weak interactions. However, evidence has been found for specific M2PYK binding partners which include HPV E7 (Human Papilloma virus E7) [42], HIF-1 [33], and the peptide hormone somatostatin [43].

M2PYK has been found to be directly targeted by the E7 oncogene of human papillomavirus (HPV) leading to dissociation of the enzyme and its inhibition [42], [44]. Activation of hypoxia inducible factor 1 (HIF-1) commonly occurs in human cancers and leads to a switch from oxidative to glycolytic metabolism [45]. HIF-1 is a transcription

factor consisting of two subunits; HIF-1α and HIF-1β. HIF-1α expression is O_2 regulated while HIF-1β is constitutively expressed [46]. The HIF-1 dimer binds to the hypoxia response element (HRE) of target genes, which includes the *MPYK* gene. M2PYK has recently been found to be a co-activator of HIF-1 [33].

M2PYK also interacts with the peptide hormone somatostatin and this interaction has been found to result in translocation of M2PYK into the nucleus and subsequent cell death by apoptosis [43]. The biological significance of this interaction is still unclear.

Table 1.1 Summary of M2PYK mutants discussed in this thesis. a= Jakub Nowak MSc rotation project report, b= Rosie Palmer (Mitchell) MSc rotation project report, c= chapter 3, d= chapter 4. Numbers in brackets are the corresponding M2PYK WT values measured in the same study. n/a = not available.

M2PYK mutant	Reason for making mutant	Kinetics – F-1,6-BP			Kinetics + F-1,6-BP			Ref.
		V_{max} U/mg	k_m [PEP mM]	k_{cat}/K_m	V_{max} U/mg	k_m [PEP mM]	k_{cat}/K_m	
V132L	SNP	0.98 (12)	n/a	n/a	32 (114)	1.1 (1.3)	28 (91)	a
I103Y	SNP	n/a	n/a	n/a	n/a	n/a	n/a	
V132L/ I103Y	SNP	0.49 (12)	n/a	n/a	0.54 (114)	Not active	Not active	a
Q310P	SNP	2.2 (12)	n/a	n/a	2.0 (114)	Not active	Not active	a
V292L	SNP	2.1 (12)	n/a	n/a	3.3 (114)	Not active	Not active	a
V71G	SNP	1.4 (12)	n/a	n/a	33 (114)	5.8 (1.3)	9.0 (91)	a
S437Y	SNP	5.7 (12)	n/a	n/a	39 (114)	6.6 (1.3)	9.8 (91)	a
E28K	SNP	28 (12)	n/a	n/a	110 (114)	2.1 (1.3)	64 (91)	a
C31F	SNP	54 (12)	n/a	n/a	98 (114)	0.75 (1.3)	137 (91)	a
P408L/ T409M	Mutated to M1PYK equivalent residues	253 (275)	0.50 (0.70)	506 (392)	301 (309)	0.12 (0.10)	2504 (3091)	b
P403S/ P408L	Mutated to M1PYK equivalent residues	236 (275)	0.36 (0.70)	656 (392)	267 (309)	0.10 (0.10)	2667 (3091)	b
K422E	Mutated to M1PYK equivalent residue	251 (275)	2.67 (0.70)	94 (392)	308 (309)	0.21 (0.10)	1466 (3091)	b
H391Y	Bloom Syndrome mutation, ↓activity	564 (724)	0.08 (0.46)	386 (83.7)	852 (810)	0.08 (0.05)	554 (101)	[47] [48]
K422R	Bloom Syndrome mutation, ↓activity	178 (724)	1.50 (0.46)	6.31 (83.7)	233 (810)	0.08 (0.05)	139 (101)	[47] [48]
K433E	No phosphotyrosine peptide binding	n/a	n/a	n/a	n/a	n/a	n/a	[49]
C31A	Cysteine oxidation	n/a	n/a	n/a	n/a	n/a	n/a	c
C358A	Cysteine oxidation	34 (97)	1.50 (0.9)	n/a	68 (110)	0.14 (0.17)	n/a	c
C358S	Cysteine oxidation	34 (97)	0.9 (0.9)	n/a	68 (110)	0.13 (0.17)	n/a	c
C423S	Cysteine oxidation	n/a	n/a	n/a	n/a	n/a	n/a	c
C424A	Cysteine oxidation	60 (97)	1.3 (0.9)	n/a	70 (110)	0.18 (0.17)	n/a	c
C424S	Cysteine oxidation	n/a	n/a	n/a	n/a	n/a	n/a	c
C424L	Cysteine oxidation	n/a	n/a	n/a	n/a	n/a	n/a	c
C326S	Cysteine oxidation	n/a	n/a	n/a	n/a	n/a	n/a	d

1.3 The relevance of studying the regulation of M2PYK activity

1.3.1 The Warburg effect and M2PYK

The Warburg effect is the name given to the observation made by Otto Warburg that cancer cells almost exclusively produce their energy from a high rate of glycolysis followed by production of lactic acid in the cytosol even in the presence of oxygen, a process that has been called "aerobic glycolysis" [50](Figure 1.7). This is in contrast to a comparatively low rate of glycolysis followed by oxidation of pyruvate in mitochondria which is observed in most differentiated tissue (Figure 1.7). Warburg's hypothesis was that cancer cells develop mitochondrial defects, leading to impaired oxidative phosphorylation and reliance on glycolytic metabolism for energy [50]. However, more recent work has shown that most cancers do not have impaired mitochondrial function. It has been suggested that cancer cells have a preference to use glucose to support cell growth rather than for oxidative phosphorylation [51]. The glycolytic gene set, including pyruvate kinase, has been found to be one of the most up regulated in tumours and expression of the M2PYK isoform has been shown to be necessary for aerobic glycolysis [51][52]. Switching pyruvate kinase expression in human cancer cell lines from M2PYK to the M1PYK isoform results in a reversal of the Warburg effect demonstrated by decreased lactate production and an increase in oxygen consumption [51].

The dependence of cancer cells on glycolysis is currently being exploited in drug discovery programmes. For example, small molecule activators of M2PYK TEPP-46, DASA-58 and ML-265 are at preclinical stages of development, having been tested in lung cancer cell lines [53]. The rationale for using activators of M2PYK is to prevent the use of glycolytic intermediates for biosynthetic processes thereby inhibiting the

proliferation of cancer cells (See section **1.3.2**). Another glycolytic enzyme that is being targeted for drug development is PGAM1, the inhibition of which should reduce glycolytic flux while at the same time compromising biosynthetic pathways due to the regulatory functions of its substrate and product on key metabolic enzymes [53]. Two small molecule inhibitors of PGAM1 are currently in drug development programmes at the preclinical stage; MJE3 and PGMI-004A. One of these, PGMI-004, has been shown to inhibit tumour growth in mice with little off-target toxicity [54].

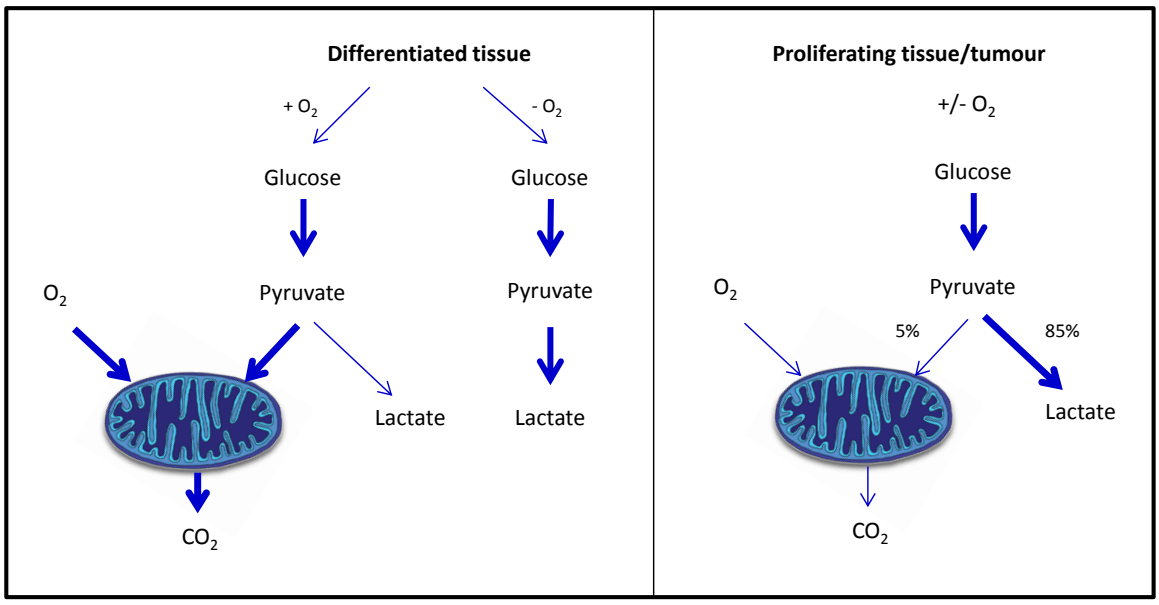

Figure 1.7 Schematic of the differences between oxidative phosphorylation, anaerobic glycolysis and aerobic glycolysis (Warburg effect) (adapted from [55]**).**

In differentiated tissue, most of the pyruvate from glycolysis is completely oxidised in the mitochondria to produce CO_2 in the process called oxidative phosphorylation. When oxygen is limiting, pyruvate is normally converted to lactate thus allowing glycolysis to continue by cycling NADH back to NAD. This process is called anaerobic glycolysis. In aerobic glycolysis, also known as the Warburg effect, most glucose (~85%) is converted to lactate regardless of whether there is oxygen present or not, and even though mitochondria remain functional. The 10% of glucose unaccounted for in the diagram is diverted to biosynthetic pathways to allow for proliferation.

1.3.2 Regulation of M2PYK allows for cell proliferation

Expression of the allosterically regulated pyruvate kinase isozyme M2PYK in cancer cells is an important regulator of the flow of glucose metabolites through the glycolytic pathway [2](Figure 1.8A). When M2PYK is active, glucose is converted to pyruvate and lactate producing ATP and recycling NAD+ for the glyceraldehyde 3-phosphate reaction of glycolysis [2]. In the case that M2PYK is inactivated, the glycolytic intermediates preceding it build up and can be used for synthetic processes allowing for cell proliferation [2])(Figure 1.8A). For example, synthesis of the amino acids serine, glycine, and cysteine uses glycerate 3-phosphate as a precursor [2] (Figure 1.8A). Dihydroxyacetone phosphate is a precursor for the synthesis of phospholipids. The pentose-phosphate pathway that utilises glucose-6-phosphate leads to production of ribose-5-phosphate, a precursor of nucleotides [2] (1.8A). All of these molecules are essential for cells with a high proliferation rate. Furthermore, expression of M1PYK in human cancer cells in which M2PYK expression has been knocked down results in a reduced ability to form tumours in nude mouse xenografts [51](Figure 1.8B). Therefore, it is likely that tight regulation of M2PYK activity provides a means of controlling the balance between energy production and synthetic processes that stem from the glycolytic pathway.

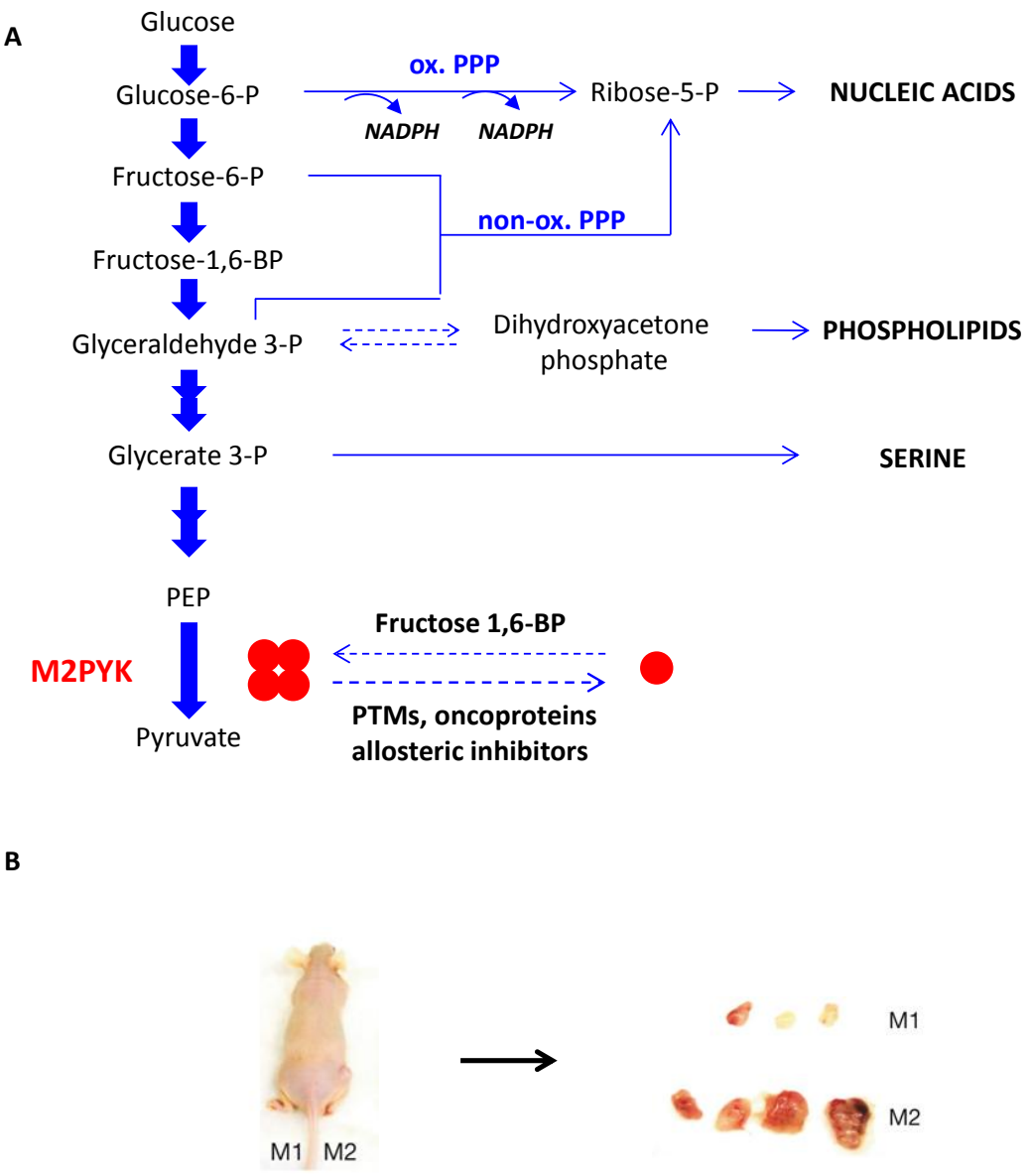

Figure 1.8 Inhibition of M2PYK allows for accumulation of glycolytic intermediates that can be used for cell proliferation.

A. Representation of the glycolytic pathway showing the intermediates that are used by the cell for proliferation and the essential building blocks that are synthesised from each of these intermediates. **B.** Nude mice were injected with M1 rescue H1299 cells on the left flank and M2 rescue H1299 cells on the right flank and then tumours dissected out [51]. The only three tumours that grew with M1PYK were much smaller than the M2PYK tumours [51].

1.3.3 Naturally occurring M2PYK polymorphisms and cancer

The COSMIC database (Catalogue Of Somatic Mutations In Cancer) is an online database of somatically acquired mutations in human cancer that curates data from published literature as well as large-scale experimental screens. The COSMIC database reports 32 missense mutations in the MPYK gene coding for M2PYK. However, the presence of a mutation does not prove that it contributes to the cancer phenotype and none of these reported M2PYK mutations have been biochemically characterised. The database therefore presents a useful resource for the further study of the importance of M2PYK polymorphisms in cancer.

There are only two published missense mutations of M2PYK that have been studied in detail, H391Y and K422R [47][48]. These were found in a patient with Bloom syndrome, a rare autosomal recessive disorder which results in many health problems including increased risk of cancer. This particular patient was prone to various types of cancer at an early age [47]. The mutation K422R is found at the C-C interface and H391Y is very close to the C-C interface. Both of these mutants were found to be less active than the wild-type M2PYK to different extents (Table 1.1). The K422R mutation had the most pronounced effect on activity which may be caused by stabilising the enzyme in a less active T-state tetramer conformation [48]. The H391Y mutation caused loss of cooperativity and allosteric behaviour evidenced by a shift of the typical sigmoidal curve, usually seen for M2PYK activity in the absence of F-1,6-BP, to a hyperbolic curve [48].

Jakub Nowak, an MSc student in this laboratory, studied the effect of nine naturally occurring M2PYK polymorphisms on the oligomeric state and activity of the enzyme. The results showed that several of these naturally occurring mutations (Q310P, V392L, I103Y and V132L/I103Y) resulted in monomeric M2PYK that was inactive even in the presence of the allosteric activator F-1,6-BP (Table 1.1). None of these mutations have

been associated with higher risk of cancer, however it seems likely that they could play a role in cancer progression given that less active M2PYK would allow for more cell proliferation due to accumulation of glycolytic intermediates (Figure 1.8A).

1.3.4 Reactive oxygen species (ROS) in cancer

Proliferation resulting from stimulation by growth factors in normal cells requires ROS signalling. It has been proposed that ROS enhances proliferation through inhibition of phosphotyrosine kinases and PTEN (phosphatase and tensin homolog) leading to an increase in signalling through the tyrosine kinase and phosphatidylinositol-3 kinase (PI-3K) pathways [56]. In cancer cells, abnormally high concentrations of ROS are produced as a result of mutations in tumour suppressor and oncogenic pathways, as well as conditions that often result from tumorigenesis such as hypoxia, matrix detachment, mitochondrial dysfunction and inflammation [57]–[66]. Cancer cells must therefore have mechanisms to maintain the subtle ROS balance that allows sufficient proliferation while preventing potentially lethals ROS levels[62]. It has been found that cancer cells overexpress thioredoxin reductase-1 (TR1), a member of the thioredoxin antioxidant system [67]. This system is translocated to the nucleus in response to oxidative stress, where it maintains the reducing environment necessary for transcription factor binding to DNA and gene expression [68]. It is probable that the increase in thioredoxin expression aids transcription in the conditions of high ROS concentration necessary for cell proliferation [67].

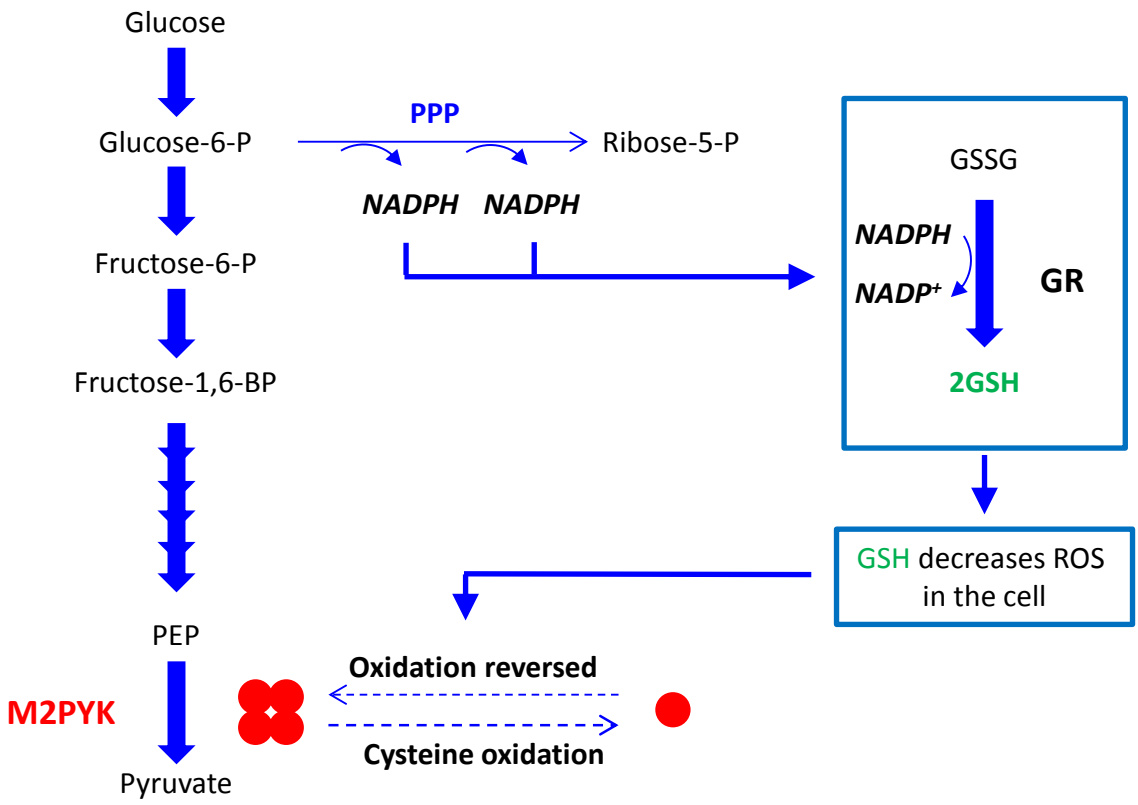

Figure 1.9 Control of M2PYK by oxidation could contribute to regulating Reactive Oxygen Species (ROS) in proliferating cells.

The proposed mechanism [34] is as follows. Cysteine oxidation causes M2PYK to become more monomeric which makes it inactive. The glycolytic intermediates earlier in the pathway build up as PEP is no longer converted to pyruvate by M2PYK. Glucose 6-phosphate enters the Pentose Phosphate Pathway (PPP) where it contributes to the production of NADPH. NAPDH is used by Glutathione Reductase (GR) to produce reduced GSH from GSSG. Increase in GSH causes a decrease in ROS, which in turn could lead to reversal of M2PYK cysteine oxidation thus allowing it to reassociate into its active tetrameric form.

1.3.5 Regulation of M2PYK by ROS

Oxidation has been found to inhibit a range of pyruvate kinase orthologues including *E. coli*, yeast and human [69]–[71]. A study carried out in A549 human lung cancer cells found that an increase in intracellular ROS concentrations lead to decreased M2PYK activity [34]. This inhibition was reversed after treatment of cells lysates with the reducing agent dithiothreitol (DTT) [34]. It was proposed that oxidation of M2PYK leads to dissociation of the homotetramer, a conclusion based on the fact that treatment of human lung cancer cells expressing FLAG-tagged M2PYK with the oxidising agent diamide prevented tagged M2PYK co-immunoprecipitating with endogenous M2PYK [34]. The significance of this for the cancer cells is explained by the authors in a model, illustrated in **figure 1.9**, in which the regulation of M2PYK by redox potential of the cell allows cancer cells to sustain antioxidant responses [34]. The idea is that inhibition of M2PYK would lead to accumulation of the glycolytic intermediate glucose-6-phosphate which would then enter the pentose phosphate pathway (PPP) thereby producing NADPH (Figure 1.9). NADPH is used by glutathione reductase (GR) to produce the reducing agent GSH from the oxidised GSSG (Figure 1.9). GSH reacts with ROS thereby decreasing the oxidising potential of the cell and allowing oxidation of M2PYK to be reversed, leading to re-activation of the enzyme (Figure 1.9).

In this same paper it was proposed that there is one cysteine in M2PYK, Cys358, that is primarily responsible for its regulation by oxidation. However, given that there are 10 cysteines in M2PYK and that many of them are accessible to solvent this hypothesis seems unlikely. The results presented in this thesis suggest that the situation is actually much more complex, involving several cysteines and different forms of oxidation, including nitrosylation.

Chapter 2: Materials and Methods

2.1 Cloning, PYK expression and purification

2.1.1 Cloning of M2PYK mutants

Mutants of M2PYK were made using the Quikchange site-directed mutagenesis kit (Stratagene) using pET28a-M2PYK as a template and following the instructions in the manual. The following mutants were generated: C31A, C326S, C358A, C358S, C423S, C424A, C424S and C424L. Mutations were confirmed by sequencing.

2.1.2 Expression of human M PYKs in *E.coli*

The following procedure was used to express M2PYK WT, M1PYK WT, and all M2PYK mutants except M2PYK C326S. Mutated plasmids were transformed into chemically competent BL21 *E. coli* cells (Novagen). Single colonies were used to inoculate 50ml LB media containing 50µg/ml kanamycin and incubated at 37°C overnight with shaking. 10ml was taken from each of the overnight cultures and used to inoculate 1L 2XTY media containing 50µg/ml kanamycin. 1L cultures were grown to an OD_{600} of 0.8 at 37°C with shaking. Cultures were incubated at 4ºC for 20 minutes before inducing expression by adding isopropyl-β-D-thiogalactopyranoside (IPTG) to a final concentration of 1mM and incubating at 20°C for 18 hours with shaking. Cells were harvested in a JLA-9.1000 rotor at 8,000 rpm for 20 minutes at 10ºC. 1L cell pellets were flash frozen in liquid nitrogen before being stored at -80ºC.

For expression of M2PYK C326S the mutated plasmid was transformed into chemically competent BL21 star *E. coli* cells (Novagen). A single colony was used to inoculate 50ml

LB media containing 50µg/ml kanamycin and incubated at 37ºC overnight with shaking. 10ml was taken from the overnight cultures and used to inoculate 1L LB media containing 50µg/ml kanamycin. This 1L culture was grown to an OD_{600} of 0.6-0.8 at 37ºC with shaking. IPTG was added to a final concentration of 1mM to induce expression and the culture was incubated at 18ºC for 3 hours with shaking. Cells were harvested in a JLA-9.1000 rotor at 8,000 rpm for 20 minutes at 10ºC. 1L cell pellets were flash frozen in liquid nitrogen before being stored at -80ºC.

2.1.3 Preparation of cell lysates

All purification steps were carried out at 4ºC unless otherwise stated. Cell pellets from 1 litre cell culture were resuspended in 30ml lysis buffer (50mM NaH_2PO_4, 300mM NaCl, 20mM imidazole, pH8.0, with EDTA free protease inhibitors (Roche)). Cells were lysed using a constant cell disruption system with pressure set to 25 MPa. The cell lysate was centrifuged at 22,000rpm for 45 minutes at 10ºC and the supernatant filtered using a 0.2 µm syringe filter.

2.1.4 Purification of bacterially expressed M PYKs

Clarified cell lysate was loaded onto a 5ml IMAC hitrap HP sepharose column pre-charged with cobalt at 2 ml/min. The flow rate was maintained at 2 ml/min for the duration of the affinity purification step. The column was washed with 10 column volumes (CV) of buffer A (50mM NaH_2PO_4, 300mM NaCl, 20mM imidazole, pH8.0) followed by an additional wash step with 15 CVs of 20% buffer B (50mM NaH_2PO_4, 300mM NaCl, 250mM imidazole, pH8.0) to wash off contaminating proteins. The His-tagged MPYK protein was eluted using a 5 CV step gradient of 100% buffer B. Eluted

fractions were pooled and loaded onto a superdex 200 26/60 XK gel filtration column pre-equilibrated with Dulbecco's phosphate buffered saline without calcium and magnesium (PBS-CM – Sigma Cat. No. D5652). A flow rate of 2.5 ml/min was used throughout the gel filtration process. Eluted fractions were pooled and concentrated using a vivaspin column with molecular weight cut-off of 30 kDa.

2.1.5 Measurement of protein concentration

Protein concentration was determined by measuring absorbance at 280nm using a nanodrop spectrophotometer and the theoretical molar absorption coefficient ε280nm = 28600 M^{-1} cm^{-1}. Protein solutions were diluted to ensure the absorbance reading was always between 0.l and 1. Concentrations were measured 5 times to ensure consistency and a mean value calculated. Accuracy of concentration measurements was checked by SDS-PAGE.

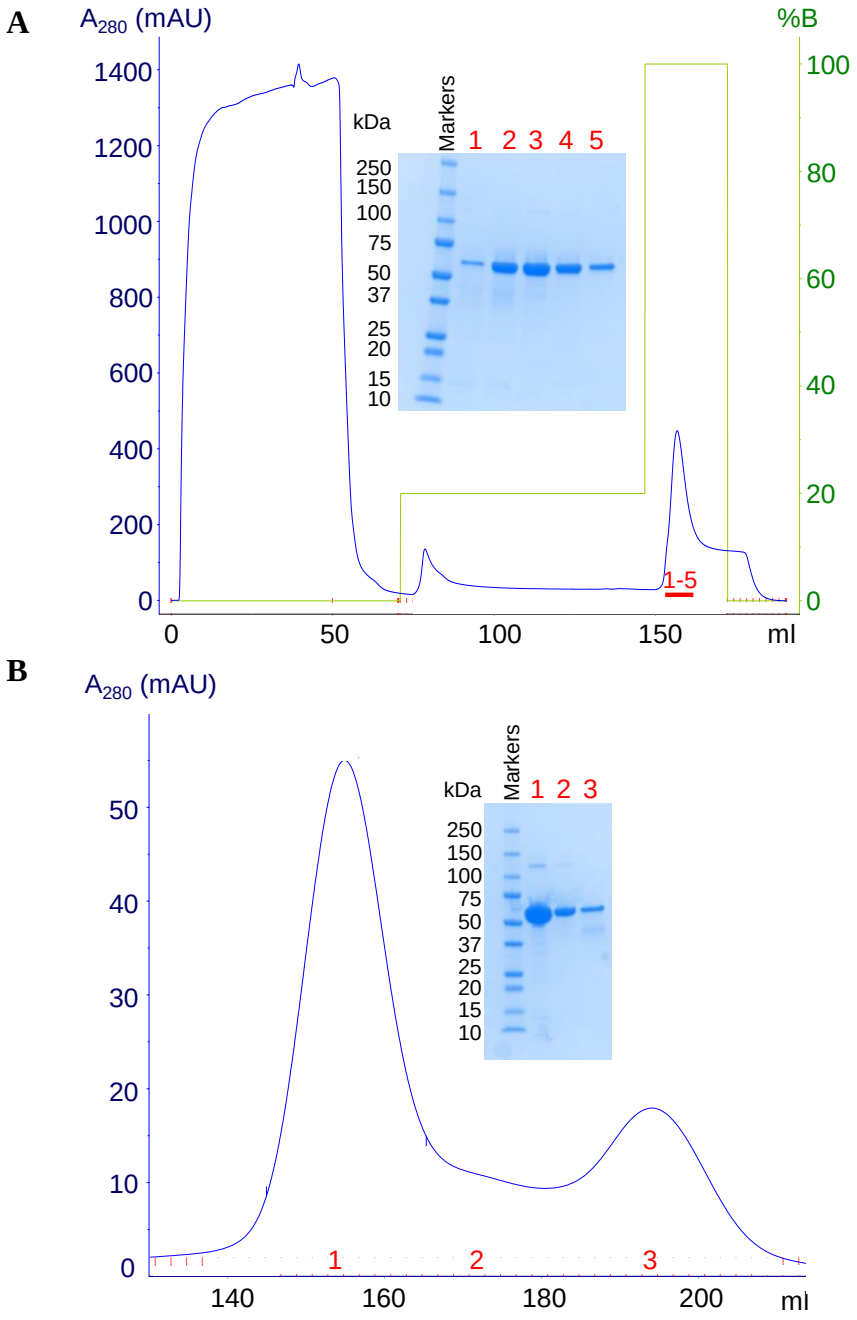

Figure 2.1 Chromatograms showing standard traces for M PYK purification with SDS-PAGE gels.

A. IMAC elution profile for M2PYK C31A with SDS-PAGE gel (inset) showing M2PYK protein at the expected size of about 60 kDa. **B**. Gel filtration elution profile for M2PYK C31A showing two peaks probably corresponding to tetramer (1) and monomer (3). There is probably also a small amount of dimeric form at the position labeled with 2, although the resolution of the column does not allow a peak to be distinguished. SDS-PAGE gel (inset) shows that protein is purified to a high level of purity.

2.2 Enzyme assays

2.2.1 Measuring PYK activity using the LDH-coupled assay

5ml protein solutions of 0.0025mg/ml M PYK were prepared by dilution in PBS-CM with or without addition of additives. The protein solutions were incubated at room temperature for 3 hours to ensure oligomeric equilibrium was reached.

Meanwhile 25ml 2x Assay buffer was made (PBS-CM, 20mM $MgCl_2$, 200mM KCl, 4mM ADP, 1mM NADH, 30 U/ml LDH). 5ml of 2x Assay buffer was taken and PEP added to a concentration of 10mM. Two-fold serial dilutions of PEP were prepared in a 96 well master block (Greiner Bio-one Cat. No. 780270) using 2x Assay buffer for dilution yielding PEP concentrations ranging from 78 µM to 10 mM (final assay concentrations 39 µM to 5 mM). A multi-channel pipette was used to transfer 50 µl of each PEP dilution to a column of a 96 well plate (Greiner Bio-one Cat. No. 655101).

The reaction (Figure 2.2) was started by adding 50 µl protein solution to the PEP titrations in the 96 well plate using a multi-channel pipette. Final concentrations of reagents were as follows: 0.00125mg/ml M PYK, 10 mM $MgCl_2$, 100 mM KCl. 2 mM ADP, 15 U/ml LDH, 0.5 mM NADH, and PEP concentrations ranging from 39 µM to 5 mM.

Plates were agitated for 10 seconds before measuring the decrease in absorbance at 340 nm for 5 minutes using a plate reader (SpectraMax M5 multimode plate reader, Molecular Devices). Initial reaction rates were obtained using the SoftMax Pro software. Substrate-velocity graphs were plotted using Kaleidograph (Synergy Software).

2.2.2 Measuring PYK activity using Kinase Glo assay

5ml protein solutions of 0.0025mg/ml M PYK were prepared by dilution in PBS-CM. Two samples were prepared for each protein; one with 10µM H_2O_2 and one with 1mM DTT. The protein solutions were incubated at room temperature for 3 hours to ensure oligomeric equilibrium was reached.

Meanwhile 25ml 2x Assay buffer was made (PBS-CM, 20mM $MgCl_2$, 200mM KCl, 4mM ADP). 5ml of 2x Assay buffer was taken and PEP added to a concentration of 2mM. A multi-channel pipette was used to transfer 25µl of 2mM PEP solution to the wells of a 96-well plate (Greiner Bio-one Cat. No. 655101).

The reaction (Figure 2.3a) was started by adding 25µl protein solution to the PEP solution in the 96-well plate using a multi-channel pipette. The final concentrations of the reagents were as follows: 0.00125mg/ml M PYK, 10 mM $MgCl_2$, 100 mM KCl. 2 mM ADP, and 1mM PEP. The reaction was incubated for 30 minutes before adding 50µl Kinase Glo Plus reagent (Promega) was added to each well using a multi-channel pipette and the reaction (Figure 2.3b) incubated at room temperature in the dark for 10 minutes. End point luminescence readings were measured using a SpectraMax M5 multimode plate reader at room temperature.

2.3 Biophysical assays

2.3.1 Dynamic light scattering

Dynamic light scattering (DLS), also known as Photon Correlation Spectroscopy (PCS) and Quasi-elastic light scattering (QELS), is a technique used for measuring the size distribution of particles in solution. A laser beam is directed through a solution and is scattered in all directions when it meets a particle. The scattered light energy is detected on a photon detector.

Particles in solution have a Brownian motion which causes laser light to be scattered in a time-dependent manner. These fluctuations can be used to derive the velocity of the Brownian motion allowing calculation of the particle size using the Stokes-Einstein relationship.

A Zetasizer Auto Plate Sampler was used for DLS measurements of M2PYK mutants. 50µl of M2PYK mutant (1mg/ml) was placed in one well of a 384-well plate. As a reference, the light scattering of PBS-CM (Sigma) only was measured. Samples were measured in a 12 µl quartz cell.

2.3.2 Thermal shift assay

The thermal shift assay takes advantage of the change in the fluorescence signal of SYPRO Orange dye when it comes into contact with a hydrophobic surface to monitor a protein undergoing thermal unfolding. A protein sample is subjected to incremental increases in temperature and the fluorescence signal monitored throughout the process. An increase in fluorescence signal indicates that the protein is unfolding and from this information a melting temperature can be deduced. The SYPRO Orange dye is supplied

by Invitrogen (catalogue no. S6650) at 5000x concentration in DMSO, and was diluted in PBS-CM before use. Test samples were prepared in a 96-well PCR plate (BioRad) before adding SYPRO Orange dye and sealing the plate with optical quality tape (BioRad). Each 50 µl sample contained 0.55 mg/ml protein in PBS-CM with 1.11mM F-1,6-BP, 1mM H_2O_2, or 1mM DTT. The 96-well plate was heated in an i-Cycler iQ5 real-time PCR detection system (BioRad) from 20 to 80 ºC in increments of 1 ºC. A charge-coupled (CCD) camera was used to monitor the fluorescence changes in the wells simultaneously using an excitation wavelength of 485nm and an emission wavelength of 575nm.

2.3.3 Analytical size exclusion chromatography

Analytical size-exclusion chromatography was carried out as described by Morgan *et al.* [22]. MPYK protein samples were incubated overnight at room temperature at 0.1mg/ml before loading independently onto a Superdex 200 PC 3.2/30 gel filtration column pre-equilibrated in PBS-CM at room temperature. A 25µl loop was used and 50 µl was injected at a rate of 0.1 ml/min. The column flow rate was maintained at 0.1 ml/min. UV absorbance was monitored at both 280nm and 214nm.

2.4 Biotin-switch assay

2.4.1 *In vitro* biotin-switch assay

In vitro biotin switch assay was performed essentially as described by Jaffrey and Snyder [72] (Figure 2.2). Protein samples were prepared by diluting to a concentration of 1mg/ml in HEN buffer (250mM HEPES-NaOH, pH7.7, 1mM EDTA, 0.1mM Neocuproine). CysNO was used as the NO donor and was prepared by mixing 10µl 100mM L-Cysteine with 10µl 100mM $NaNO_2$ resulting in 50mM solution of CysNO which was diluted to 10mM with HEN buffer. CysNO was added to protein samples and the reaction incubated in the dark for 20 minutes. CysNO donor was removed by passing the samples through pre-equilibrated zeba-spin columns. MMTS blocking buffer (HEN buffer, 2.5% SDS, 20mM MMTS) was added to block unmodified cysteines and the reaction incubated at 50ºC for 20 minutes. 2 volumes of -20ºC acetone were then added and the samples incubated at -20ºC for 2 hours. Precipitated protein was pelleted by centrifuging at 14,000xg for 15 minutes. Supernatant was removed and residual acetone allowed to evaporate by placing tubes uncapped in a 37ºC incubator. Protein pellets were resuspended in 50µl HENS buffer (HEN buffer with 1% SDS). Biotin-labeling solution (4.5mM ascorbate, 1mM Biotin-HPDP) was added and the samples were incubated at 4ºC overnight before running on two SDS-PAGE gels. One of the gels was stained with coomassie stain and the other was used for western blot with anti-biotin-HRP antibody using 5000:1 dilution.

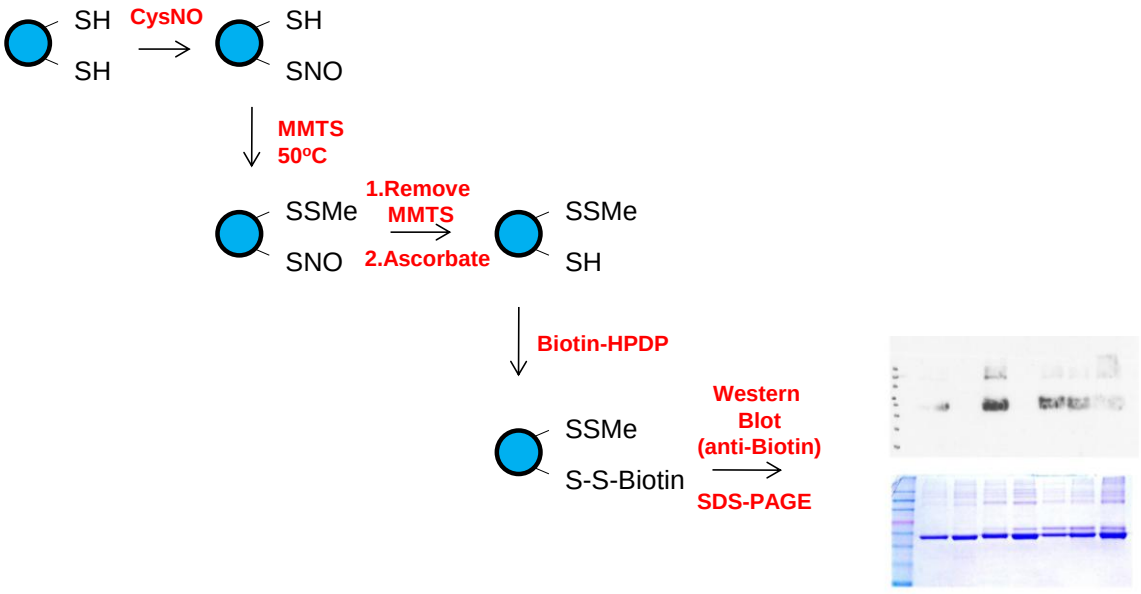

Figure 2.2 Biotin-switch assay workflow.

Protein samples are nitrosylated using a nitrosylating agent such as CysNO followed by removal of nitrosylating agent using a desalt column. Free cysteines that are not nitrosylated are then blocked by reaction with methylmethanethiosulfonate (MMTS) in denaturing conditions (50˚C). Residual MMTS is then removed by precipitating protein with acetone and collecting the protein pellet. Ascorbate is then added to remove NO group from nitrosylated cysteines before labeling with biotin-HPDP. Protein samples are then separated by SDS-PAGE and a western blot carried out using anti-biotin-HRP antibody.

2.4.2 Mass spectrometry of biotinylated protein

2.4.2.1 Sample Digestion

The coomassie stained SDS-PAGE gel of biotin-switch assay samples was used to obtain samples for mass spectrometry analysis to identify biotinylated peptides. Prominent protein bands of the expected size for M PYK were excised from lanes corresponding to samples for M1PYK with and without CysNO treatment and M2PYK with and without CysNO treatment. In-gel digestion was similar to the protocol published in Nature by Schevchenko and colleagues [73]. DTT and iodoacetamide were not used to avoid reduction and alkylation of the peptides. Gel pieces were incubated in 300µl of 200mM ammonium bicarbonate (ABC) in 50% acetonitrile (ACN) at room temperature for 30 minutes to remove SDS. This was followed by 3 washes with 500µl 20mM ABC in 50% ACN. The washed gel pieces were then covered with 100% ACN for about 5 minutes, ACN was removed and gel pieces allowed to air dry. Trypsin (29µl 50mM ABC + 1µl 0.4µg/µg trypsin) was then added to the dehydrated gel pieces at 4ºC. The gel pieces were left to swell at 4ºC for a few minutes before transferring the tubes to 32ºC and incubating overnight.Samples were cleaned on ziptip, dried under low pressure (Speedvac from Thermo Jouan) and stored at -20 ºC. The dried peptide aliquots were re-suspended in 7µl Buffer A (2.5%v/v acetonitrile, 0.1%v/v formic acid in water) and were filtered using Millex filter (Millipore, UK) before subjecting to HPLC-MS analysis.

2.4.2.2 LC-MS analysis

Nano-HPLC-MS/MS analysis was performed using an on-line system consisting of a nano-pump (Dionex Ultimate 3000, Thermo-Fisher, UK) coupled to a QExactive instrument (Thermo-Fisher, UK) with a pre-column of 300 µm x 5 mm (Acclaim Pepmap, 5 µm particle size) connected to a column of 75 µm x 50 cm (Acclaim Pepmap, 3 µm particle size). Samples were analyzed on a 2 hour gradient in data dependent analysis (1 survey scan at 70k resolution followed by the top 5 MS/MS at 17.5k resolution).

2.4.2.3 Label free quantitation

Progenesis (Nonlinear Dynamics, UK) was used for LC-MS label-free quantitation. Only MS/MS peaks with a charge of 2+, 3+ or 4+ were taken into account for the total number of 'Feature' (signal at one particular retention time and m/z) and only the five most intense spectra per 'Feature' were considered in the analysis. Normalization was first performed based on the sum of the ion intensities of these sets of multi-charged ions (2+, 3+, and 4+). The associated unique peptide ion intensities for a specific protein were then summed to generate an abundance value. The abundance was then transformed using an ArcSinH function (a log transform is not ideal considering the significant amount of near zero measurements generated by the current method of detection). Based on the abundance values, within group means were calculated and from there the fold changes (in comparison to control) were evaluated. One-way ANOVA was used to calculate the p-value based on the transformed values.

2.4.2.4 Protein identification

Data from MS/MS spectra was searched using MASCOT Versions 2.4 (Matrix Science Ltd, UK) against an in-house database with maximum missed-cut value set to 2 and assuming trypsin cleavage. The following features were used in all searches: i) variable methionine oxidation, ii) cysteine either blocked with methylthio or HDPD-biotin, iii) precursor mass tolerance of 10 ppm, iv) MS/MS tolerance of 0.05 amu, v) significance threshold (p) below 0.05 (MudPIT scoring) and vi) final peptide score of 20.

2.5 X-ray crystallography

2.5.1 Crystallisation screening procedures

Purified M2PYK C358A, M2PYK C358S and M2PYK C424A samples that had been stored at -80ºC were used for the experiments. Proteins were thawed on ice before mixing with ligands. Crystallisation experiments were carried out by the vapour diffusion method and the hanging drop technique at 18ºC (M2PYK C358A and M2PYK C424A) or 4ºC (M2PYK C358S).

Crystallisation conditions were based on those used by Morgan *et al.* [22]. The drops were set up by mixing 1.5 µl of well solution with 1.5 µl of 10 mg/ml protein sample containing 5mM of each ligand. The well solution consisted of 6-16% PEG 3350, 100mM sodium cacodylate (pH 6), 20 mM Triethanolamine-HCl buffer (pH 7.2), 50 mM $MgCl_2$, 100mM KCl. **Table 2.1** shows the procedure for setting up the well solutions**.** The drops were equilibrated against 1ml of well solution.

Table 2.1 Procedure for preparation of well solutions used for crystallization. 1x metals buffer was prepared from a 10x metals buffer stock: 200mM TEA, pH7.2, 500mM $MgCl_2$, 1M KCl. All solutions were filtered using a 0.2µm syringe filter before use.

Stock solutions	**Final concentration of PEG 3350 (%)**					
	6	**8**	**10**	**12**	**14**	**16**
40% PEG 3350	150 µl	200 µl	250 µl	300 µl	350 µl	400 µl
1M Sodium cacodylate pH6.0	100 µl	100 µl	100 µl	100 µl	100 µl	100 µl
1x metals buffer	100 µl	100 µl	100 µl	100 µl	100 µl	100 µl
H_2O	650 µl	600 µl	550 µl	500 µl	450 µl	400 µl
Total volume	1 ml	1 ml	1 ml	1 ml	1 ml	1 ml

2.5.2 Data collection and processing

X-ray intensity data from crystals were collected at the Diamond synchrotron radiation facility in Oxfordshire, United Kingdom on beamline IO2. Prior to data collection crystals were equilibrated over a well solution containing a high concentration of PEG-3350 to help dehydrate the crystal and eliminate the appearance of ice-rings. The intensity data were collected from single crystals flash frozen in liquid nitrogen at 100K. Processing was carried out by the Xia2 automated data reduction system

2.5.3 Model building and refinement

The M2PYK C358S structure was solved by molecular replacement using MolRep using the AC domains of the M2PYK structure with PDB ID 3SRH [74]. Because the B domains of the M2PYK C358S structure have very poor density they were solved separately. One of the B domains was found by using a B domain of M2PYK 3SRH separately in MolRep refinement. The other three B domains were placed by finding the corresponding B domains in the rabbit M2PYK structure with PDB ID 1PKN. The structure was then refined using REFMAC5 [75].

The M2PYK C424A structure was solved by molecular replacement using MolRep [74]. The M2PYK structure with PDB ID 3SRD was used as the search model because the two crystals are isomorphous (Tables 5.1 and 5.6). The structure was then refined using REFMAC5 [75].

Chapter 3: Characterisation of seven M2PYK cysteine point mutants

3.1. Introduction

3.1.1 M2PYK is regulated by oxidation

Oxidation has been found to inhibit a range of pyruvate kinase orthologues including *E. coli*, yeast and human [69]–[71]. A study carried out in A549 human lung cancer cells found that an increase in intracellular ROS concentrations lead to decreased M2PYK activity [34]. This inhibition was reversed after treatment of cells lysates with the reducing agent dithiothreitol (DTT) [34]. It was proposed that oxidation of M2PYK leads to dissociation of the homotetramer, a conclusion based on the fact that treatment of human lung cancer cells expressing FLAG-tagged M2PYK with the oxidising agent diamide prevented tagged M2PYK co-immunoprecipitating with endogenous M2PYK [34].

3.1.2 The possible role of M2PYK in regulating ROS in proliferating cells

Expression of the allosterically regulated M2PYK in cancer cells is an important regulator of the flow of glucose metabolites through the glycolytic pathway [2]. Tight regulation of M2PYK activity provides a means of controlling the balance between energy production and synthetic processes that stem from the glycolytic pathway [2]. One of these synthetic processes is the pentose phophate pathway (PPP). The PPP produces the precursor to nucleic acid synthesis ribose-5-phosphate while also generating NADPH which is used by glutathione reductase to maintain GSH antioxidant levels in the cell

[76]. It is therefore concievable that expression of M2PYK could play an important role in the cancer cell's antioxidant defence response.

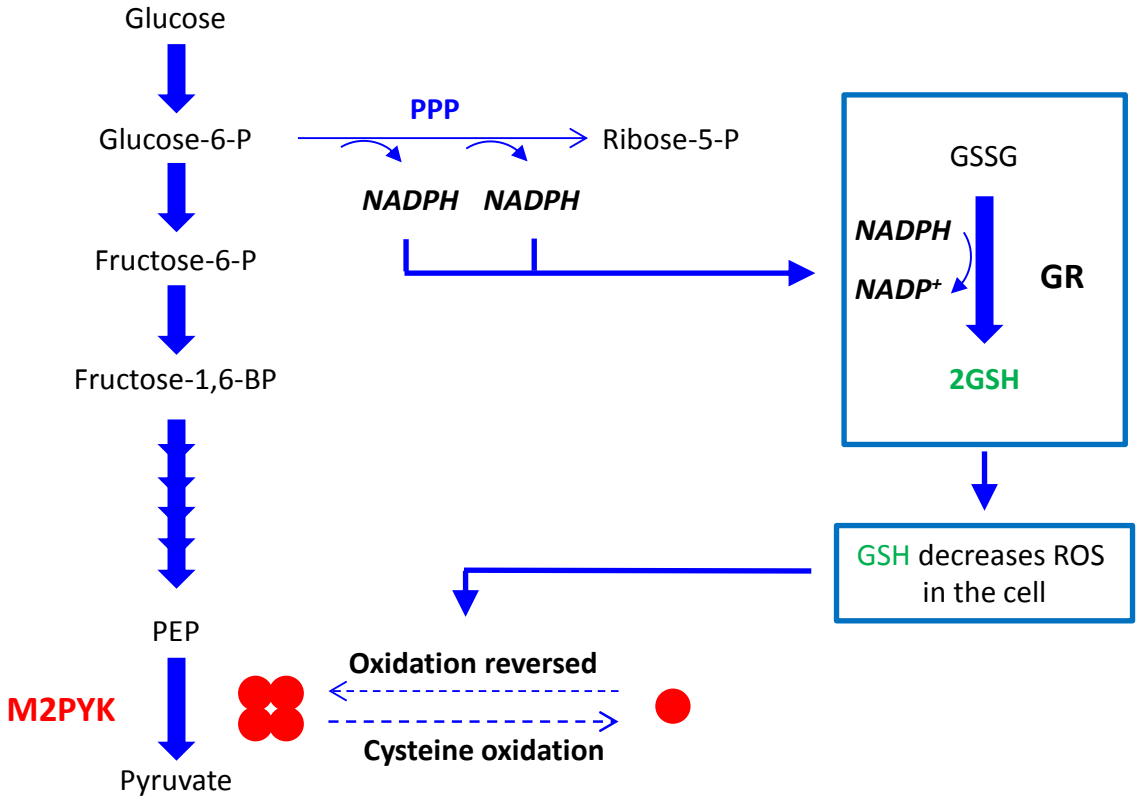

Figure 3.1 Control of M2PYK by oxidation could contribute to regulating Reactive Oxygen Species (ROS) in proliferating cells.

The proposed mechanism [34] is as follows. Cysteine oxidation causes M2PYK to become more monomeric which makes it inactive. The glycolytic intermediates earlier in the pathway build up as PEP is no longer converted to pyruvate by M2PYK. Glucose 6-phosphate enters the Pentose Phosphate Pathway (PPP) where it contributes to the production of NADPH. NAPDH is used by Glutathione Reductase (GR) to produce reduced GSH from GSSG. Increase in GSH causes a decrease in ROS, which in turn could lead to reversal of M2PYK cysteine oxidation thus allowing it to reassociate into its active tetrameric form.

3.1.3 M2PYK contains ten cysteine residues

Ten cysteines are found in the sequence of M2PYK (1.9%) (Figure 3.2). A cysteine content of 1.9% is about average for a mammalian intracellular protein, which has been calculated to be 1.6±0.9% [77]. Many of the cysteines of M2PYK are readily accessible to solvent and thus modification by oxidising agents, suggesting that regulation of M2PYK by oxidation may be complex and involve multiple cysteines. However, it has been suggested that there is one cysteine, cysteine 358, that is primarily responsible for the regulation of M2PYK by oxidation [34]. This cysteine is situated in the β barrel close to the active site and its buried location makes it a surprising candidate for oxidation (Figure 3.2). The aim of this study was to investigate the claim that Cys358 is primarily responsible for the regulation of M2PYK by oxidation. To this end, M2PYK point mutants have been made and their behaviours *in vitro* have been studied.

3.1.4 Which cysteine(s) of M2PYK are involved in its regulation by oxidation?

In order to study the role of cysteine oxidation in the regulation of M2PYK, cysteine point mutations were made. The cysteines mutated were chosen based on the results of the cysteine oxidation prediction program (COPP) web interface [78]. The M2PYK structure 1T5A was used as the input for this program which identifies cysteines susceptible to oxidation based on proximity to nearest cysteine sulphur atom, solvent accessibility, and pKa [78]. The Cysteine Oxidation Prediction Algorithm is based on a database of the physicochemical properties of 161 oxidation-susceptible cysteines and 161 oxidation-non-susceptible cysteines taken from a total of 100 polypeptides, called the balanced oxidation susceptible cysteine thiol database (BALOSCTdb). The program is capable of correctly classifying about 80% of cysteines, with 77.8% of cysteines from

transferases being correctly classified [78]. The BALOSCTdb is heavily biased towards oxidoreductases, this being the authors' particular interest, with 119 cysteines out of the total 322 cysteines being from oxidoreductases [78]. There are obvious drawbacks to using such an algorithm, most importantly that does not take into account the dynamic nature of protein architecture. Since the oxidation susceptibility of reversibly oxidised protein thiols has been found to be largely based on solvent accessibility, protein conformation would be an important determinant in cysteine oxidation [78]. Also, success of the algorithm at predicting oxidation susceptibility is dependent on the types of oxidation, as well as the types of proteins, that are present in the database used. In this case, it was found that COPA was generally unsuccessful at predicting oxidation suscuptibility of thiols that form intermolecular disulfides due to the fact that there are only 5 examples of these in the database and because this type of oxidation is generally found to involve large changes in protein conformation [78]. However, at the time of writing, COPA is the only algorithm developed that predicts oxidation susceptibility of reversibly oxidised protein thiols, and with a success rate of around 80% it gives a reasonable starting point for experimentation.

The cysteines predicted to be susceptible to oxidation by the COPP web interface were Cys31, Cys423 and Cys424 (Table 3.1). Cys358 was not predicted by this program to be susceptible to oxidation but it was included in the study due to the experimental findings by Cantley's group (Table 3.1)[34]. The cysteines were mutated to alanine to remove the cysteine group and serine to mimic a cysteine residue that cannot be oxidised (Table 3.1). Cys424 was also mutated to Leu, the equivalent residue in M1PYK due to the finding that this mutation in rat M2PYK leads to loss of allosteric regulation and maintainance of active R state in the absence of F-1,6-BP [79].

Table 3.1 M2PYK point mutations made and reasons for choosing these cysteines

M2PYK mutant	Reason for making mutant
C31A	Identified by COPP web interface as being susceptible to oxidation. Mutating to alanine removes the reactive cysteine group.
C423S	Identified by COPP web interface as being susceptible to oxidation. Mutation to serine is to mimic a reduced cysteine that cannot be oxidised.
C424A	Decreased allosteric effect [79]
C424S	Mutation to serine to mimic a reduced cysteine that cannot be oxidised
C424L	Loss of allosteric regulation, and protein in active R-state in absence of activators [79]
C358A	Identified by Cantley's group as the key cysteine residue regulating M2 PYK activity [34]
C358S	

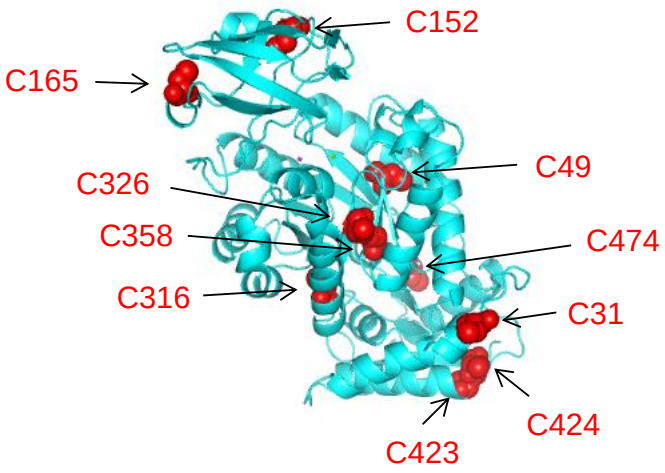


```
          10         20         30         40         50         60         70
....|....|....|....|....|....|....|....|....|....|....|....|....|....|....|
MSKPHSEAGTAFIQTQQLHAAMADTFLEHMCRLDIDSPPITARNTGIICTIGPASRSVETLKEMIKSGMN

          80         90        100        110        120        130        140
....|....|....|....|....|....|....|....|....|....|....|....|....|....|....|
VARLNFSHGTHEYHAETIKNVRTATESFASDPILYRPVAVALDTKGPEIRTGLIKGSGTAEVELKKGATL

         150        160        170        180        190        200        210
....|....|....|....|....|....|....|....|....|....|....|....|....|....|....|
KITLDNAYMEKCDENILWLDYKNICKVVEVGSKIYVDDGLISLQVKQKGADFLVTEVENGGSLGSKKGVN

         220        230        240        250        260        270        280
....|....|....|....|....|....|....|....|....|....|....|....|....|....|....|
LPGAAVDLPAVSEKDIQDLKFGVEQDVDMVFASFIRKASDVHEVRKVLGEKGKNIKIISKIENHEGVRRF

         290        300        310        320        330        340        350
....|....|....|....|....|....|....|....|....|....|....|....|....|....|....|
DEILEASDGIMVARGDLGIEIPAEKVFLAQKMMIGRCNRAGKPVICATQMLESMIKKPRPTRAEGSDVAN

         360        370        380        390        400        410        420
....|....|....|....|....|....|....|....|....|....|....|....|....|....|....|
AVLDGADCIMLSGETAKGDYPLEAVRMQHLIAREAEAAIYHLQLFEELRRLAPITSDPTEATAVGAVEAS

         430        440        450        460        470        480        490
....|....|....|....|....|....|....|....|....|....|....|....|....|....|....|
FKCCSGAIIVLTKSGRSAHQVARYRPRAPIIAVTRNPQTARQAHLYRGIFPVLCKDPVQEAWAEDVDLRV

         500        510        520        530
....|....|....|....|....|....|....|....|.
NFAMNVGKARGFFKKGDVVIVLTGWRPGSGFTNTMRVVPVP
```

Figure 3.2 Positions of cysteines in M2PYK sequence and structure

Top, cartoon of M2PYK monomer showing positions of cysteines in folded structure. Bottom, sequence of M2PYK showing positions of 10 cysteines (indicated by red dots)

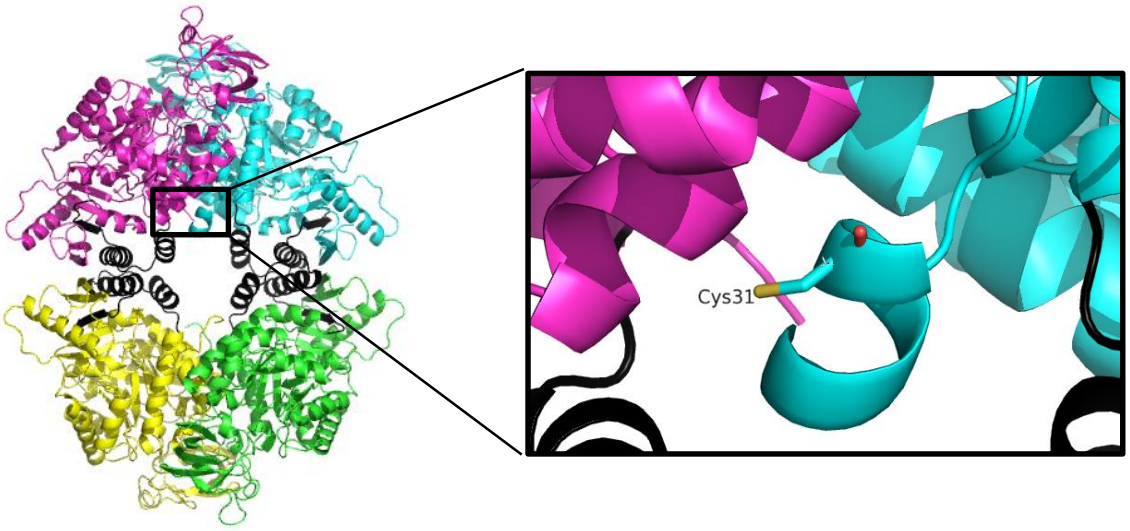

Figure 3.3 Cysteine 31 is located on the A-A interface.

It is identified in COPP web interface as being susceptible to oxidation.

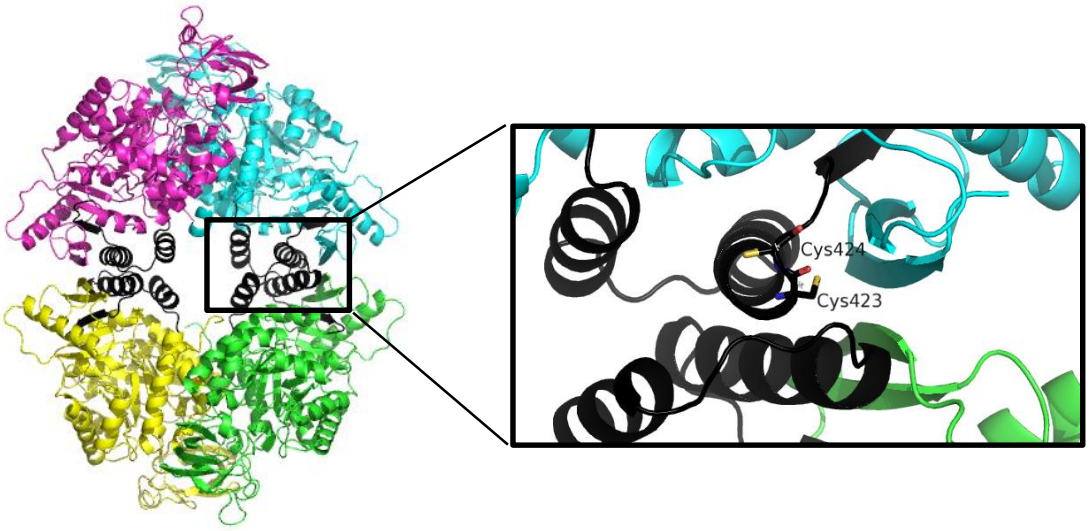

Figure 3.4 Cysteines 423 and 424 are located in the alternatively spliced region of M2 PYK on the C-C interface.

Cys424 is specific to M2 PYK, the equivalent residue in M1 PYK being a leucine. It has been found that mutating this residue in rat M2 PYK to the M1 equivalent residue resulted in loss of allosteric regulation [79]. Both cysteines are identified by the COPP web interface as being susceptible to oxidation.

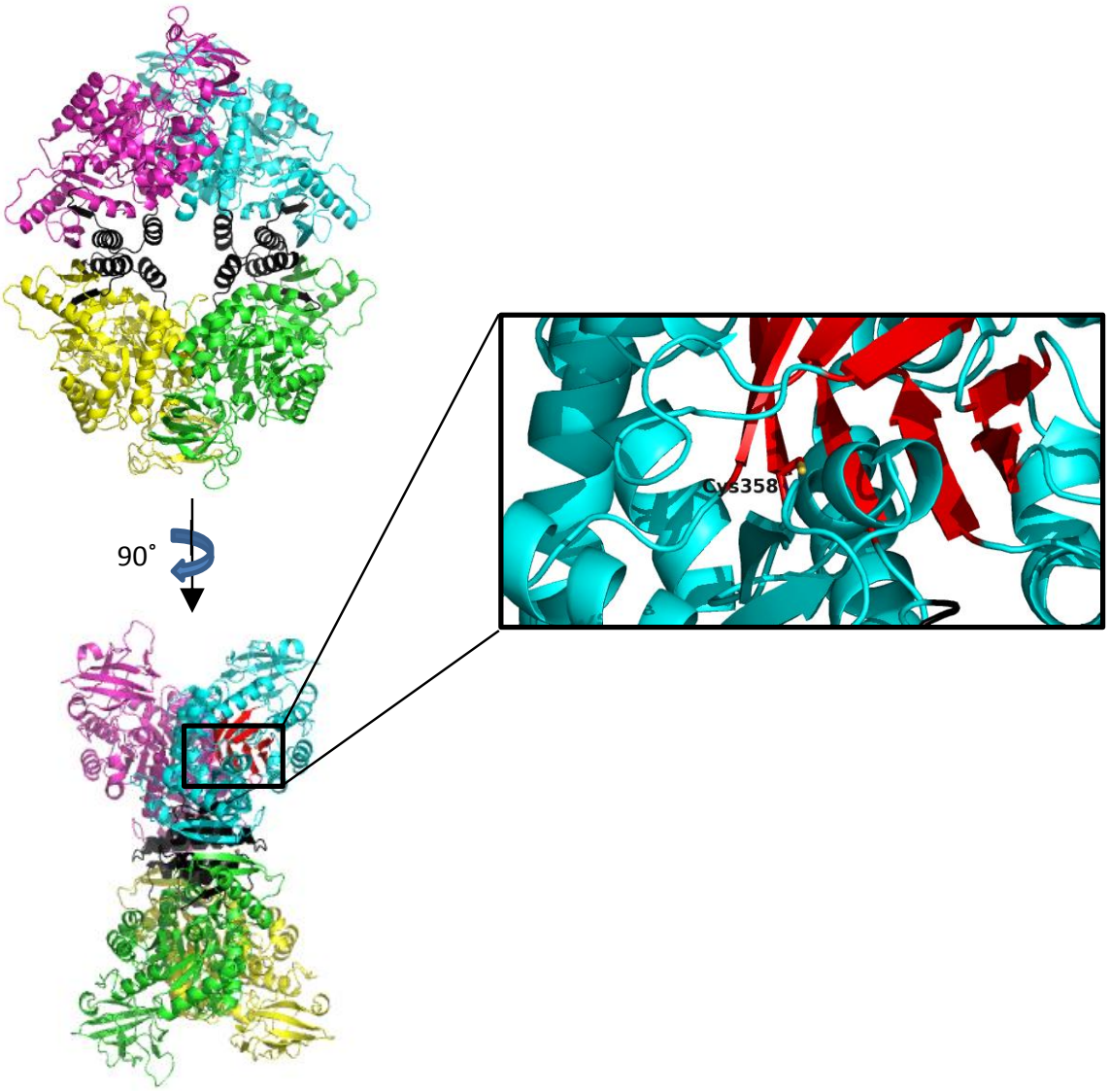

Figure 3.5 Cysteine 358 is located in a β barrel that includes essential catalytic residues.

β barrel is shown in red and C358 is located at the bottom of one of the β strands. It is this cysteine that Cantley's group claims is the cysteine primarily responsible for inhibition of M2PYK by oxidation [34]. The COPP web interface predicts that this cysteine is not susceptible to oxidation. The algorithm used by COPP (COPA) utilises structural data to predict the susceptibility of cysteine thiols to reversible oxidation with an accuracy of about 80% [78].

3.2. Results and Discussion

3.2.1 Aims

The aims of this part of the project were to produce, purify and biochemically characterise seven cysteine point mutants of human M2PYK in order to investigate which cysteine(s) are involved in the regulation of M2PYK by oxidation.

3.2.2 Expression and purification of M2PYK and mutants

His_6M1PYK, His_6M2PYK, and His_6M2PYK mutants were overexpressed in BL21 *E. coli* cells (Novagen). All proteins expressed under the same conditions (Figure 3.4). Cell pellets were lysed and the soluble fraction passed over a 5ml IMAC Hitrap HP sepharose column (GE Healthcare), precharged with cobalt at 2ml/min. Eluted M PYK was pooled and loaded onto a superdex 200 26/60 XK gel filtration column pre-equilibrated with PBS-CM (Sigma). Fractions containing M PYK were pooled and concentrated a vivaspin column with molecular weight cut-off of 30 kDa. Chromatograms and SDS-PAGE gels of relevant fractions are shown in figures 3.7 to 3.11.

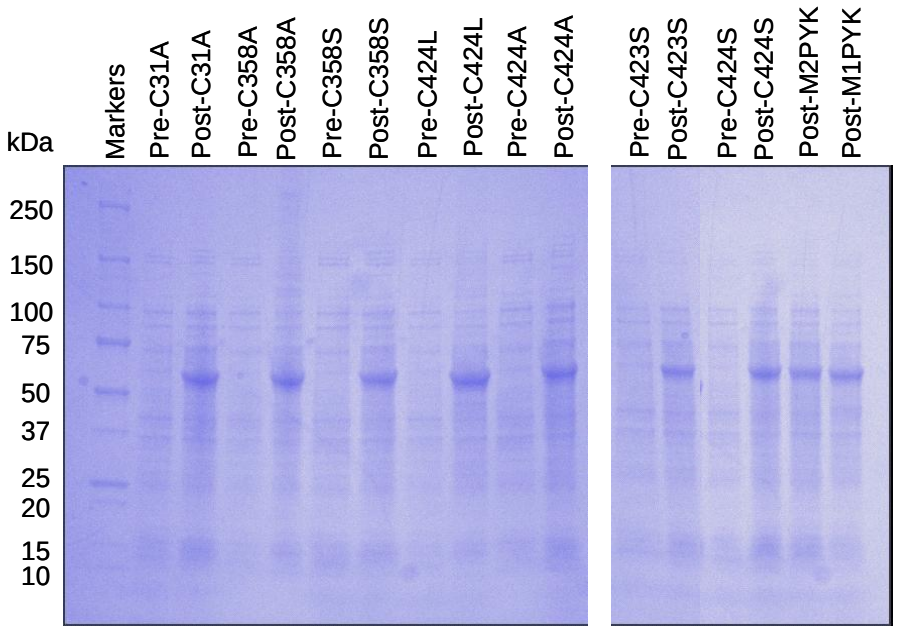

Figure 3.6 M2PYK cysteine mutant expression gels

SDS-PAGE of whole cell extracts pre- and post-induction of M PYK cultures with 1mM IPTG in 2xTY media at 18ºC overnight. Results show that all cysteine mutants express well under these conditions, the same as wild-type (Compare lanes Post-C31A, Post-C358A, Post-C358S, Post-C424L, Post-C424A, Post-C423S, and Post-C424S with Post-M2PYK)

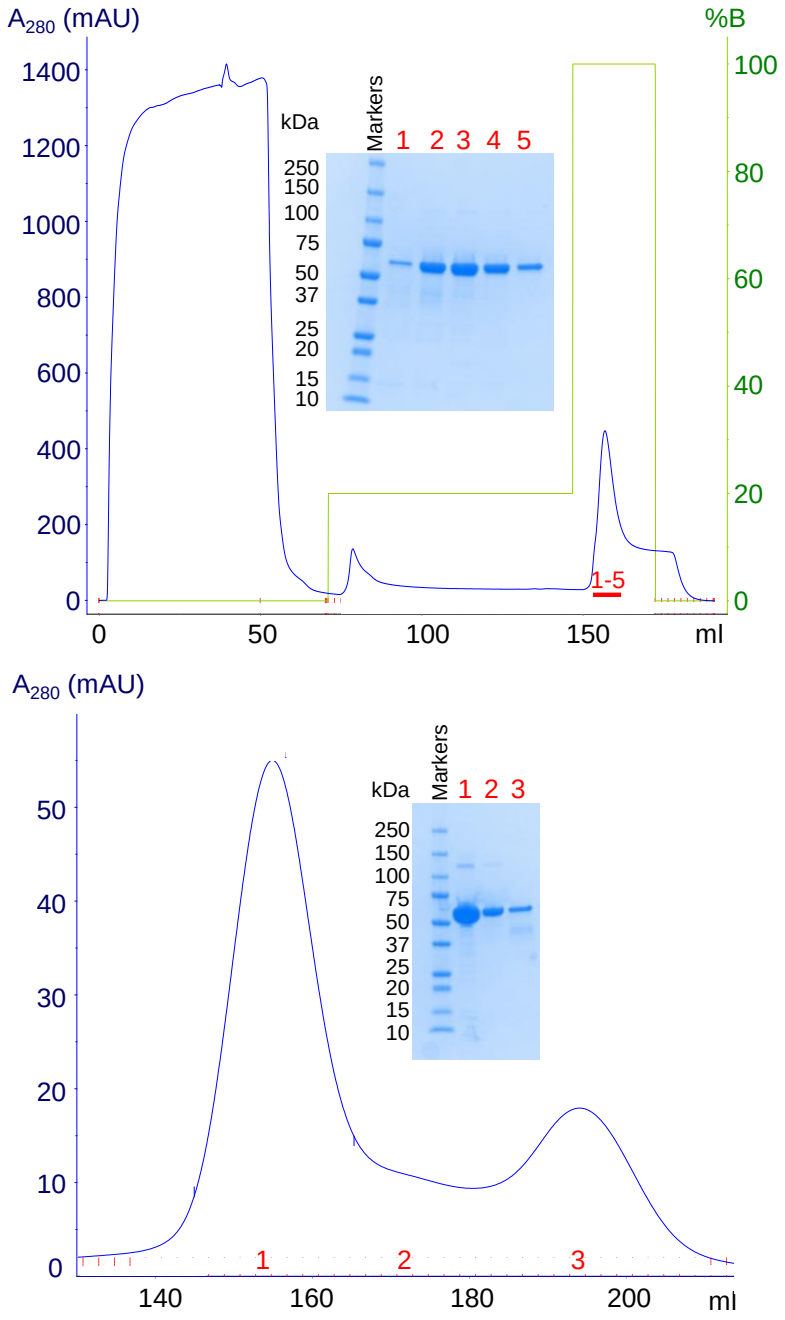

Figure 3.7 Purification of M2PYK C31A.

Top panel, IMAC elution profile from a 5ml IMAC hitrap HP column. Inset, SDS-PAGE gel of indicated fractions 1-5. Bottom panel, gel filtration elution profile from a superdex 200 26/60 XK gel filtration column. Inset, SDS-PAGE gel of indicated fractions 1-3 showing that protein was obtained to a high level of purity.

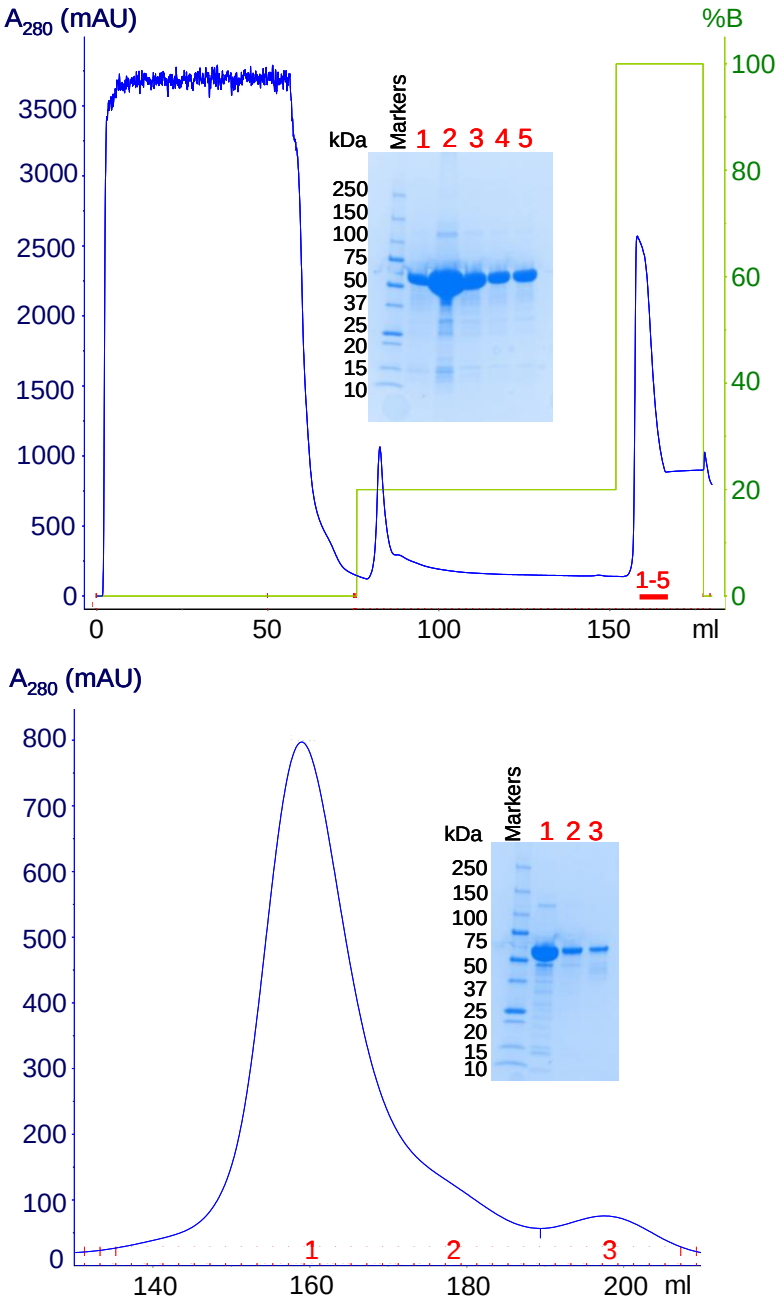

Figure 3.8 Purification of M2PYK C358A.

Top panel, IMAC elution profile from a 5ml IMAC hitrap HP column. Inset, SDS-PAGE gel of indicated fractions 1-5. Bottom panel, gel filtration elution profile from a superdex 200 26/60 XK gel filtration column pre-equilibrated in PBS-CM. Inset, SDS-PAGE gel of indicated fractions 1-3 showing that protein was obtained to a high level of purity.

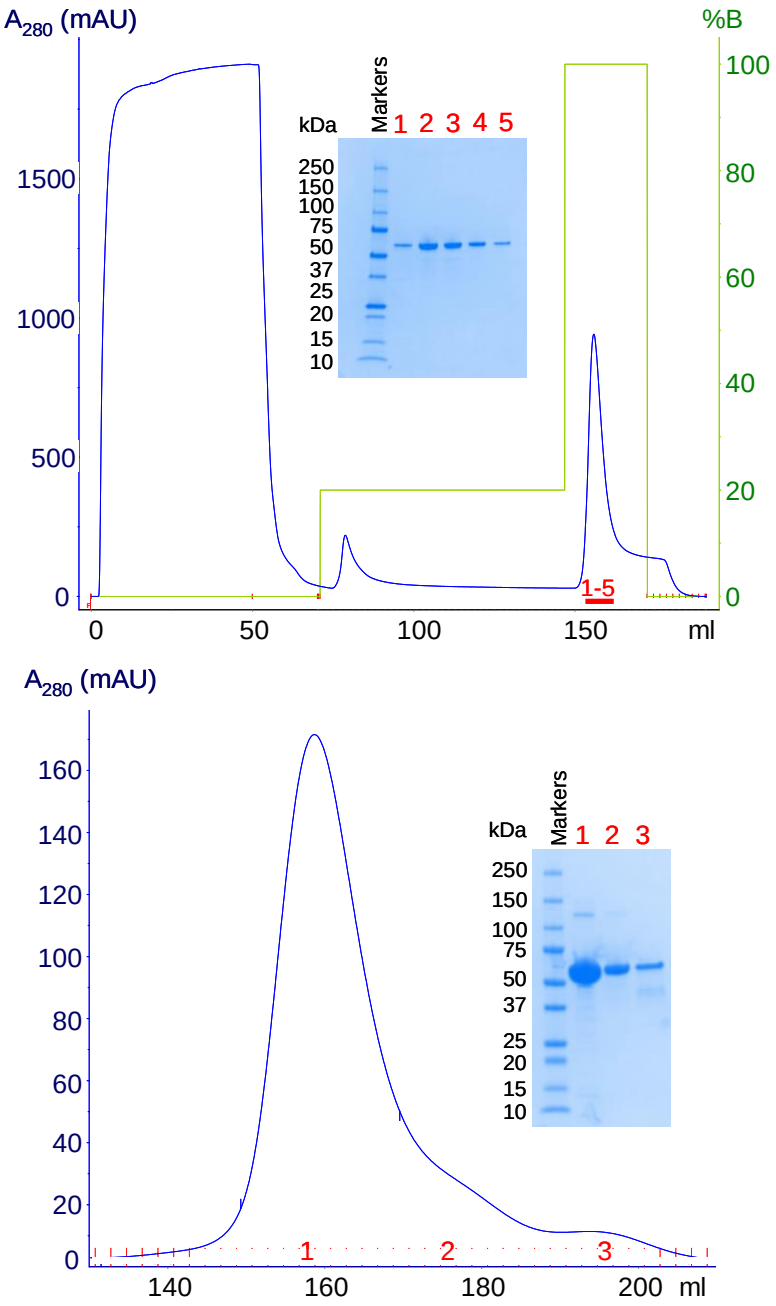

Figure 3.9 Purification of M2PYK C358S.

Top panel, IMAC elution profile from a 5ml IMAC hitrap HP column. Inset, SDS-PAGE gel of indicated fractions 1-5. Bottom panel, gel filtration elution profile from a superdex 200 26/60 XK gel filtration column pre-equilibrated in PBS-CM. Inset, SDS-PAGE gel of indicated fractions 1-3 showing that protein was obtained to a high level of purity.

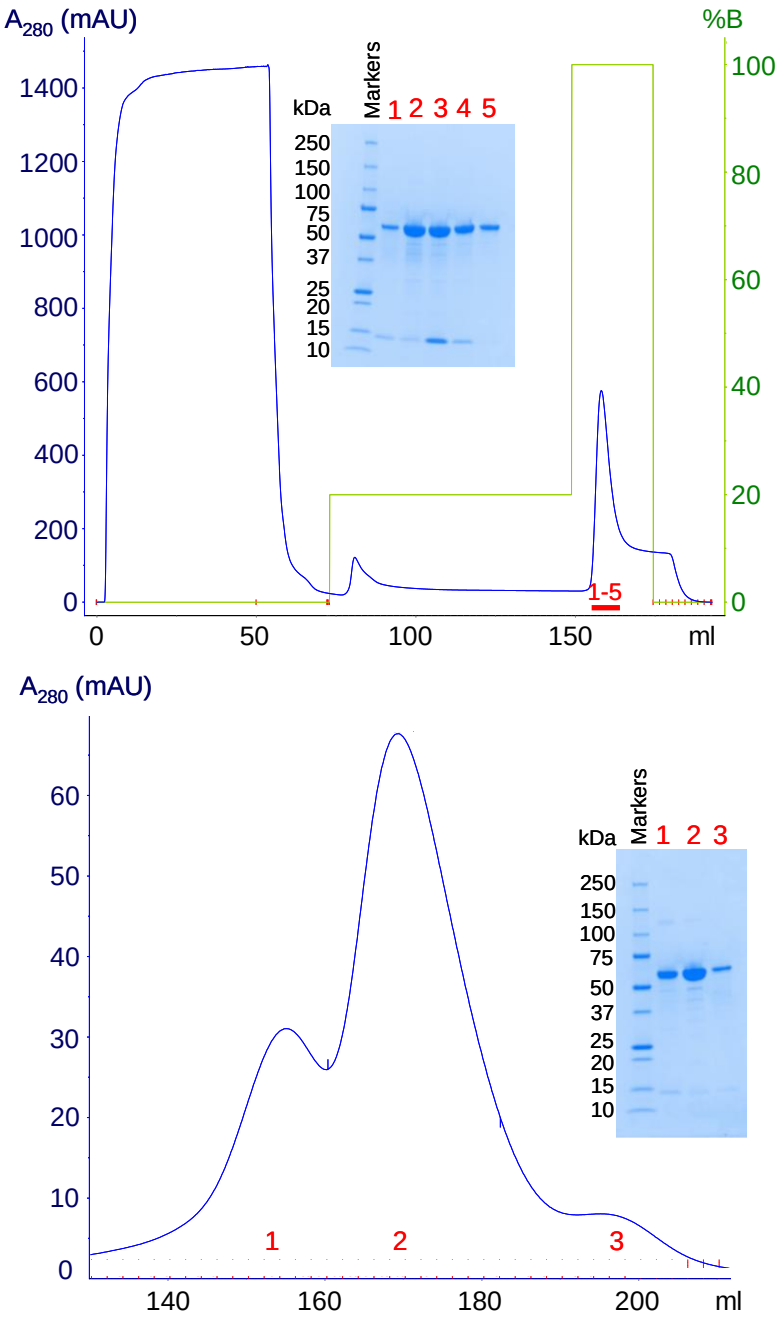

Figure 3.10 Purification of M2PYK C423S.

Top panel, IMAC elution profile from a 5ml IMAC hitrap HP column. Inset, SDS-PAGE gel of indicated fractions 1-5. Bottom panel, gel filtration elution profile from a superdex 200 26/60 XK gel filtration column pre-equilibrated in PBS-CM. Inset, SDS-PAGE gel of indicated fractions 1-3 showing that protein was obtained to a high level of purity.

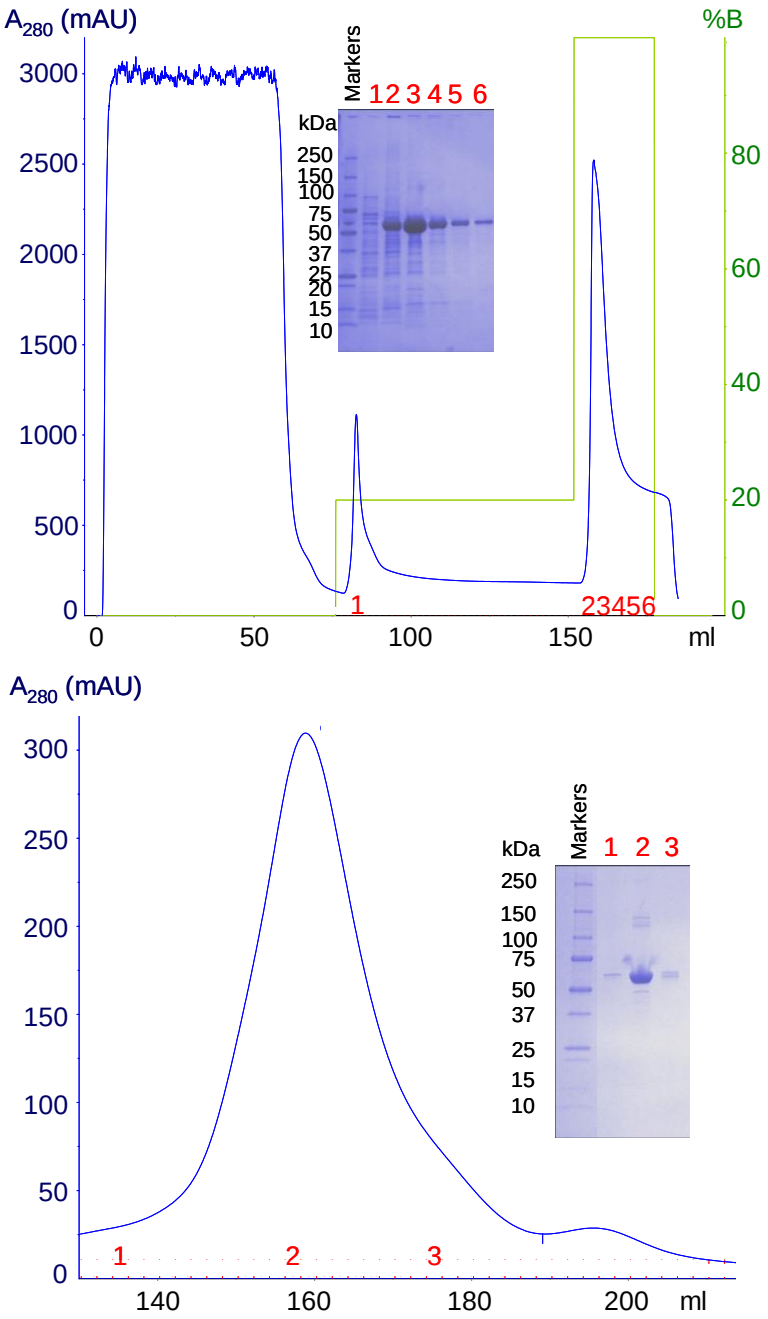

Figure 3.11 Purification of M2PYK C424A.

Top panel, IMAC elution profile from a 5ml IMAC hitrap HP column. Inset, SDS-PAGE gel of indicated fractions 1-6. Bottom panel, gel filtration elution profile from a superdex 200 26/60 XK gel filtration column pre-equilibrated in PBS-CM. Inset, SDS-PAGE gel of indicated fractions 1-3 showing that protein was obtained to a high level of purity.

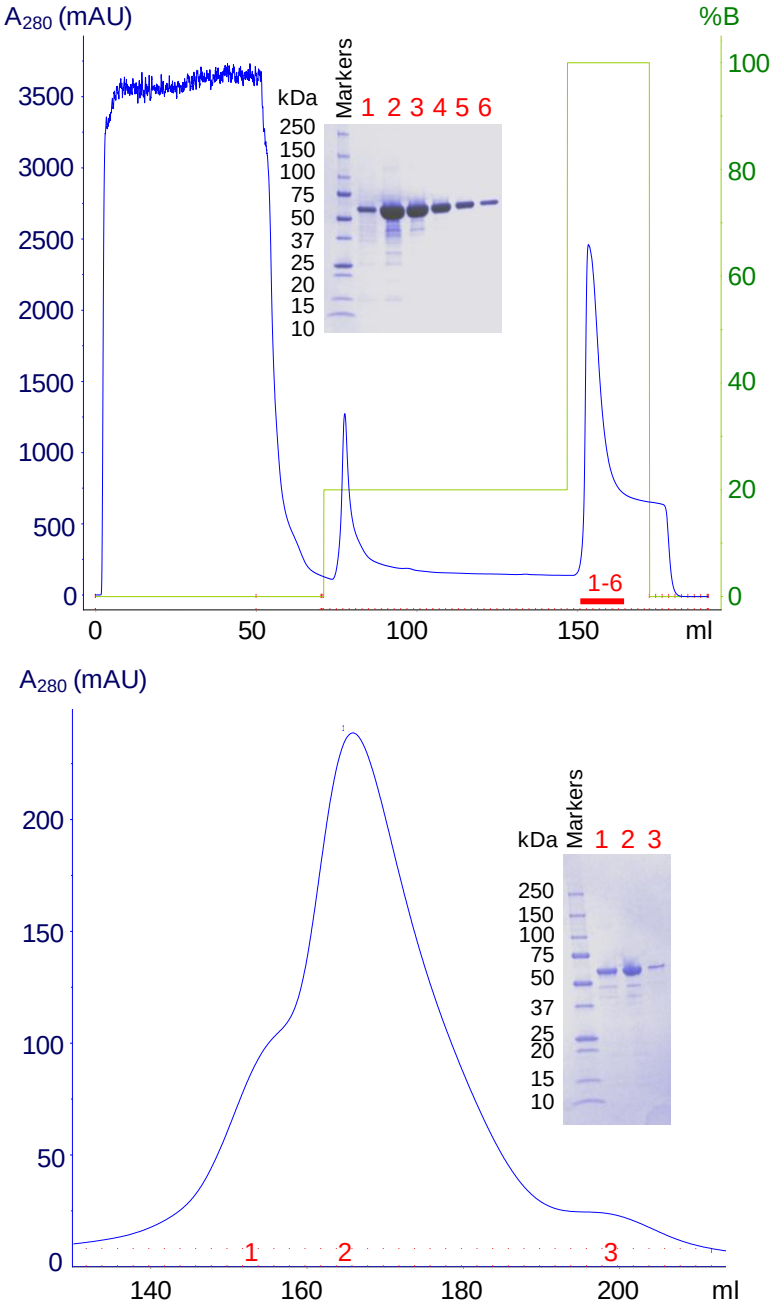

Figure 3.12 Purification of M2PYK C424S.

Top panel, IMAC elution profile from a 5ml IMAC hitrap HP column. Inset, SDS-PAGE gel of indicated fractions 1-6. Bottom panel, gel filtration elution profile from a superdex 200 26/60 XK gel filtration column pre-quilibrated in PBS-CM. Inset, SDS-PAGE gel of indicated fractions 1-3 showing that protein was obtained to a high level of purity.

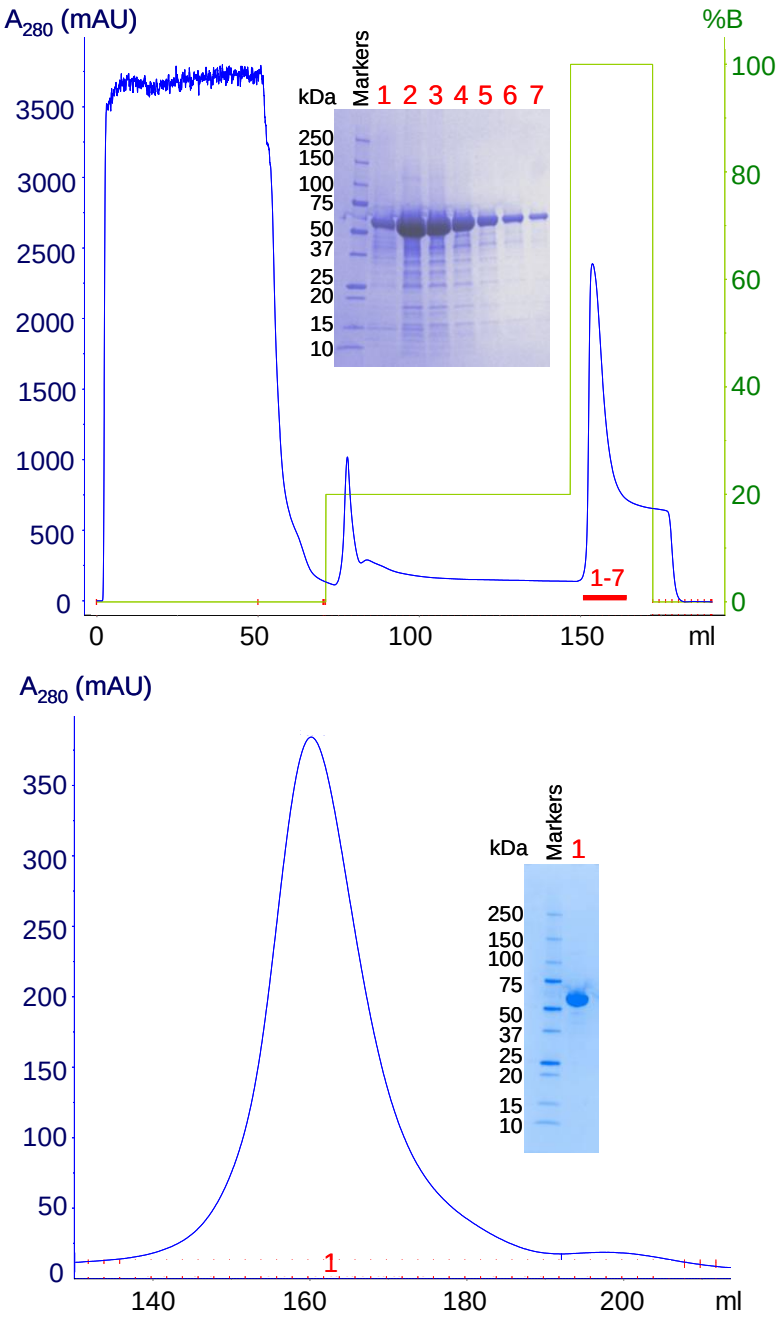

Figure 3.13 Purification of M2PYK C424L.

Top panel, IMAC elution profile from a 5ml IMAC hitrap HP column. Inset, SDS-PAGE gel of indicated fractions 1-7. Bottom panel, gel filtration elution profile from a superdex 200 26/60 XK gel filtration column pre-equilibrated in PBS-CM. Inset, SDS-PAGE gel of indicated fraction 1 showing that protein was obtained to a high level of purity.

All M2PYK cysteine mutants were purified to high level of purity and with good yields. The difference in gel filtration elution profiles suggest that mutation of these cysteines has an effect on tetramer:dimer:monomer equilibrium of M2PYK, although it would be necessary to carry out analytical gel filtration to confirm this (Figures 3.7-3.11, bottom panel).

3.2.3 DLS of M2PYK cysteine mutants

DLS was carried out on all M2PYK cysteine mutants after storage at -80ºC. The results are shown in Figure 3.12. The "size distribution by volume" graphs show a single peak of particles at close to the expected size of about 240kDa for a M2PYK tetramer. The molecular weights are estimated by the DLS software and are based on empirical mass vs. size calibration curve. The difference between the estimated molecular weights and the actual size of a M2PYK tetramer is probably due to the equilibrium between tetramer, dimer and monomer. The estimated molecular weight would therefore be an average of the different oligomeric states present. The mutants with smaller estimated molecular weights may have a higher proportion of monomer and dimer than those with higher estimated molecular weights.

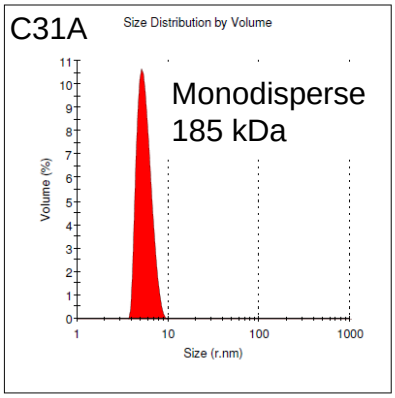

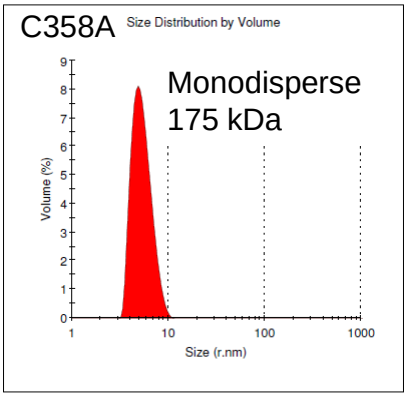

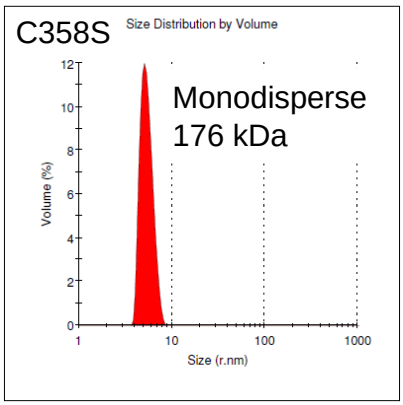

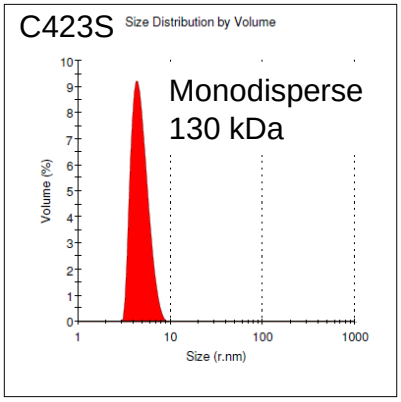

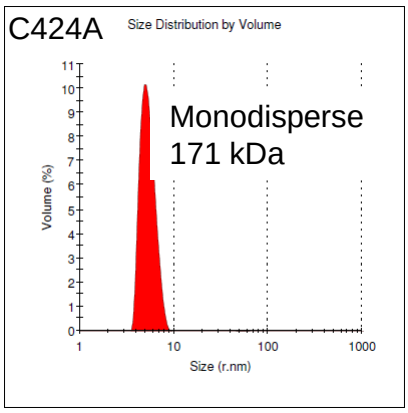

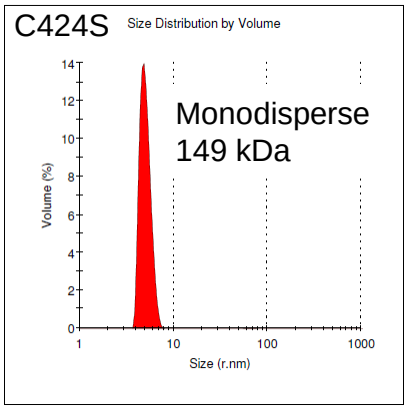

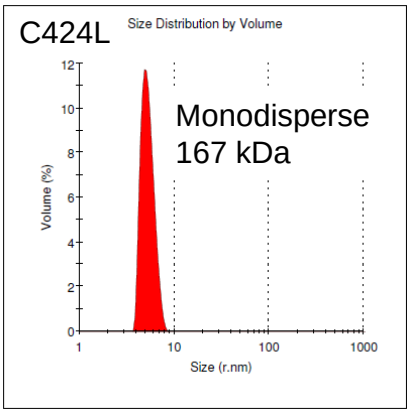

Figure 3.14 Dynamic light Scattering (DLS) analysis of M2PYK cysteine mutants shows that all are stable after storing at -80ºC in PBS-CM.
The molecular weights are estimated by the DLS software and are based on empirical mass vs. size calibration curve. Actual Molecular weight is about 240 kDa.

3.2.4 M2PYK cysteine point mutations effect on enzyme activity

The activity of M2PYK WT, M1PYK WT and M2PYK cysteine mutants were analysed using the LDH-coupled assay in the presence of 1mM PEP and 1mM DTT. Consistent with previously published results using rat M2PYK, the human M2PYK C424L mutant had similar activity to M1PYK WT [79]. Most of the cysteine mutations result in decreased activity compared to M2PYK WT, with M2PYK C358A showing the most significant reduction (Figure 3.15). This finding is in agreement with published results which show that Cys358 is important for M2PYK regulation by oxidation [34].

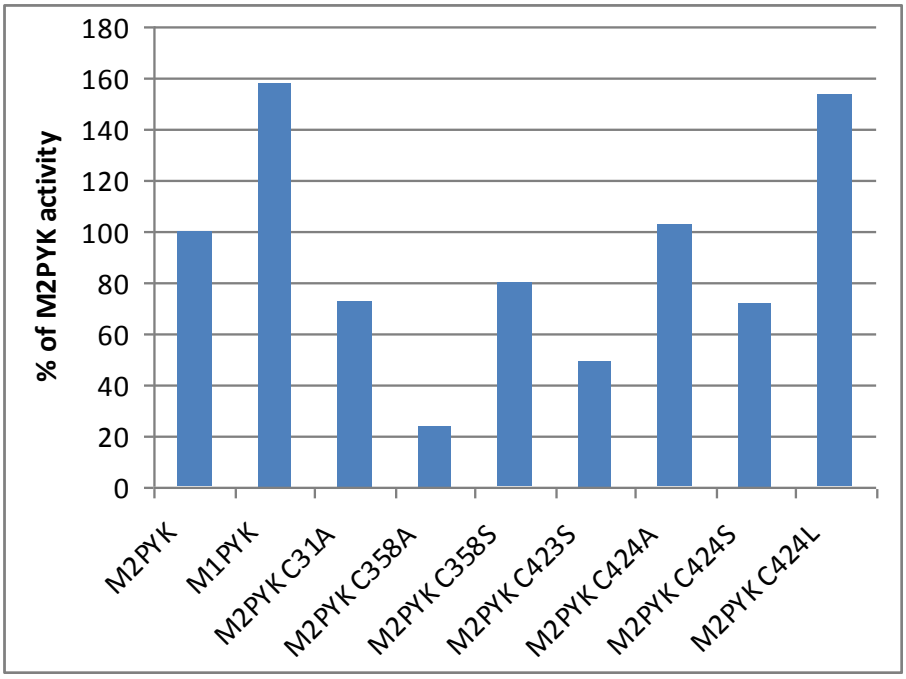

Figure 3.15 M2PYK C358A shows most significant reduction in activity compared to M2PYK WT. Activity was measured using the LDH-coupled assay in the presence of 1mM PEP and 1mM DTT, without F-1,6-BP. Velocity values (in Abs units/sec) were calculated and are presented here as a percentage of the M2PYK WT velocity. Results show that most mutants result in decreased activity compared to M2PYK WT, with the exception of M2PYK C424A and M2PYK C424L. M2PYK C358A mutation results in the most significant reduction in activity compared to M2PYK WT.

3.2.5 Cysteine point mutants do not protect M2PYK from oxidative damage

Activity assays in the presence of 1mM DTT or 10µM H_2O_2 were carried out using the Kinase Glo reagent (Promega) in order to investigate whether any single cysteine is important for regulation of M2PYK by regulation. If one cysteine was of particular importance then it would be expected that mutating it to a residue resistant to oxidative damage would result in maintenance of M2PYK activity in presence of H_2O_2. However, the results of this experiment show that none of the cysteine point mutations protect M2PYK from oxidative damage (Figure 3.16). As a control, M1PYK WT activity is unaffected by treatment with 10µM H_2O_2.

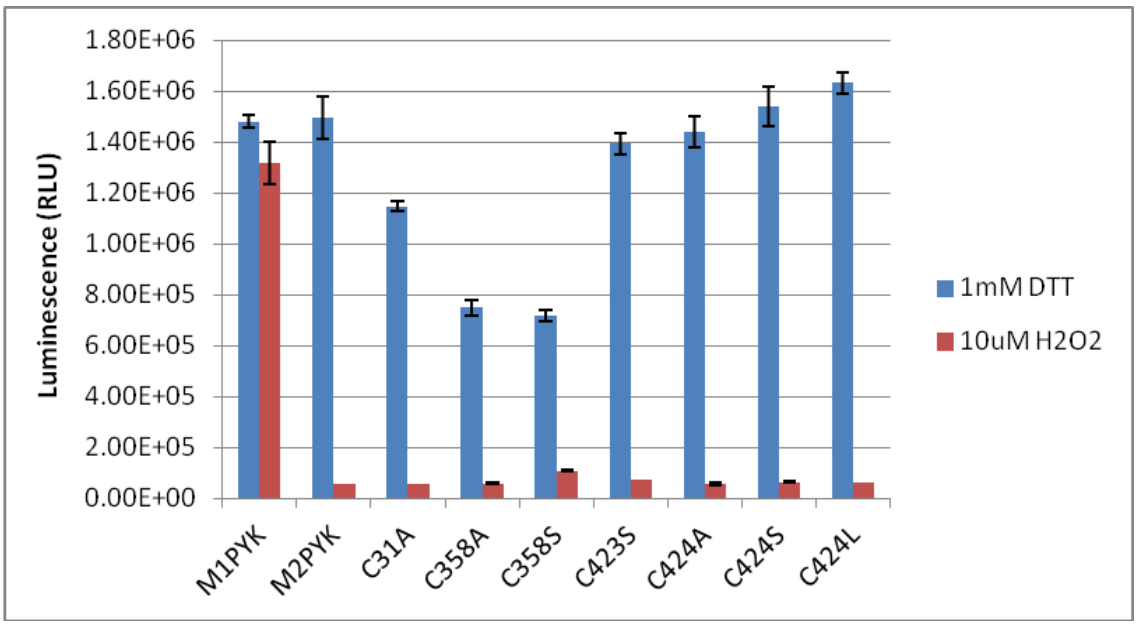

Figure 3.16 M2PYK cysteine point mutants do not prevent oxidation of M2PYK. M1PYK is unaffected by treatment with 10µM H_2O_2, whereas the activities of M2PYK and all cysteine mutants are dramatically decreased by H_2O_2. Error bars are based on triplicate measurements.

3.2.6 Kinetics of M2PYK mutants

Kinetics data for three of the M2PYK cysteine mutants as well as M2PYK WT was measured using the LDH-coupled assay varying the concentration of the substrate PEP. The mutants chosen were M2PYK C358A, M2PYK C358S, and M2PYK C424A. M2PYK C358A and M2PYK C358S were chosen for further study due to the apparent importance of this cysteine in the regulation of M2PYK as shown by Anastasiou *et al.* [34]. M2PYK C424A was chosen for further study because this cysteine is the only cysteine that is present in M2PYK but not M1PYK. The results are shown in Table 3.2 and Figure 3.17. The K_m values for M2PYK WT of 0.9mM PEP without F-1,6-BP and 0.14mM PEP with F-1,6-BP are similar to previously obtained values (Table 1.1). V_{max} values vary significantly between studies from as little as 12 U/mg (Table 1.1; Jakub Nowak MSc report) to as much as 724 U/mg (Table 1.1; [48]). This could be due to differences in the way the kinetics assays were carried out as the longer M2PYK is left at the low concentrations used for these assays, the more it dissociates into the less active dimeric and inactive monomeric states. In these experiments, as well as those carried out by Jakub Nowak, M2PYK protein was left at low concentrations at room temperature for 2-3 hours before measuring activity in order to allow the tetramer:dimer:monomer ratio to reach equilibrium. The details of the protocol used for the published paper, in which a V_{max} of 724 U/mg was obtained, are not described but perhaps they used a higher concentration of M2PYK and/or did not leave the protein to reach oligomeric equilibrium at low concentrations before measuring the activity leading to a higher proportion of active tetramer at the time of measurement [48].

Table 3.2 Summary of kinetics data collected for M2PYK cysteine point mutants.

Protein	Activity	Kinetics (no F-1,6-BP)*		Kinetics (+ F-1,6-BP)*	
		V_{max} (U/mg)	**K_m [PEP mM]**	**V_{max} (U/mg)**	**K_m [PEP mM]**
M2PYK WT	Active	97	0.9	110	0.17
M2PYK C358A	Active	34	1.5	68	0.14
M2PYK C358S	Active	34	0.9	68	0.13
M2PYK C424A	Active	60	1.3	70	0.18

All three mutants studied showed a significant decrease in V_{max} compared to M2PYK WT and small differences in K_m (Table 3.3 and Figure 3.16). M2PYK C358A has the highest K_m value which is in agreement with the activity results shown in Figure 3.15 in which M2PYK C358A was found to have the lowest activity measured in the presence of 1mM PEP. Based on the results from the thermal denaturation assay, which show that M2PYK C358S thermal stability is unaffected by the presence of F-1,6-BP (Table 3.3), it was expected that F-1,6-BP would not activate this mutant. However, all three mutants were found to be allosterically activated by F-1,6-BP (Table 3.2 and Figure 3.17). The reason for this could be based on the fact that the C358S mutation appears to stabilise the tetrameric form of M2PYK (Figure 4.7). The increase in melting temperature on addition of F-1,6-BP to M2PYK WT could be due to the fact that F-1,6-BP causes M2PYK to form more stable tetramers. Since M2PYK C358S is already mostly tetrameric, addition of F-1,6-BP would not be expected to make much difference to the stability of the protein. Perhaps M2PYK C358S is a tetramer, similar in conformation to M2PYK with phenylalanine, and binding of F-1,6-BP changes the conformation of the mutant to the active R-state [22]. This is a conceivable hypothesis given that C358 is situated close to the phenylalanine binding pocket and the pivot point of the rigid body rotation that occurs in the transition of inactive T-state to active R-state [22].

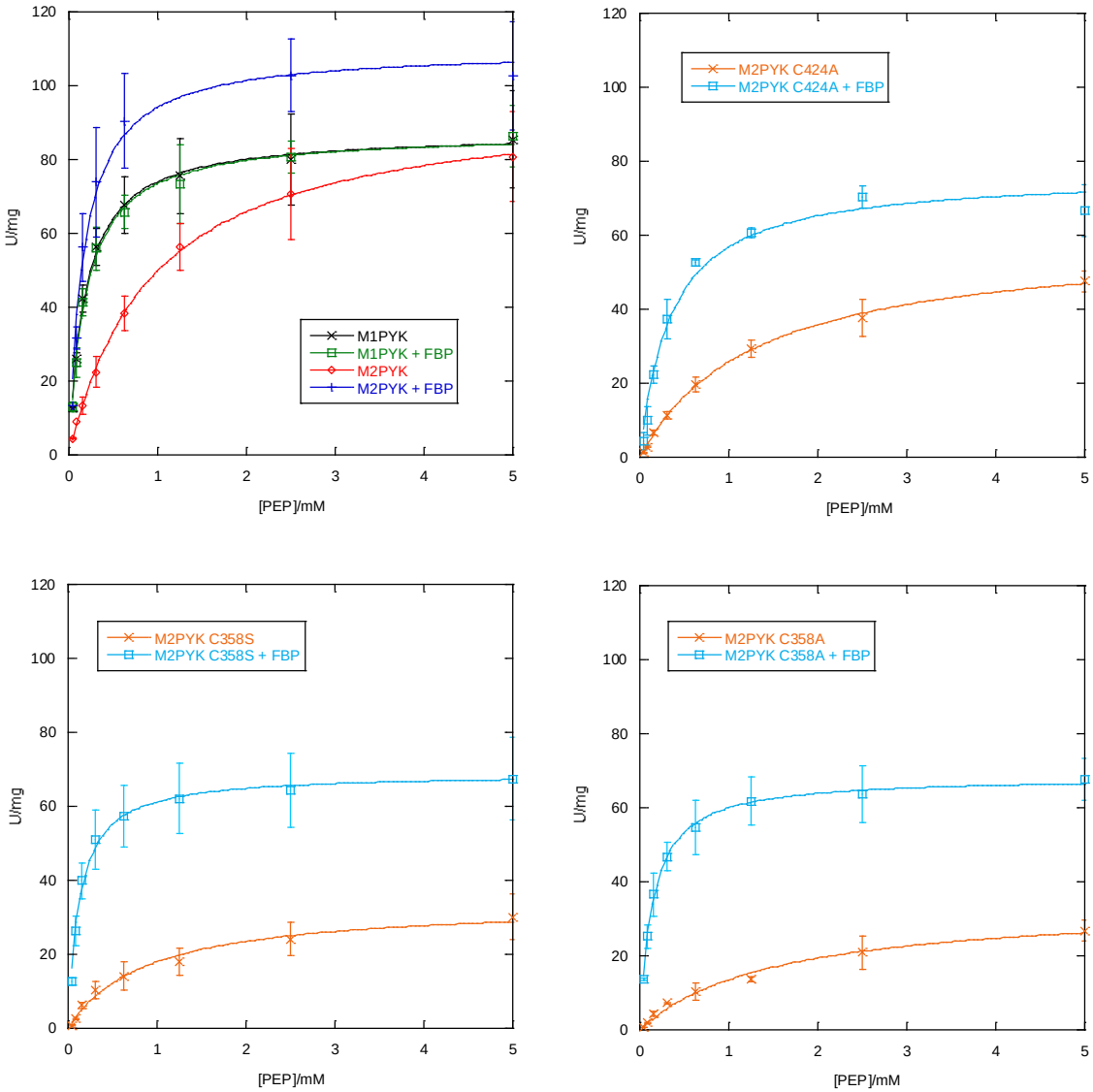

Figure 3.17 Kinetics of M2PYK cysteine mutants show that the mutants have decreased activity compared to M2PYK WT. Kinetics data for M2PYK WT and M1PYK WT (Top left), M2PYK C424A (Top right), M2PYK C358S (Bottom left), and M2PYK C358A (bottom right). PYK activity was measured using the LDH-coupled assay at room temperature. PYK samples were incubated at 0.0025 mg/ml for 3 hours at room temperature before measuring activity in order to ensure oligomeric equilibrium was reached. FBP = Fructose-1,6-bisphosphate.

3.2.7 How do the cysteine point mutations affect thermal stability of M2PYK?

Thermal denaturation assay results show that all mutations except C424A and C424L destabilise M2PYK (Figure 3.18 and Table 3.3). M2PYK C424A has the same melting temperature as M2PYK WT without additives and M2PYK C424L has a melting temperature 3ºC higher than M2PYK WT without additives (Figure 3.21).

As expected, the allosteric activator F-1,6-BP has no effect on M1PYK thermal stability whereas it shifts the melting temperature of M2PYK WT by +5ºC (Table 3.3). All M2PYK cysteine mutants except M2PYK C358S have a shift in melting temperature in response to F-1,6-BP similar to M2PYK WT. This is an interesting and unexpected observation given the distance of C358S from the F-1,6-BP binding site, however it is supportive of the theory that C358 is an important cysteine in the regulation of M2PYK by oxidation.

In the presence of 1mM H_2O_2 the melting temperature of M2PYK WT is decreased by 5ºC indicating that the structure of the enzyme is destabilised by oxidation, whereas it has no effect on the melting temperature of M1PYK (Table 3.3). The mutant M2PYK C423S is the only one for which oxidation has little effect on its melting temperature (Table 3.3). Interestingly, this mutant also has two melting peaks in the presence of DTT and is the only protein investigated which is significantly stabilised by DTT (+9ºC) (Figure 3.18 and Table 3.3). These results indicate that C423 could also be involved in the regulation of M2PYK by oxidation.

The effect of H_2O_2 and DTT on the melting temperatures of the M PYK proteins in the presence of F-1,6-BP was also measured to find out if stabilisation of the protein by the allosteric activator could protect it from oxidative damage (Table 3.3). This is of interest given the hypothesis put forward by Cantley's group that M2PYK is protected from oxidation when in the active R state [34]. The results show that M2PYK is destabilised

by H_2O_2 even in the presence of F-1,6-BP which could suggest that M2PYK is not protected from oxidation when in the R-state (Table 3.3). However, another explanation could be that the addition of H_2O_2 at the same time as F-1,6-BP allowed the H_2O_2 to have an effect before the conformational change was induced by F-1,6-BP.

Table 3.3 Summary of thermal denaturation data. * = Broad peak in -dRFU/dT plot, ** = Protein denatured at start of data collection. Two values in the same cell indicates a two phase melting event shown by two peaks in the –d(RFU)/dT plot.

Protein	Melting temperature (˚C) with:					
	No additive	1mM H_2O_2	1mM DTT	1mM FBP	1mM FBP + 1mM H_2O_2	1mM FBP + 1mM DTT
M2PYK	49	44	49-50	54	49	55
M1PYK	50/63	50/63	50/63	-	-	-
M2PYK C31A	44	41*	46	52	44*	53
M2PYK C358A	45	38/44	47	52	48*	53
M2PYK C358S	45	**	46	45	40*	47
M2PYK C423S	46	46*	46/55	54	49*	55
M2PYK C424S	46	**	47	51	**	52
M2PYK C424A	49	46	49/53	55	50*	55
M2PYK C424L	49/**52**	43	49/52	55	50	55

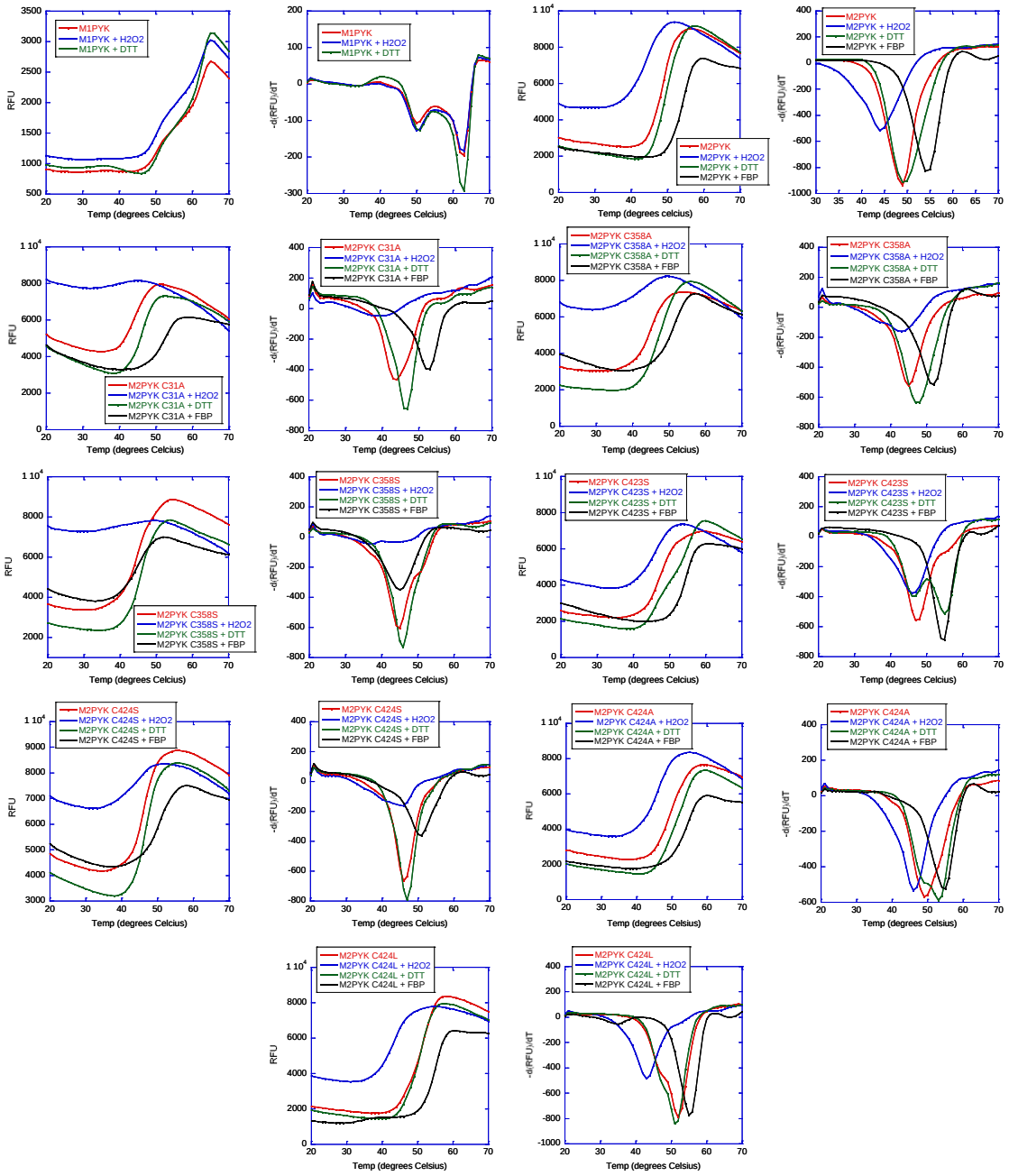

Figure 3.18 Thermal stability of M2PYK cysteine mutants

Thermal denaturation data for M PYKs and mutants in the presence of 1mM DTT (green), 1mM H_2O_2 (blue), 1mM F-1,6-BP (black), or with no additives (red). Row 1, M1PYK and M2PYK WT. Row 2, M2PYK C31A and M2PYK C358A. RowM2PYK C31A and M2PYK C358A. Row 3, M2PYK C358S and M2PYK C423S. Row 4, C424S and M2PYK C424A. Row 5, M2PYK C424L. RFU = relative fluorescence units, -d(RFU)/dT = negative derivative of RFU.

3.3 Conclusions

In conclusion, seven M2PYK cysteine mutants were successfully expressed in E.coli and purified to a high level of purity and with good yields (Figures 3.6-3.13). Differences in gel filtration profiles indicate that modification of these cysteines could have an effect on the tetramer:dimer:monomer equilibrium of M2PYK (Figures 3.7-3.13). Furthermore, DLS results show that all M2PYK cysteine mutants store well at -80˚C in PBS-CM. Enzyme activity assay results show that M2PYK C424L has high activity comparable to M1PYK even in the absence of F-1,6-BP. This is consistent with published results using rat M2PYK in which the same mutation resulted in loss of allostery and activity similar to M1PYK [79]. M2PYK C424A has activity very similar to M2PYK WT, whereas all other cysteine mutants studied showed decreased activity compared to wild-type, with the most pronounced reduction seen for M2PYK C358A (Figure 3.15). It was also shown that no single cysteine mutation could protect M2PYK from decrease in enzyme activity caused by H_2O_2, whereas M1PYK activity was mostly unaffected by the same treatment (Figure 3.16).

As expected, the thermal stability of M1PYK was unaffected by addition of F-1,6-BP whereas the melting temperature of M2PYK was increased by 5˚C by the allosteric activator (Table 3.3). Additionally it was found that all M2PYK cysteine mutants show a shift in melting temperature in response to F-1,6-BP similar to M2PYK WT, with the exception of M2PYK C358S (Table 3.3). It is unclear why this should be the case because F-1,6-BP clearly has an affect on the activity of C358S (Table 3.2 and Figure 3.17). However, the different behaviour of this mutant in the presence of F-1,6-BP despite its distance from the F-1,6-BP binding site could be supportive of the theory that C358 is an important cysteine in the regulation of M2PYK by oxidation.

The addition of 1mM H_2O_2 has no affect on the thermal stability of M1PYK whereas it decreased the melting temperature of M2PYK WT by 5˚C indicating that oxidation has a destabilising effect on the structure of M2PYK but no effect on M1PYK (Table 3.3 and Figure 3.18). This agrees with the enzyme activity results which show that M1PYK activity is unaffected by H_2O_2. The thermal denaturation results also show that oxidation by H_2O_2 has little affect on M2PYK C423S (Table 3.3). This mutant is also the only protein in this study that is significantly stabilised by addition of DTT (Table 3.3). These results suggest that M2PYK C423 could be an important cysteine in the regulation of M2PYK by oxidation.

It is interesting to speculate that oxidation and effector binding compete so that M2PYK would be protected from oxidation when in the active R-state. Although the results shown in Table 3.3 (1mM FBP + 1mM H_2O_2) do not appear to support this hypothesis, this may be due to the simultaneous addition of F-1,6-BP and H_2O_2 to the protein. It seems likely that F-1,6-BP binding would prevent oxidation because it is known that addition of F-1,6-BP induces tetramerisation [22]. Since the majority of M2PYK cysteines likely to be involved in M2PYK oxidation are located at the tetramerisation interfaces it is logical to conclude that these cysteines would be protected from oxidation in the M2PYK tetramer. In support of this hypothesis, another protein Galectin-1 has been found to have reduced sensitivity to oxidative inactivation after binding of its ligand lactose, which enhances dimer formation [80]. In order to accurately test the hypothesis that M2PYK binding to F-1,6-BP prevents oxidation it would be necessary to repeat the thermal denaturation assays incubating M2PYK in the presence of F-1,6-BP to allow transition to the active R-state before adding H_2O_2.

Chapter 4: The role of nitric oxide in M2PYK regulation (- *In vitro* biotin switch assay shows that human M2PYK is S-nitrosylated)

4.1. Introduction

4.1.1 Nitric oxide as a signalling molecule

Nitric oxide (NO) was thought only to be an atmospheric pollutant until, in 1987 and the years that followed, it was found to be synthesised *in vivo* and to have extremely similar biochemical properties to the previously described endothelium-derived relaxation factor (EDRF) [81]. NO is a by-product of the metabolism of L-arginine to L-citrulline catalysed by the enzyme nitric oxide synthase (NOS) (Figure 4.1)[82]. There are three known isoforms of NOS; NOS1, NOS2 (iNOS) and NOS3. NOS1 and NOS3 are also known as nNOS and eNOS, due to the fact that they were initially cloned in neural and endothelial cells respectively, and are dependent on Ca^{2+}-calmodulin [83]. NOS2, also known as iNOS, was first identified in macrophages and its binding to calmodulin is independent of calcium allowing it to consistently produce high levels of NO for long periods [84]. Many cell types have been found to express one or more of these isoforms [85]. NO typically acts via two types of pathway, cyclic guanosine monophosphate (cGMP)-dependent or cGMP-independent [86]. In the cGMP-dependent pathway, NO interacts with the soluble guanylyl cyclase as well as cGMP-dependent protein kinase G, phosphodiesterases and cyclic nucleotide-gated channels [87].

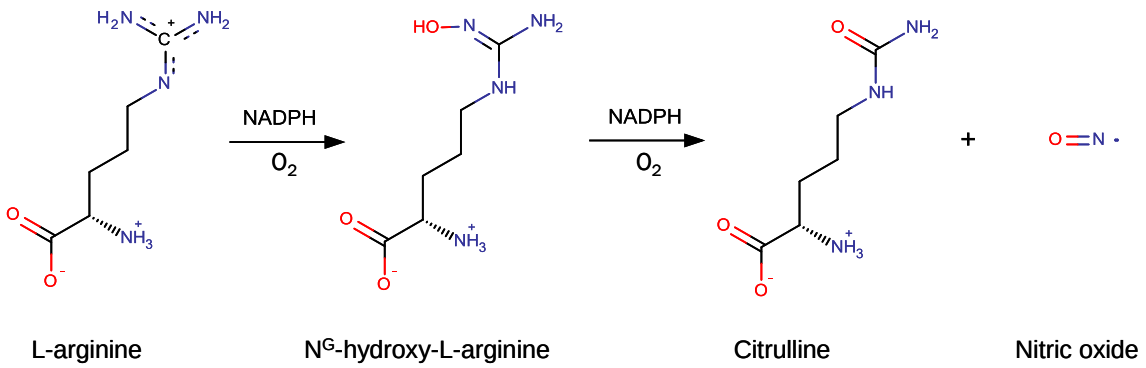

Figure 4.1 Reaction catalysed by Nitric oxide synthase (NOS).
NOS converts L-arginine to citrulline and nitric oxide via a N^G-hydroxy-L-arginine intermediate.

One of the ways that NO can function independently of cGMP is by post-translational modification of proteins by the coupling of a nitroso moiety to a reactive thiol group on a cysteine, a process known as S-nitrosylation [88]. It is thought that dinitrogen trioxide (N_2O_3) is the likely S-nitrosating species as NO itself is known to be a poor nitrosating agent [89]. N_2O_3 is produced from the reaction of NO with O_2 (Eq. (1)(2)(3)).

$$\cdot NO + O_2 \rightleftharpoons ONOO\cdot \qquad (1)$$

$$ONOO\cdot + \cdot NO \longrightarrow 2\cdot NO_2 \qquad (2)$$

$$\cdot NO_2 + \cdot NO \rightleftharpoons N_2O_3 \qquad (3)$$

The reaction mechanism for S-nitrosylation of glutathione by N_2O_3 is shown in Figure 4.2. In the first step, the thiol hydrogen is transferred to the N_2O_3 forming the reactive thiyl and a •NO radicals which then react in the second step to form the final S-nitrosothiol product.

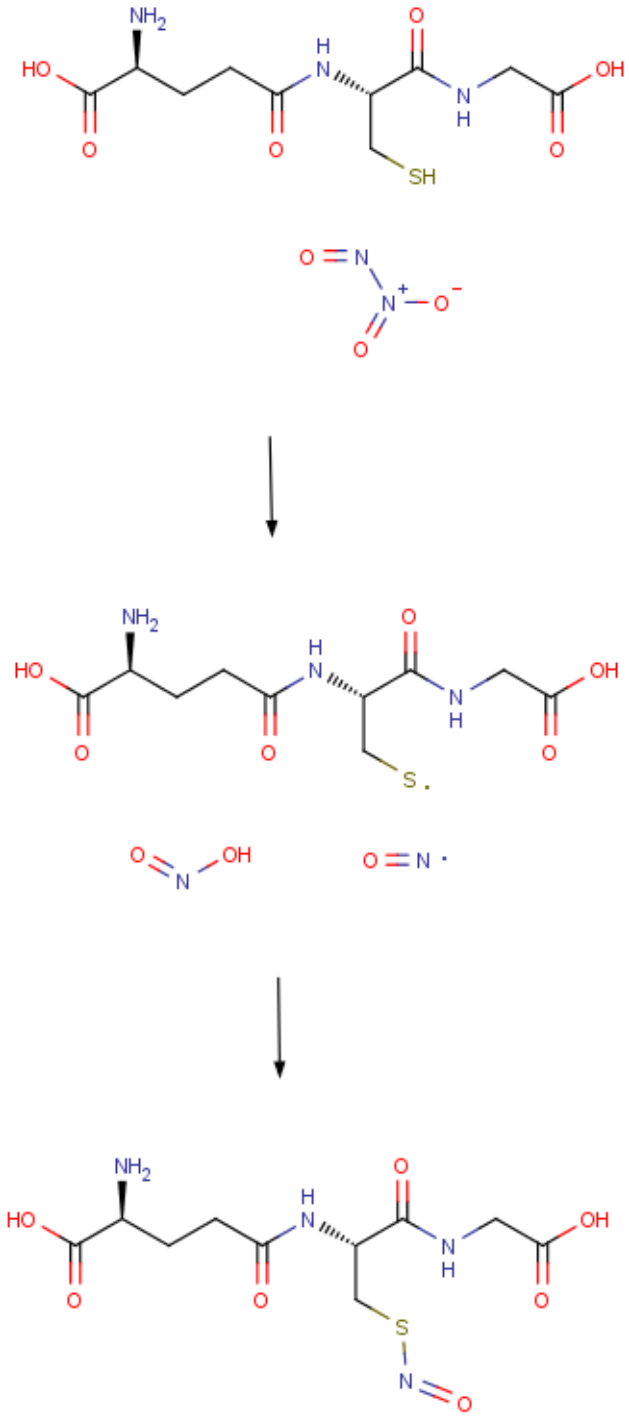

Figure 4.2 Possible chemical mechanism for the S-nitrosylation of glutathione by dinitrogen trioxide (N_2O_3).

In the first step, the thiol hydrogen is transferred to the N_2O_3 forming the reactive thiyl and a •NO radicals which then react in the second step to form the final S-nitrosothiol product.

Transfer of the nitroso moiety between proteins can also occur via nucleophilic attack on the nitrogen atom of the SNO, a process known as tranS-nitrosylation [89][90].

It is believed that S-nitrosylation of proteins could be involved in regulation and signalling in a similar way to phosphorylation because, although there are multiple cysteine residues in a protein accessible for S-nitrosylation, only a few are specifically modified. There are a few different theories put forward as to how this specificity is achieved. Firstly, specific motifs around cysteine residues may allow for selective nitrosylation by creating the right chemical environment for the reaction to take place [91][92]. Secondly, subcellular co-localisation of S-nitrosylated proteins with NOS isoforms may allow for specificity by bringing target proteins into proximity with the relevant NOS isoform [93][94][95][96]. Finally, several "protein nitrosylases" have been described that directly transfer nitroso groups to target proteins via tranS-nitrosylation [97][98][99].

4.1.2 Nitric oxide and carcinogenesis

Carcinogenesis often involves the elevated expression, overproduction, or abnormal activation of various mediators of inflammation, which include iNOS and NO [100]. Furthermore, the expression of iNOS has been found to be upregulated in many tumour types including lung [101][102], colon [103][104], melanoma [105], and breast cancers [106]–[108]. There are many laboratory and population-based studies that suggest a link between inflammatory damage and carcinogenesis [109]. For example, gastric inflammation, chronic hepatitis, cholecystisis, inflammatory atrophy of the prostate, and chronic pancreatitis are linked to cancers of the stomach, liver, gallbladder, prostate and pancreas, respectively [109].

The normal production of ROS/RNS during cellular metabolism is important for a variety of cellular functions, however oxidative stress can occur when a defect in the body's ROS/RNS detoxification pathways is coupled with excessive production of ROS/RNS as a consequence of environmental stress, infection, or a metabolic disorder [110]. NO, and its derivative peroxynitrite, promotes inflammation-associated carcinogenesis through various mechanisms. These include the reaction of peroxynitrite with DNA to form 8-nitroguanine, a biomarker of inflammation-associated cancers [111]–[113], suppression of DNA repair enzymes, and altered expression and covalent modification of numerous proteins leading to abnormal growth and proliferation of cells [86], [110].

4.1.3 Nitric oxide and tumour progression

NO derived from tumour cells has been reported to both promote and inhibit tumour progression [114][115]. The effect of NO on tumour progression is thought to be dependent upon the duration of NO exposure, cellular sensitivity to NO, and the type, activity and localisation of NOS isoforms expressed [116]. There are four explanations proposed for how NOS expression in tumour cells promotes tumour progression [116]. Firstly, migration and invasion of breast cancer and colon cancer cells have been found to be enhanced by iNOS and eNOS by acting through soluble guanylate cyclase (sGC) and the mitogen-activated protein kinase (MAPK) pathway [117]–[119]. Secondly, a correlation between iNOS expression and increased cell proliferation has been found in T-lymphoma cells [120]. Thirdly, NO may induce immune cell dysfunction thus allowing tumour cells to escape from immunosurveillance [121]. Finally, induction of iNOS in tumour cells has been found to increase expression of VEGF, which promotes angiogenesis leading to increased microvascular density and tumour progression [122][123].

Although induction of iNOS in tumour cells has been found to promote angiogenesis, there a few studies reporting that iNOS expression does not correlate with tumour progression [107][126]. Other studies have shown that there is no correlation between iNOS expression and VEGF expression in some human tissues [124]. This conflict may arise from the differences in tumour type, host tissues or tumour models. Also, in most of the studies the distribution and concentration of NO was not determined [116]. It has been reported that the response of tumour cells to iNOS induction is dependent on the status of p53, with one study showing that in p53 mutant cells induction of iNOS expression resulted in increased expression of VEGF, angiogenesis and tumour growth, whereas in p53 wild-type cells tumour growth was decreased [122](Figure 4.3).

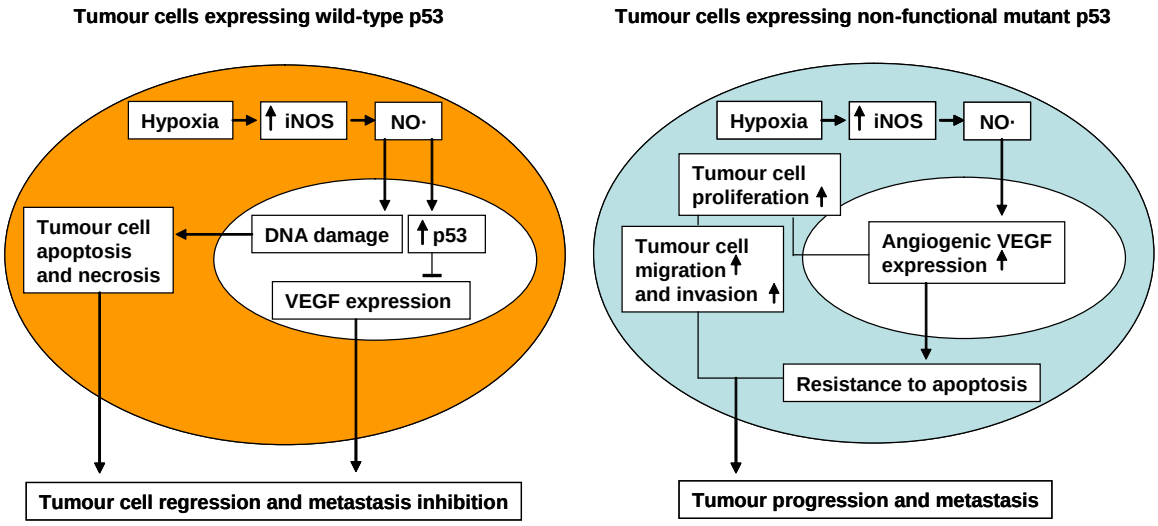

Figure 4.3 Diagram summarising the relationship between p53 and NO signalling in cancer.

Hypoxia induces NOS expression which leads to endogenous production of NO. High concentrations of NO lead to DNA damage, which results in apoptosis and necrosis, and p53 expression, which inhibits expression of the angiogenic factor VEGF thereby inhibiting metastasis. In tumour cells which express mutated non-functional p53, expression of VEGF is not inhibited and increases in response to endogenously produced NO resulting in resistance to apoptosis and increased tumour cell proliferation, migration and invasion.

4.1.3 S-nitrosylation of M2PYK

In 2001, Jaffrey and Snyder published a paper describing the biotin-switch technique for isolating S-nitrosylated proteins [72]. This opened up the opportunity to map out the S-nitrosylated proteome. In 2005, the S-nitrosylated proteome of murine macrophages was published which combined the biotin-switch technique with MALDI-TOF mass spectrometry (MS) to sequence and identify the isolated proteins [127]. It was in this study that M1/M2PYK was first identified as being S-nitrosylated. More recent studies have combined liquid chromatography with MS/MS to get more detail about peptides within the S-nitrosylated proteins that are S-nitrosylated and using this technique four M2PYK cysteines have been identified as being S-nitrosylated (Table 4.1 and Figure 4.4).

Table 4.1 Summary of M2PYK cysteines previously reported as being S-nitrosylated

M2PYK cysteine nitrosylated	Type of tissue	Reference
C49	Murine macrophages Different mouse tissues	[128] [129]
C326	Rat cerebellum Different mouse tissues	[130] [129]
C423/C424	Murine macrophages	[128]

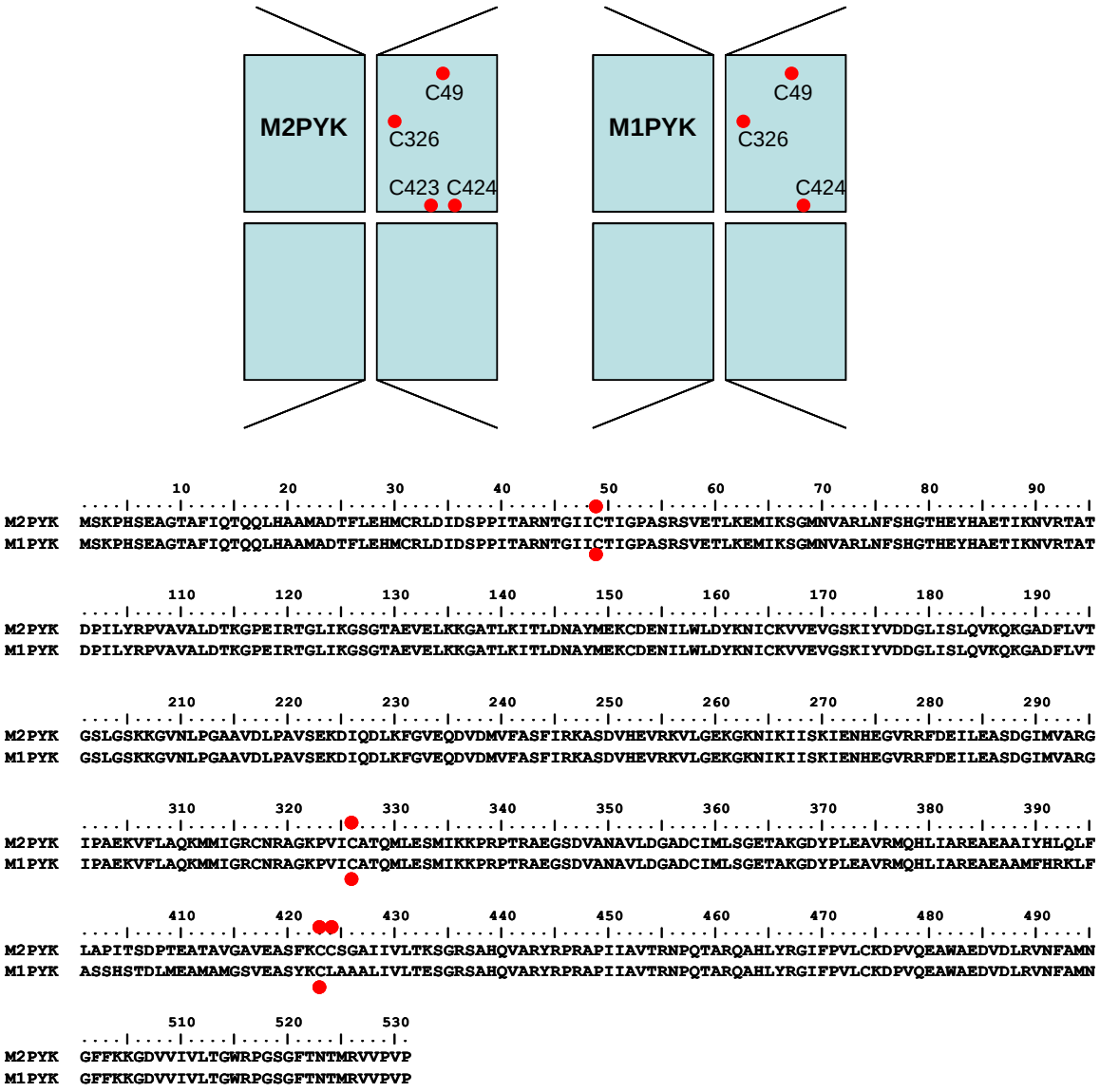

Figure 4.4 Positions of cysteines found to be nitrosylated in M1/M2PYK.

Only one of the cysteines, C424, is present in M2PYK but not M1PYK. Top; cartoon representation of M1PYK and M2PYK tetramers with the positions of those cysteines that can be S-nitrosylated shown as red circles. Bottom; sequence alignment of human M1PYK and human M2PYK with positions of those cysteines that previously reported to be S-nitrosylated indicated by the red circles.

Another glycolytic enzyme that has been reported to be S-nitrosylated is glyceraldehyde-3-phosphate dehydrogenase (GAPDH) [131]. GAPDH S-nitrosylation at its active site, Cys145, promotes interaction of GAPDH with the E3 ubiquitin ligase Siah1 and results in nuclear translocation of the SNO-GAPDH-Siah1 complex leading to mechanisms that promote cell death [131]. Interestingly, M2PYK has been found to interact with the SUMO-E3 ligase PIAS3 which induces the sumoylation and subsequent nuclear translocation of M2PYK [132]. Nuclear M2PYK has been implicated in the enhancement of cell proliferation through various different mechanisms, for example phosphorylation of the ε-amino group of L-lysine of histone H_1 by M2PYK leads to destabilisation of the nucleosome and chromatin thus allowing for DNA replication and cell proliferation [133], M2PYK interacts with and positively regulates the activity of the transcription factor Oct4 which is important in maintaining the pluripotent state of embryonic stem cells [134], and M2PYK has been found to translocate to the nucleus in response to interleukin-3 (IL-3) stimulation and to enhance cell proliferation in the absence of IL-3 [135]. It is interesting to speculate that S-nitrosylation could promote nuclear translocation in a similar manner to GAPDH thus allowing for increased proliferation of tumour cells.

4.2. Results and Discussion

4.2.1 Aims

The aims of this part of the project were to investigate whether human M2PYK is regulated by cysteine S-nitrosylation and, if so, to identify which cysteine(s) are modified.

4.2.2 Human M2PYK is S-nitrosylated *in vitro*

The biotin-switch assay was carried out on M1PYK WT, M2PYK WT, and three of the M2PYK mutants described in chapter 3 – M2PYK C423S, C424S and C358S (Figure 4.4). A workflow of the biotin-switch assay is shown in Figure 4.5A. Protein samples were treated with the nitrosylating agent CysNO followed by blocking of the free cysteines with methylmethanethiosulfonate (MMTS). NO groups were then removed and the resulting free cysteines labelled with biotin-HPDP before running samples on SDS-PAGE gel and carrying out a western blot with anti-biotin antibody to identify biotinylated proteins (Figure 4.5A). The results show that both M1PYK and M2PYK are nitrosylated, but M1PYK is nitrosylated to a lesser extent than M2PYK (Figure 4.5B). Mutation of Cys358 to serine results in almost complete loss of the biotin signal (Figure 4.5B). A naïve analysis would suggest that this cysteine is the main target of S-nitrosylation, however this does not take into consideration the possibility that the mutation could lead to change in conformation and/or oligomeric state that could result in masking of other important cysteines.

4.2.3 Mass spectrometry identifies biotinylated peptide containing Cys326

Analysis of the protein samples in the SDS-PAGE gels of WT M2PYK by mass spectrometry did not detect any peptide containing biotin labelled Cys358. However, a peptide containing Cys326 was found to be biotinylated in both M1PYK and M2PYK (Figure 4.5C). This is an interesting finding because it has been reported that M2PYK Cys326 is stably nitrosylated in a study in which it was discovered that there are a subset of proteins that are not subject to de-nitrosylation by cytosolic reducing agents [130]. In another paper, M2PYK Cys326 was found to be nitrosylated in mouse [136].

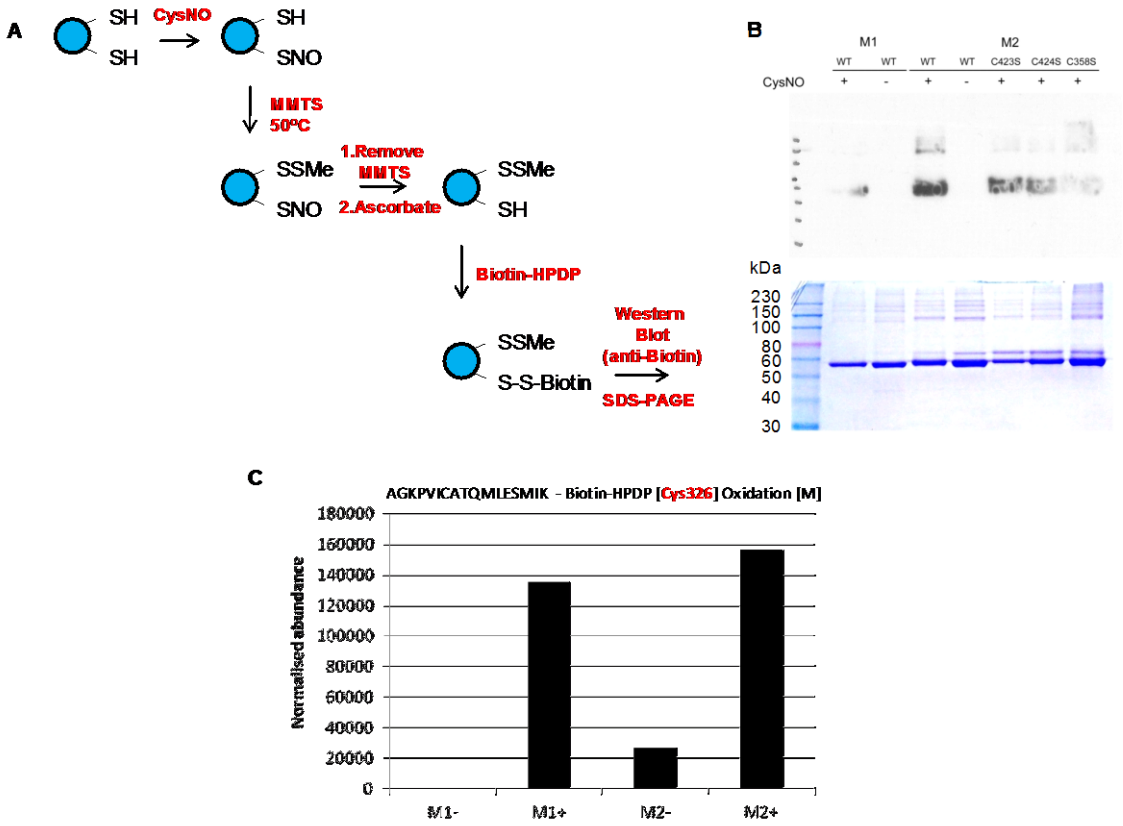

Figure 4.5 *In vitro* biotin-switch assay shows that M2PYK can be nitrosylated and that mutation of cysteine 358 to serine prevents this nitrosylation from occurring.

A. Diagram showing workflow of biotin-switch assay. **B.** SDS-PAGE and western blot of M1- and M2PYK and mutants that have undergone the biotin-switch assay. Molecular weight markers are ColorPlus Prestained protein ladder. (Carried out by Dr. Manda Yu) **C.** Bar chart showing normalised abundance of the peptide containing biotin-labelled Cys326 from mass spectrometry analysis of SDS-PAGE bands (Carried out by Dr. Thierry LeBihan) M1- = M1PYK without CysNO treatment, M1+ = M1PYK with CysNO treatment, M2- = M2PYK without CysNO treatment, M2+ = M2PYK with CysNO treatment.

4.2.4 Tetramerisation of M2PYK C358S could mask C326 from nitrosylation

Cys326 is located at the large A-A interface of M2PYK with only Arg294 masking it from the solvent when M2PYK is monomeric (Figure 4.6). Due to this location, Cys326 would be completely masked from the solvent when M2PYK is tetrameric and therefore would not be available for nitrosylation. A possible explanation for the lack of nitrosylation of M2PYK C358S is that this mutation causes M2PYK to be much more tetrameric thus shielding Cys326 from nitrosylation. The proximity of Cys358 to the phenylalanine binding pocket means that this hypothesis is feasible [22]. Phenylalanine is an allosteric inhibitor of M2PYK and acts by holding M2PYK as an inactive tetramer [22]. In order to test this hypothesis, analytical gel filtration was carried out on M2PYK C358S in order to find out its oligomeric equilibrium compared to M2PYK WT. The results were striking and show that M2PYK C358S has a much higher proportion of tetramer than M2PYK WT (Figure 4.6).

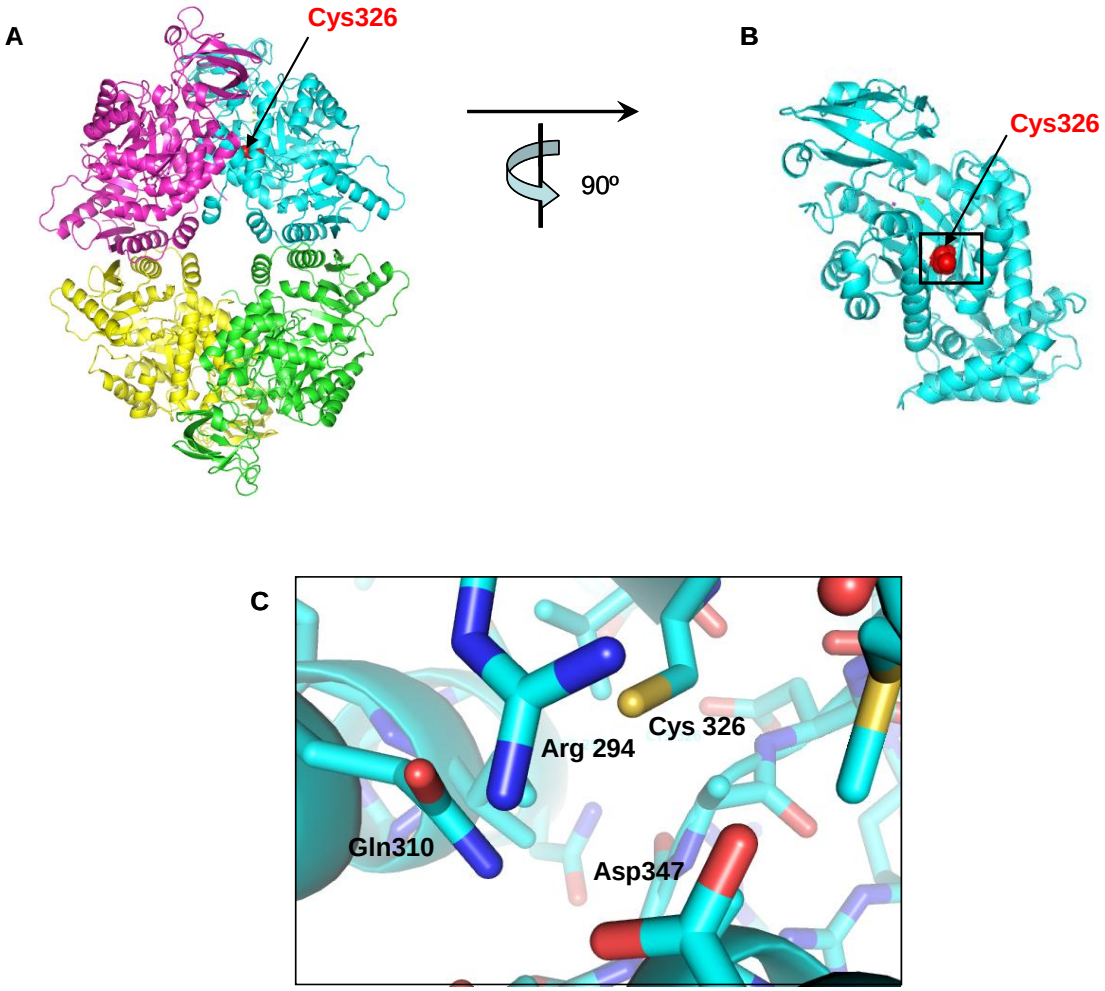

Figure 4.6 Cys326 is located on the A-A interface with only Arg294 between it and the solvent when M2PYK is monomeric.

A. M2PYK tetramer showing that Cys326 (red spheres) is buried. **B.** M2PYK monomer rotated 90º to show that when M2PYK is monomeric Cys326 is exposed to the solvent. **C.** Zoom in of boxed region in **B** showing that Arg294 is the only residue between Cys326 and the solvent. In this structure (PDB ID: 3SRD), Arg294 appears to be held in place by hydrogen bonding with Asp347.

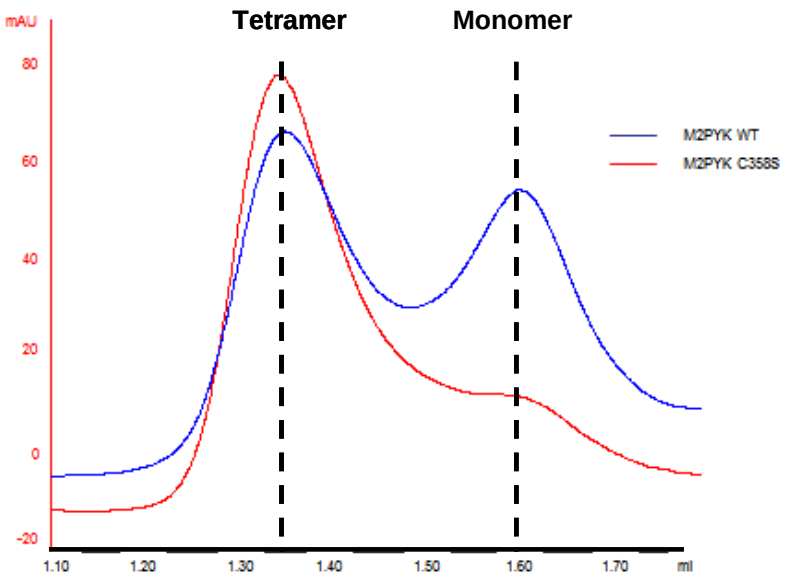

Figure 4.7 M2PYK C358S has a higher proportion of tetramer compared to M2PYK WT.

Analytical gel filtration was carried out using a superdex 200 PC 3.2/30 with a protein concentration of 0.1mg/ml. Protein samples were incubated at 0.1 mg/ml overnight at room temperature in order to allow oligomeric equilibrium to be reached. Absorbance was measured at 214nm.

4.2.5 Expression of M2PYK C326S

In order to test the hypothesis that Cys326 is the cysteine residue that is nitrosylated in human M2PYK *in vitro*, the point mutation M2PYK C326S was made using the QuikChange Lightening site-directed mutagenesis kit (Agilent technologies). This mutant did not express at all under the same conditions as the wild type and other mutants so expression trials were carried out. Mutated plasmid was transformed into three different cell lines; BL21*, C41(DE3), and C43(DE3). Expression was induced with 1mM IPTG at 20ºC, 30ºC, and 37ºC and expression was tested by SDS-PAGE after induction for 3 hours and overnight in LB media and 2xTY media (Figure 4.8). Expression was also tested in Enpresso media (BioSilta) (Figure 4.8). The conditions chosen for expression of

His_6M2PYK C326S were inducing at 30ºC for 3 hours using BL21* cell line in LB media (Figure 4.8, top right).

4.2.6 Purification of M2PYK C326S

Purification of M2PYK C326S was carried out by Meng Yuan essentially as described in **sections 2.1.3 and 2.1.4** with a few changes due to the instability of this mutant. Cell pellets containing overexpressed His_6M2PYK C326S were lysed and the soluble fraction was passed over a 5ml IMAC Hitrap FF sepharose column (GE Healthcare) precharged with cobalt at a constant flow rate of 2ml/min (Figure 4.9, top). Eluted M2PYK C326S protein was pooled and concentrated using a vivaspin column with molecular weight cut-off of 30 kDa. The concentrated protein was then loaded onto a Hiload superdex 200 16/60 column pre-equilibrated in PBS-CM with 10% glycerol (Figure 4.9, bottom). Eluted protein was pooled and concentration using a vivaspin column with molecular weight cut-off of 30 kDa. The concentration of the concentrated protein was measured as described in **section 2.1.5** using a nanodrop spectrophotometer. The final concentration achieved was 1.7 mg/ml. Purified protein was frozen in liquid nitrogen and stored at -80˚C.

BL21* 2xTY

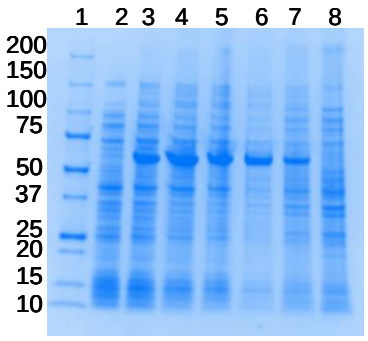

BL21* LB

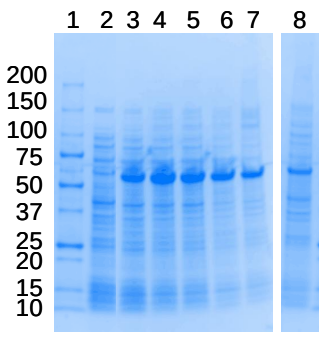

C41(DE3) 2xTY

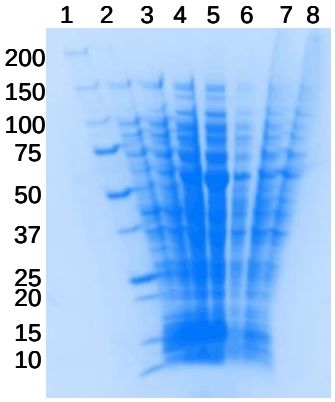

C41(DE3) LB

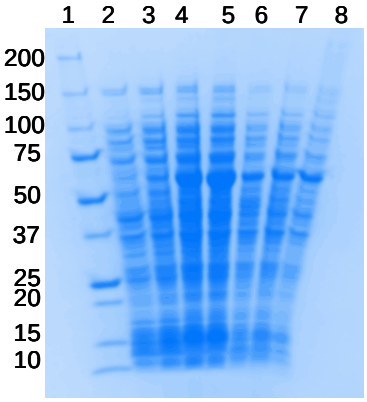

C43(DE3) 2xTY

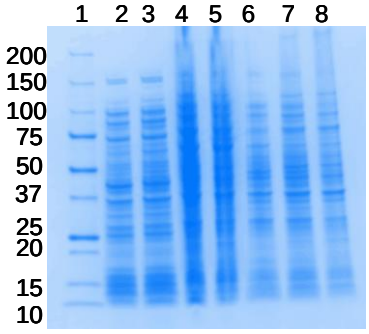

C43(DE3) LB

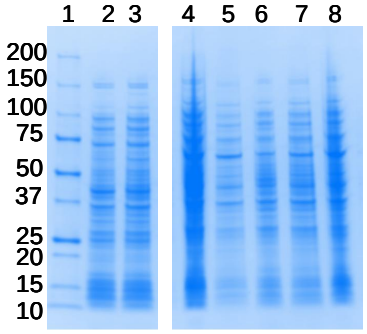

Enpresso

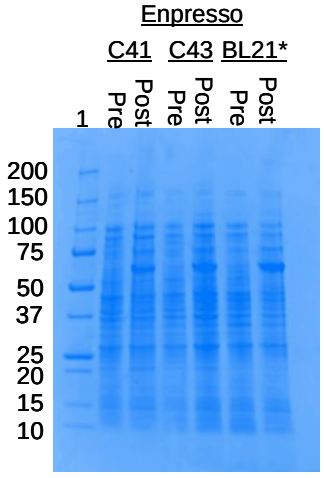

Figure 4.8 M2PYK C326S expression trials.

M2PYK C326S pET28a was transformed into three different cell lines; C41(DE3), C43(DE3), and BL21*. Expression was tested in LB media and 2xTYmedia at 3 different temperatures and 2 incubation times. Enpresso media was also tested using the standard protocol. Labels: **1**-molecular weight markers, **2**-Pre-induction, **3**-3h post induction at 20ºC**, 4**-3h post induction at 30ºC, **5**-3h post induction at 37ºC, **6**-overnight post induction at 20ºC, **7**-overnight post induction at 30ºC, **8**-overnight post induction at 37ºC. Gels were run by Meng Yuan.

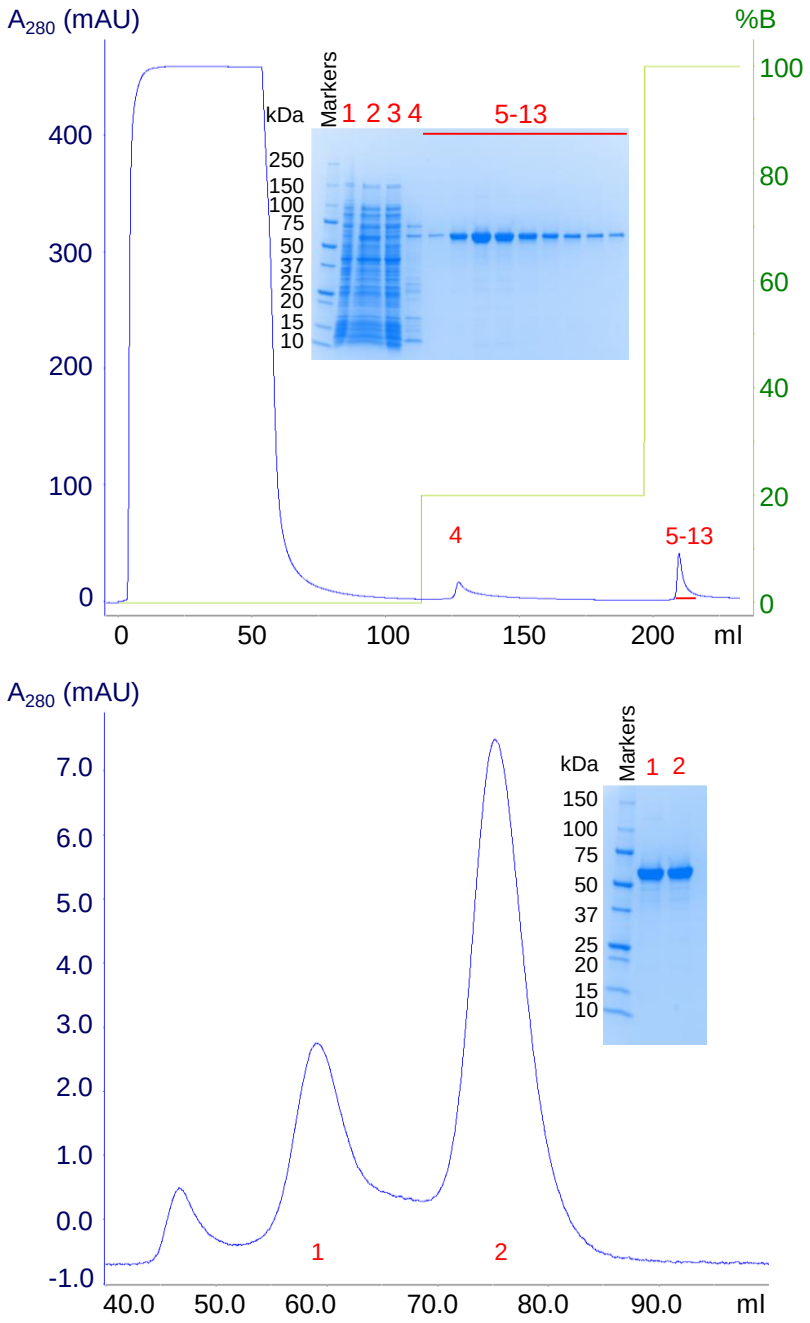

Figure 4.9 Purification of M2PYK C326S.

Top panel, IMAC elution profile from a 5ml Hitrap FF sepharose column pre-charged with cobalt. Inset, SDS-PAGE gel of indicated fractions. Lane 1 = pre-induction, lane 2 = sample loaded onto IMAC column, lane 3 = flow through. Bottom panel, gel filtration elution profile from a Hiload superdex 200 16/60 column pre-equilibrated in PBS-CM with 10% glycerol. Inset, SDS-PAGE gel of indicated fractions.

4.2.7 M2PYK C326S mutation prevents tetramerisation

M2PYK C326S was found to form a cloudy precipitate very soon after purification when stored in PBS-CM and did not respond well to concentrating. Addition of 10% glycerol to the protein after purification was effective to prevent formation of the precipitate. Analytical gel filtration was used to compare the oligomeric state of the M2PYK C326S mutant with M2PYK WT. The protein samples were incubated overnight at a concentration of 0.1 mg/ml at room temperature before loading onto a superdex 200 PC 3.2/30 column. As expected, M2PYK WT protein eluted in two prominent peaks corresponding to tetramer and monomer (Figure 4.10). However, M2PYK C326S protein eluted as a single peak corresponding to monomer (Figure 4.10). The apparent inability of the M2PYK C326S mutant to form tetramers highlights the importance of this cysteine in regulating the oligomeric state of M2PYK. It is therefore an interesting possibility that S-nitrosylation of C326 could result in the monomerisation of M2PYK thus allowing for interaction with protein partners and nuclear translocation of M2PYK in a similar manner to that observed for SNO-GAPDH [131].

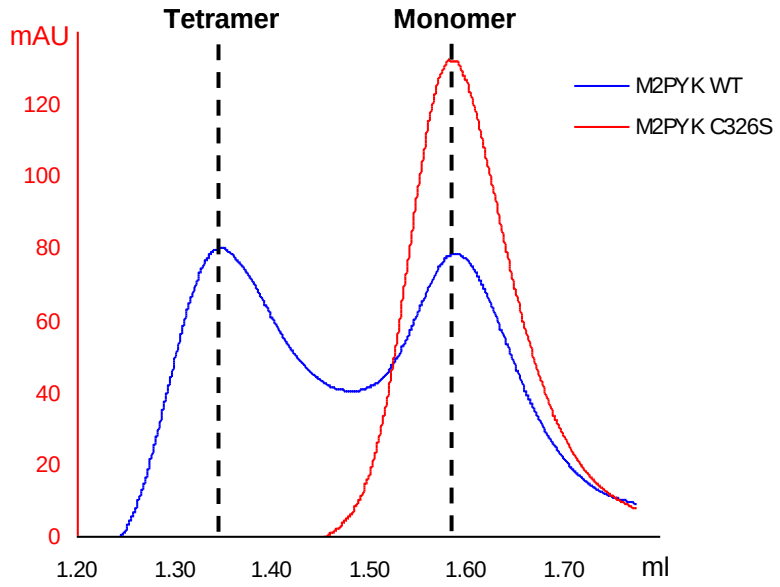

Figure 4.10 M2PYK C326S is monomeric.

Analytical gel filtration of M2PYK WT and M2PYK C326S with a superdex 200 PC 3.2/30 column after incubation at 0.1 mg/ml for 12 hours shows that M2PYK C326S is exclusively monomeric.

4.2.8 Use of serine as a cysteine substitute

Serine is commonly used as a substitute for non-disulphide bond forming cysteines due to the apparent similarity in the side-chains, the only difference being a change from an oxygen atom in serine to a sulphur atom in cysteine. However, the results from this study show that substitution of cysteine with serine can have a significant effect on the oligomeric state and stability of a protein. Substitution of Cys358 with serine resulted in a much higher proportion of tetramer compared to M2PYK WT at physiologically relevant concentration and changing Cys326 to serine resulted in exclusively monomeric protein (Figures 4.7 and 4.10). The effect of the M2PYK C358S mutation on oligomeric state is important to consider when interpreting the results published by Cantley's group in which the M2PYK C358S mutant was used to demonstrate that oxidation of this cysteine in

M2PYK effects oligomeric state [34]. They used co-precipitation experiments to show that exposing M2PYK to oxidising conditions in the cell, induced by addition of diamide to cell growth media, resulted in no co-precipitation of Flag-M2PYK WT with endogenous M2PYK. However, Flag-M2PYK C358S co-precipitated with endogenous M2PYK even in the presence of oxidising conditions [34]. Given the results found here (Figure 4.7), it is possible that the formation of hetero-oligomers of M2PYK C358S with endogenous M2PYK WT could push the oligomeric equilibrium more towards tetramer. It is also probable that mutation of Cys358 to serine also changes the conformation of the protein given that, although M2PYK C358S is mostly tetrameric and would therefore be expected to have stability similar to M1PYK, thermal denaturation assay results show that M2PYK C358S is less thermally stable that M2PYK WT (Figure 3.21 and Table 3.2). This adds another layer of complexity to interpretation of the experiments carried out by Cantley's group using M2PYK C358S because the mutant is not equivalent to M2PYK WT in either oligomeric state or activity (Table 3.3)

4.3 Conclusions

In conclusion, it is shown here for the first time that both human M2PYK and M1PYK are S-nitrosylated *in vitro* using the biotin-switch assay (Figure 4.5). M1PYK is S-nitrosylated to a lesser extent than M2PYK (Figure 4.5). In addition, mutation of Cys358 to serine results in almost complete loss of S-nitrosylation whereas the other cysteine mutants tested were largely unaffected (Figure 4.4). These results indicate that Cys358 could be the main target of S-nitrosylation. However, analysis of the biotinylated protein samples failed to detect any peptide containing biotin-labelled Cys358. Instead a peptide containing biotinylated Cys326 was detected in both M1PYK and M2PYK (Figure 4.5C). This is in agreement with two published studies; one found M2PYK to be amongst a subset of stably nitrosylated proteins with Cys326 being the S-nitrosylated cysteine, the other identified mouse M2PYK to be nitrosylated on Cys326 [137][136].

One possible explanation for the fact that Cys358 was not detected by mass spectrometry is that this cysteine is not the nitrosylated cysteine. Instead, the mutation of this cysteine to serine could cause a conformational change in the protein which results in Cys326 being buried and inaccessible to nitrosylating agents. It has been shown here that M2PYK C358S is much more tetrameric than wild-type M2PYK at physiological concentrations (Figure 4.7). The tetrameric nature of this mutant would shield Cys326 from nitrosylation due to the location of this cysteine in the A-A interface of the M2PYK tetramer (Figure 4.6).

To test this hypothesis, the mutant M2PYK C326S was made, expressed and purified with the goal of carrying out the biotin-switch assay with it (Figures 4.8 and 4.9). This mutant was more difficult to express and was mostly found in the insoluble fraction. As a result the yields were relatively low. The protein product was found to be unstable and

required 10% glycerol to remain in solution. Analytical gel filtration shows that M2PYK C326S is completely monomeric at physiological concentrations indicating that modification of this cysteine could be important in regulating the oligomeric state of M2PYK and thus its activity (Figure 4.10). Furthermore it has been found that this mutant is inactive (data not shown).

Before the M2PYK C326S mutant is used for further experimentation, the structural integrity of the protein should be tested. Although DNA sequencing of the plasmid used for expression of the mutant has been carried out and the correct DNA sequence confirmed, it may be advisable to analyse the purified protein by mass spectrometry to confirm that the correct mutation is present. The overall conformation and fold of the mutant could also be analysed using circular dichroism in order to confirm that the loss of activity is not due to incorrect protein folding.

Serine is commonly used as a substitute for cysteines because it appears that their side-chains are very similar, only differing in one atom. The results presented here show that substitution of cysteine with serine can result in dramatic changes in the conformation of a protein. Therefore, the commonly held assumption that proteins with cysteines mutated to serine are structurally equivalent to wild-type, other than there susceptibility to oxidation, needs to be treated with caution.

Chapter 5: Structural studies of M2PYK mutants

5.1. Introduction

5.1.1 Human M1- and M2PYK structures

There are 17 M2PYK structures and one M1PYK structure deposited in the PDB. The details of these structures are recorded in **Table 5.1**. The resolution of the structures ranges from 1.60 Å to 2.90 Å, with the majority being above 2.00 Å (Table 5.1). The most common space group seen is P 2_1 with unit cell dimensions of α=γ=90˚, β= 90-106˚, a= 80-170 Å, b= 70-156 Å, c= 91-170 Å (Table 5.1).

Only two of the deposited M2PYK structures include point mutations and both of these are located in the F-1,6-BP binding pocket (Table 5.1, 4FXJ and 3G2G). 4FXJ is the structure of M2PYK R489A in complex with the allosteric inhibitor phenylalanine. This mutant was made *in vitro* to prevent F-1,6-BP contamination during expression and purification of the protein in order to allow crystallisation of the protein in the inactive conformation [22]. 3G2G is the structure of M2PYK S437Y, which is a naturally occurring M2PYK SNP resulting in reduced binding of the allosteric activator F-1,6-BP.

5.1.2 M2PYK mutants discussed in this chapter

The structures of two cysteine point mutants of M2PYK, C358S and C424A, are presented in this chapter. The locations of these cysteines in the structure of the M2PYK monomer is shown in **figure 5.1**. Diffracting crystals of M2PYK C358A were also obtained, although they did not diffract to a high enough resolution for further processing. It has been shown previously that mutation of the equivalent cysteine to more hydrophobic residues in rat M2PYK resulted in loss of allosteric regulation [79]. In

chapter 4 it was shown that mutation of C358 to Ser resulted in M2PYK becoming more tetrameric (Figure 4.7). The analysis of the structures of these mutants could give interesting insights into the cause of these observed changes.

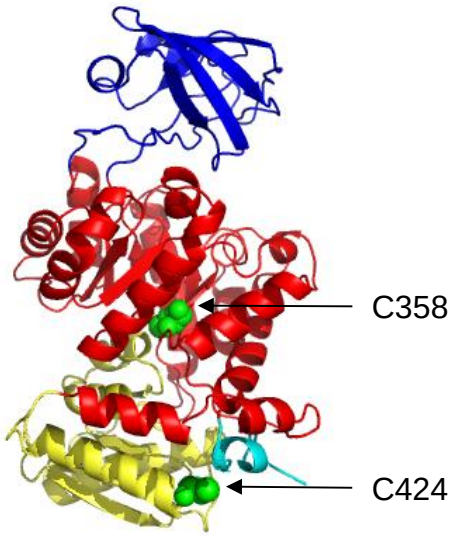

Figure 5.1 Positions of C358 and C424 in M2PYK monomer
View of M2PYK monomer showing the positions of C358 and C424 (Green spheres)

Table 5.1 Summary of human M1- and M2PYK structures deposited in the PDB. TLA= L-Tartaric acid *M2PYK activators; **DZG**= 1-(2,3-dihydro-1,4-benzodioxin-6-ylsulfonyl)- 4-[(4-methoxyphenyl)sulfonyl]piperazine, **DYY**= 1-[(2,6-difluorophenyl)sulfonyl]-4-(2,3-dihydro- 1,4-benzodioxin-6-ylsulfonyl)piperazine, **D8G**= 6-(2-fluorobenzyl)-2,4-dimethyl-4,6-dihydro- 5H-thieno[2',3':4,5]pyrrolo[2,3-d]pyridazin- 5-one, **3SZ**= 3-{[4-(2,3-dihydro-1,4-benzodioxin-6-ylsulfonyl)- 1,4-diazepan-1 yl]sulfonyl}aniline, **O7T**= 6-(3-aminobenzyl)-4-methyl-2-methylsulfinyl-4,6-dihydro-5H-thieno[2',3':4,5]pyrrolo[2,3- d]pyridazin-5-one, **NZT**= N-(4-{[4-(pyrazin-2-yl)piperazin-1-yl]carbonyl}phenyl)quinoline-8-sulfonamide, **1OX**= 2-(1H-benzimidazol-1-ylmethyl)-4H-pyrido[1,2- a]pyrimidin-4-one

Protein	PDB ID	Ligands	Space Group	Unit cell angles	Unit cell dimensions	Resolution (Å)
M2PYK	1T5A	F-1,6-BP, oxalate, K^+, Mg^{2+}	P 2_1 2_1 2_1	α= 90.00 β= 90.00 γ= 90.00	a= 108.21 b= 145.01 c= 159.26	2.80
	1ZJH	none	I 2 2 2	α= 90.00 β= 90.00 γ= 90.00	a= 120.00 b= 120.90 c= 120.90	2.20
	3BJF	F-1,6-BP, oxalate, K^+, Mg^{2+}	P 1	α= 74.63 β= 69.91 γ= 66.10	a= 80.76 b= 81.46 c= 106.89	2.03
	3BJT	oxalate, Mg^{2+}	P 1	α= 69.82 β= 77.74 γ= 67.97	a= 74.63 b= 80.71 c= 107.60	2.50
	3GQY	DZG*, F-1,6-BP, TLA	P 2_1	α= 90.00 β= 103.28 γ= 90.00	a= 81.15 b= 152.95 c= 93.16	1.85
	3GR4	ADP, DYY*, F-1,6-BP, TLA	P 2_1	α= 90.00 β= 102.91 γ= 90.00	a= 81.28 b= 153.21 c= 93.14	1.60
	3H6O	D8G*, F-1,6-BP,	P 2_1	α= 90.00 β= 108.04 γ= 90.00	a= 81.34 b= 155.69 c= 101.79	2.00
	3ME3	3SZ*, F-1,6-BP, sulphate	P 2_1	α= 90.00 β= 103.17 γ= 90.00	a= 80.88 b= 152.56 c= 93.04	1.95
	3SRD	F-1,6-BP, oxalate, K^+, Mg^{2+}	P 2_1	α= 90.00 β= 113.56 γ= 90.00	a= 95.05 b= 117.37 c= 110.46	2.90

	3SRH	PO_4	P 2_1	α= 90.00 β= 105.59 γ= 90.00	a= 81.20 b= 154.31 c= 98.59	2.60
	3U2Z	O7T*, F-1,6-BP	P 2_1	α= 90.00 β= 102.94 γ= 90.00	a= 80.76 b= 151.16 c= 93.21	2.10
	4B2D	F-1,6-BP, Mg^{2+}, serine	P 2_1	α= 90.00 β= 102.01 γ= 90.00	a= 80.61 b= 151.10 c= 91.79	2.30
	4FXF	ADP, F-1,6-BP, oxalate, K^+, Mg^{2+}	P 2_1	α= 90.00 β= 90.52 γ= 90.00	a= 81.60 b= 139.35 c= 111.28	2.55
	4G1N	NZT*, Mg^{2+}, oxalate	C 2	α= 90.00 β= 99.39 γ= 90.00	a= 168.12 b= 94.14 c= 146.15	2.30
	4JPG	1OX*, F-1,6-BP	P 2_1	α= 90.00 β= 103.45 γ= 90.00	a= 80.97 b= 153.61 c= 93.48	2.33
M2PYK R489A	4FXJ	phenylalanine, PO_4	P 2_1	α= 90.00 β= 105.72 γ= 90.00	a= 97.26 b= 70.60 c= 167.60	2.90
M2PYK S437Y	3G2G	sulphate	P 2_1 2_1 2_1	α= 90.00 β= 90.00 γ= 90.00	a= 105.55 b= 137.88 c= 155.68	2.00
M1PYK	3SRF	K^+, Mg^{2+}, PO_4, pyruvate	C 2	α= 90.00 β= 90.00 γ= 90.00	a= 238 b= 192.22 c= 109.06	2.85

5.2 Results and discussion

5.2.1 Aims

The aim of this part of the project was to crystallise and collect x-ray diffraction data for human M2PYK cysteine mutants of interest in order to obtain structures for investigation of the effect of these point mutations on the conformation of M2PYK.

5.2.2 Crystallisation

As described in chapter 2, crystals were prepared using the vapour diffusion method and the hanging drop technique at 18˚C (M2PYK C358A and M2PYK C424A) or 4˚C (M2PYK C358S) against 1ml of well solution. Crystallisation conditions were based on those used by Morgan *et al.* [22]. To prepare the drops, 1.5µl of well solution was mixed with 1.5µl of 10 mg/ml protein sample with 5mM of each ligand if applicable. The well solution contained 6-16% PEG 3350, 100mM sodium cacodylate (pH6.0), 20mM Triethanolamine-HCl buffer (pH7.2), 50mM $MgCl_2$, 100mM KCl. **Table 2.3** shows how the well solutions were prepared.

A summary of the conditions in which each of the M2PYK mutant crystals were grown is shown in **table 5.2**. Photos of the crystals that were grown are shown in **figure 5.2**. It was not possible to get a photo of crystals of M2PY C358S because they were grown in the cold room where there was no camera available.

Table 5.2 Summary of crystallisation conditions

M2PYK mutant	Temperature	Ligands	% PEG 3350
C358A	18˚C	F-1,6-BP, oxalate, ATP	14
C358S	4˚C	F-1,6-BP,oxalate, ATP	12
C424A	18˚C	F-1,6-BP, oxalate, ATP	18.5

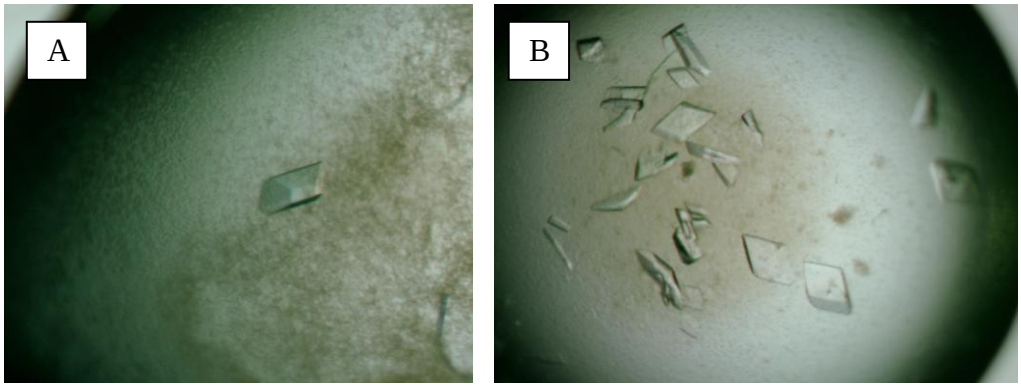

Figure 5.2 Photos of M2PYK mutant crystals.
A. M2PYK C358A. B. M2PYK C424A

5.2.3 Data collection

As described in chapter 2, x-ray intensity data was collected at the Diamond synchrotron radiation facility in Oxfordshire, United Kingdom on beamline IO2. The data was collected from single crystals flash frozen in liquid nitrogen at 100K. Crystals were dehydrated by equilibration over a well solution containing a high concentration of PEG-3350 in order to eliminate the appearance of ice-rings. Summaries of the data collection statistics are shown in **table 5.4** and **table 5.6**.

M2PYK C358S was co-crystallised with F-1,6-BP, oxalate and ATP and diffracted to a maximum resolution of 3.10Å (Table 5.4). The crystal has an unusual space group of C2 2 2_1 not seen in any of the M2PYK structures deposited in the PDB (Table 5.1). It also

has unusually large unit cell dimensions (Table 5.4). The data set has a completeness of 99.8%.

M2PYK C424A was also co-crystallised with F-1,6-BP, oxalate and ATP and diffracted to a maximum resolution of 2.87Å (Table 5.6). This crystal has the more commonly seen space group of P 2_1 and unit cell dimensions comparable to those of 3SRD (Table 5.6 and Table 5.1). This data set has a completeness of 90.5%.

M2PYK C358A was co-crystallised with F-1,6-BP, oxalate and ATP. The crystal obtained diffracted but not sufficiently for any processing.

An example diffraction image from the M2PYK C424A crystal is shown in **figure 5.3**.

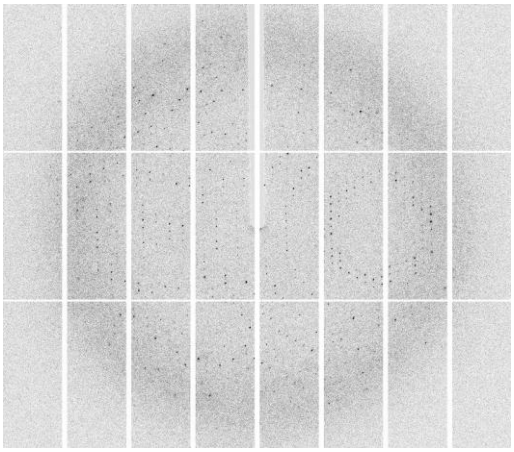

Figure 5.3 Diffraction image from a crystal of M2PYK C424A

5.2.4 M2PYK C424A structure determination

As described in chapter 2, the M2PYK C424A structure processed by Xia2 automated data reduction system and was then solved by molecular replacement using MolRep [74]. The M2PYK structure with PDB ID 3SRD was used as the search model because it has the same space group and similar unit cell dimensions (Tables 5.1 and 5.4). The structure was then refined using REFMAC5 [75]. The refined structure has an R factor of 18.5 and R_{free} of 24.1.

5.2.5 M2PYK C358S structure determination

As described in chapter 2, the M2PYK C358S structure was processed by Xia2 automated data reduction system. The structure was then solved by molecular replacement using MolRep using the AC domains of the M2PYK structure with PDB ID 3SRH [74]. Because the B domains of the M2PYK C358S structure have very poor density they were solved separately. One of the B domains was found by using a B domain of M2PYK 3SRH separately in MolRep refinement. The other three B domains were placed by finding the corresponding B domains in the rabbit MPYK structure with PDB ID 1A49, a holo MPYK structure in which the B domains adopt different conformations [138]. The structure was then refined using REFMAC5 [75]. The refined structure has an R factor of 23.4 and R_{free} of 30.0

Table 5.3 Summary of crystals

Protein	Crystallisation method	Ligands	Resolution (Å)
M2PYK C358A	co-crystallisation	F-1,6-BP, oxalate, ATP	n/a
M2PYK C358S	co-crystallisation	No ligands	3.10
M2PYK C424A	co-crystallisation	F-1,6-BP, oxalate, ATP	2.87

Table 5.4 Crystallographic data statistics

		M2PYK C358S	M2PYK C424A
Spacegroup		C 2 2 2_1	P 2_1
Unit cell parameters			
a (Å)		90.12	94.36
b (Å)		135.91	115.26
c (Å)		449.45	109.40
α (˚)		90.00	90.00
β (˚)		90.00	114.43
γ (˚)		90.00	90.00
Wavelength (Å)		0.9795	0.9200
High resolution limit		3.10	2.87
Low resolution limit		74.91	49.88
R_{merge} (%)		7.7	9.4
Completeness		99.8	90.5
Anomolous completeness		96.2	83.8
Multiplicity		4.8	3.5
Anomolous multiplicity		2.4	1.7
I/sigma		12.8	8.3
Reflections	Total	244922	153526
	Unique	50619	43988

Table 5.5 Refinement statistics

	M2PYK C358S	M2PYK C424A
Number of reflections	50549	41736
Resolution range (Å)	67.14 – 3.10	49.88-2.87
R factor	0.234	0.1815
R_{free}	0.30	0.2397
Mean B factor ($Å^2$)	59.9	33.3
R.m.s deviation from ideal		
Bond lengths (Å)	0.0138	0.0112
Bond angles (˚)	1.7822	1.5132
Ramachandran plot (%)		
Residues in favoured region	87.9	92.3
Residues in allowed region	9.3	3.6
Outliers	2.8	1.2

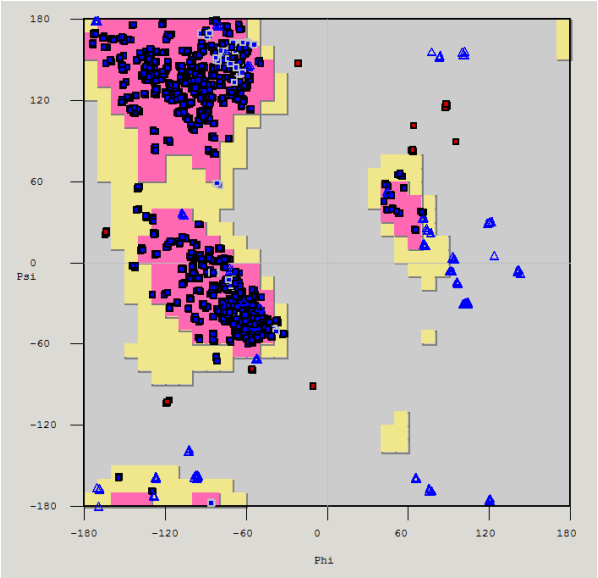

Figure 5.4 Ramachandran plot for M2PYK C424A

Ramachandran plot for M2PYK C424A refined structure shows that most residues have configurations within the favoured or allowed regions.

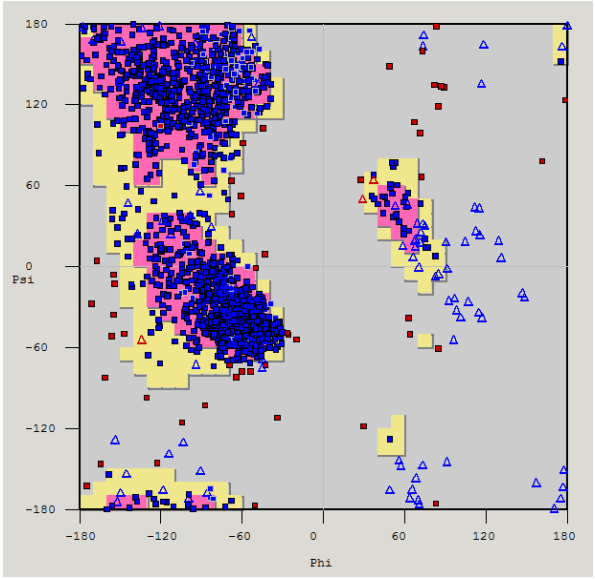

Figure 5.5 Ramachandran plot for M2PYK C358S

Ramachandran plot for M2PYK C358S refined structure shows that the majority of residues have configurations within the favoured or allowed regions.

5.2.6 M2PYK C424A mutation is present in structure

A model of M2PYK WT (PDB code 3SRD) was used to calculate the $|F_o-F_c|$ difference electron density map with M2PYK C424A. The difference electron density map clearly shows that the mutation has been successful as indicated by strong negative peaks where the cysteine has been mutated to alanine in the C424A structure (Figure 5.5).

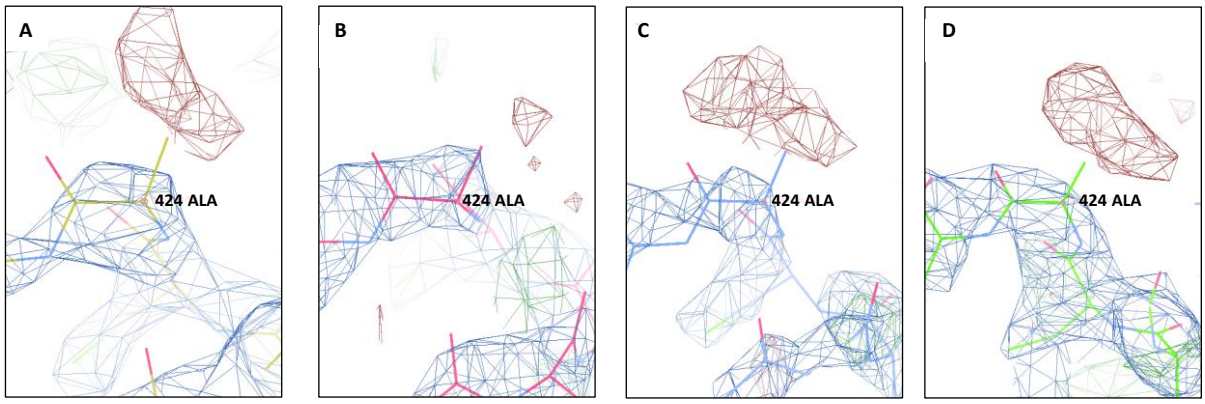

Figure 5.6 M2PYK C424 was successfully mutated to alanine

Electron density maps for M2PYK C424A structure showing that the cysteine was successfully mutated to alanine in all chains (A, B, C, and D). The electron density map was calculated from a model of M2PYK WT (PDB code 3SRD). The $|F_o-F_c|$ difference electron density map using the M2PYK WT model (with Cys424) shows strong negative peaks corresponding to the "missing" sulfhydryl group in the M2PYK C424A structure.

5.2.7 M2PYK C358S mutation is present in structure

The mutation of cysteine to serine in the M2PYK C358S is much more subtle than the mutation of cysteine to alanine in the M2PYK C424A mutant. At a resolution of only 3.1Å it is not possible to detect the density difference between a sulphur atom and an oxygen atom. However, comparison of the B factors in the structure refined with cysteine

in position 358 and those in the structure refined with serine in position 358 gives a good indication of which atom (sulphur or oxygen) is the best fit to the electron density measured. In the usual case, it would be expected that all the atoms of the same residue would have similar B factors. When the M2PYK C358S structure is refined with cysteine in position 358 then the B factor of the sulphur atom is much higher than those of the other atoms in the residue suggesting that this atom is not a good fit to the electron density measured (Table 5.6). Replacement of the cysteine with a serine followed by another refinement step shows that the oxygen atom of the serine has a B factor very similar to those of the other atoms in the residue showing that the oxygen atom is a good fit to the electron density measured (Table 5.6). In this way it can be shown that the M2PYK C358S mutation has been successful.

Table 5.6 Comparison of B factors of atoms in residue 358 in each chain of M2PYK C358S after refinement with cysteine or serine.

Atom in residue	**B factor**							
	Chain A		**Chain B**		**Chain C**		**Chain D**	
	Cys358	**Ser358**	**Cys358**	**Ser358**	**Cys358**	**Ser358**	**Cys358**	**Ser358**
N	79.8	75.7	90.3	84.1	77.0	77.2	48.2	45.3
CA	82.4	78.5	87.9	80.1	77.2	76.4	50.1	45.0
C	88.4	85.5	93.8	89.3	78.1	75.9	47.7	44.9
O	83.2	78.6	92.2	89.2	75.3	71.4	46.3	43.5
CB	85.1	78.1	86.7	77.0	84.4	80.9	54.0	46.5
S/O	103.5	81.0	111.7	83.3	95.3	78.4	82.8	54.6

5.2.8 Comparison of M2PYK C424A structure to M2PYK WT

The overall fold of the M2PYK mutant structure is similar to that of the wild type enzyme structure. The structural architecture of wild type M2PYK was briefly introduced in chapter 1 and was first described by Dombraukas *et al.* [139]. M2PYK is a tetrameric enzyme with each monomer consisting of four domains that are named A, B, C, and N (Figure 1.4). The tetramer is described as being a dimer-of-dimers with the intermolecular contacts for the first dimer occurring between the A domains of each monomer, and tetramerisation occurring via dimerisation along the C domain surfaces of each dimer [139] (Figure 1.5). The A-domain contains a α_8/β_8 barrel and the mobile B domain consists of a combination of β sheets and random coils [139]. The active site is situated in a cleft between the A and B domains [139] (Figure 1.5). The F-1,6-BP binding pocket is located entirely within the C-domain, which consists of both α and β structural elements [139] (Figure 1.5).

Superposition of the M2PYK C424A structure with that of the M2PYK WT holo structure (PDB code 3SRD) results in an overall RMS deviation of 0.57Å. The maximum displacement between M2PYK WT holo and M2PYK C424A is 3Å which occurs at around residue 126 on each of the four chains (Figure 5.7A). This difference is caused by the B domain of the M2PYK C424A structure adopting a slightly more closed orientation than in the M2PYK WT structure, although this difference is probably not significant given the highly flexible nature of the B domain (figure 5.7A). The structure around the mutated residue at the C-C interface also shows very little changes (Figure 5.7B). It is remarkable that a mutation which has such a significant effect on enzymatic activity has such a negligible effect on overall protein structure. One possible explanation for the activity loss could be that the mutation results in a more rigid structure. Such a

phenomenon can be observed when comparing thermophilic enzymes to mesophilic enzymes. Although the structure and architecture of thermophilic enzymes are generally highly homologous to their mesophilic counterparts, they have much lower activity at the lower temperatures at which most related enzymes are fully active due to their increased structural rigidity required to protect the protein against heat denaturation.

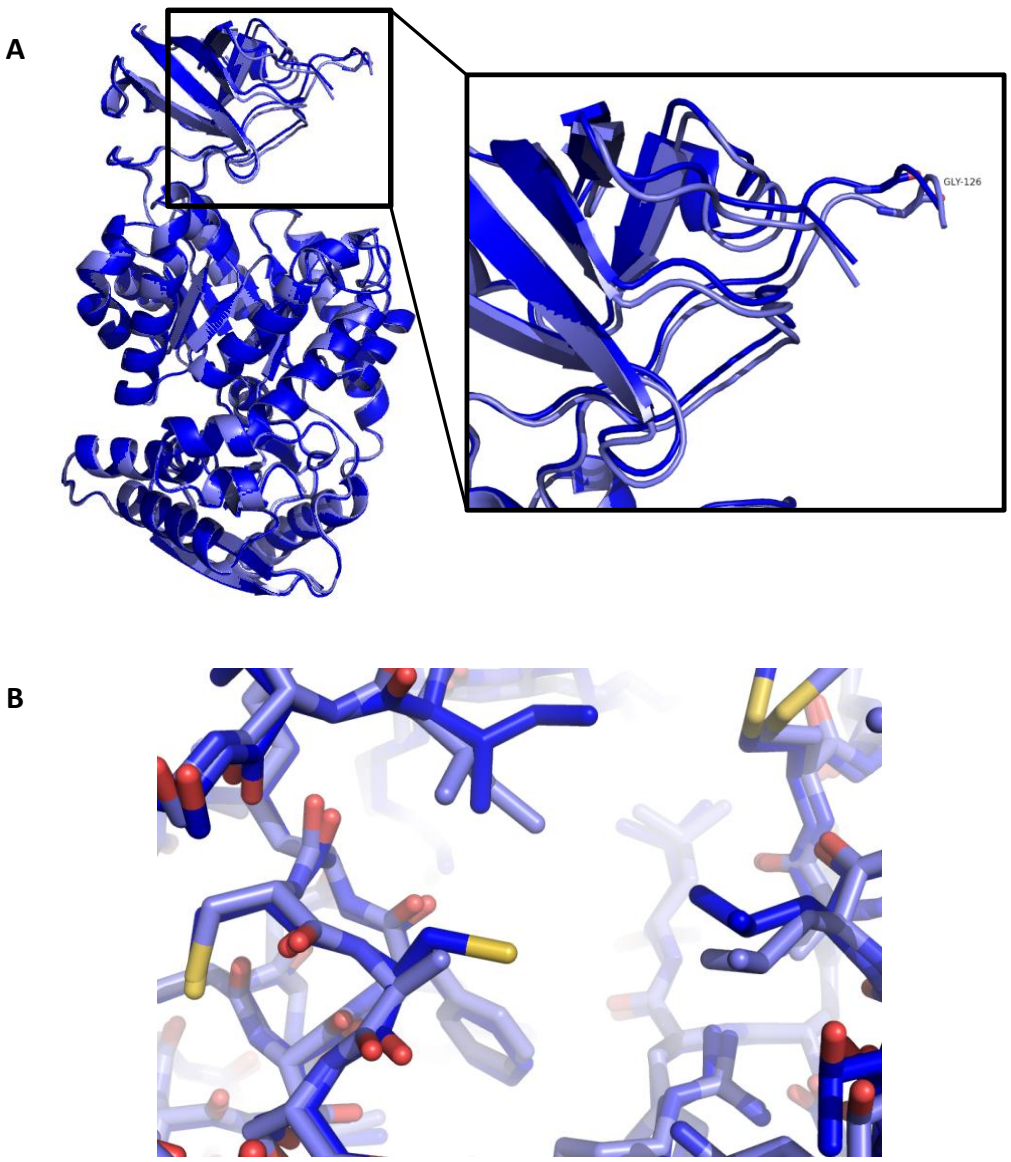

Figure 5.7 Alignment of M2PYK WT and M2PYK C424A structures.

A. Superimposed monomers of M2PYK WT (PDB code 3SRD) and M2PYK C424A showing that there is not significant change in B domain position as a result of the mutation. **B.** Enlarged view of area around mutated residue of chain A showing that there are only minor differences in side-chain positions as a result of the mutation.

5.2.9 Comparison of M2PYK C358S structure to M2PYK WT

The most noticeable difference between the M2PYK WT structure and the M2PYK C358S structure is that there is Mg^{2+}-ATP and Mg^{2+}-oxalate in the M2PYK C358S active site whereas there is only Mg^{2+}-oxalate bound in the M2PYK structure (PDB ID: 3SRD). In fact, the M2PYK C358S structure is the only human muscle PYK structure with ATP in the active site even though others have been crystallised with ATP present (e.g. M2PYK C424A, Dombrauckas). The only other mammalian PYKs with ATP in the active site is rabbit muscle PYK (PDB ID: 1A49) and human liver PYK with mutation C436M (PDB ID: 4IMA). It is interesting that the only other human PYK structure with ATP in the active site is also a cysteine point mutant.

Structural alignment of the M2PYK C358S structure with the M2PYK WT structure (PDB ID: 3SRH) results in an overall RMS deviation of about 0.6 Å, which shows that the structures are very similar. The biggest variation in structure is in the position of the B domain; M2PYK C358S B domain is in a more closed position than the M2PYK WT B domain due to the presence of ATP in the M2PYK C358S active site (Figure 5.8, top). A closer comparison around the mutated residue shows that there are no significant changes in backbone conformation, however as a consequence of the low resolution of the M2PYK C358S structure it is not possible to analyse the significance of any changes in side-chain position (Figure 5.8, bottom).

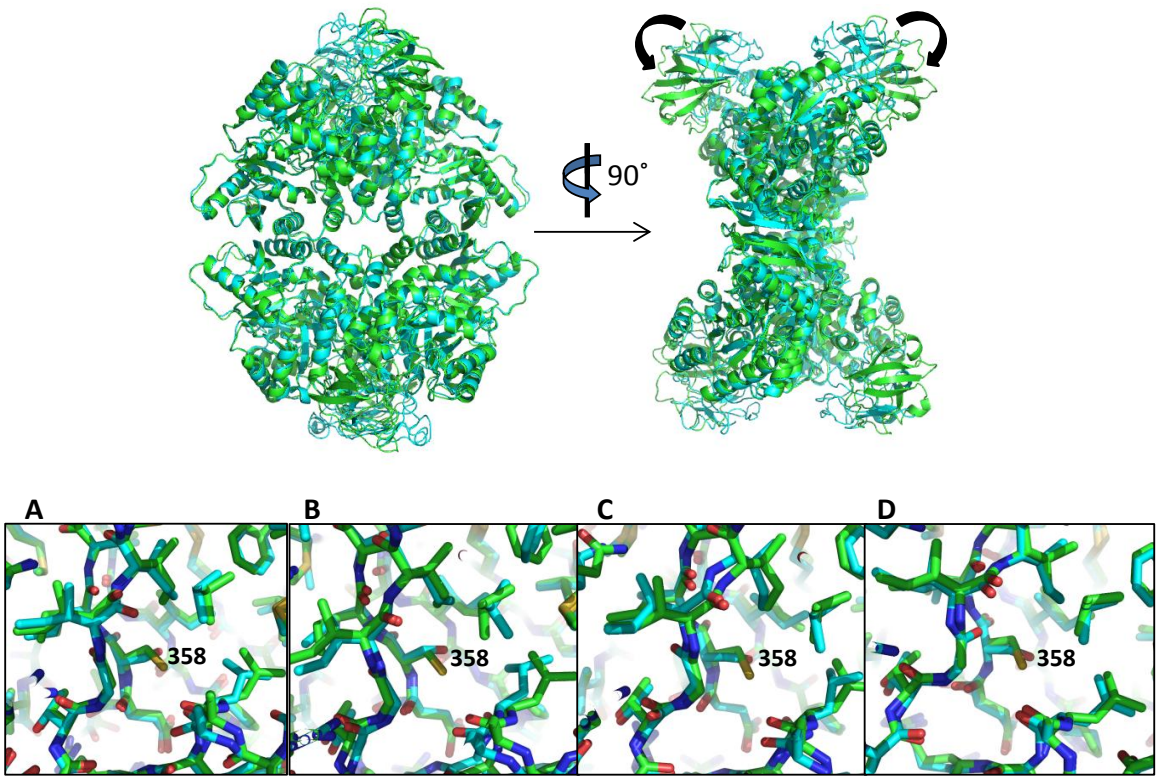

Figure 5.8 Alignment of M2PYK WT and M2PYK C358S structures.

Top. M2PYK WT (PDB code 3SRH) and M2PYK C358S superimposed tetramers; M2PYK WT = green, M2PYK C358S = cyan. Bottom. Enlarged view of area around mutated residue for each of the chains A, B, C and D. This shows that there are only minor differences in side-chain positions as a result of mutation, however the low resolution of the M2PYK C358S structure means it is not possible to analyse the significance of these changes.

5.2.10 Differences in ATP binding within the M2PYK C358S tetramer

Figure 5.9 shows the electron density maps of the three active sites of M2PYK C358S that show density for ATP. The density for ATP in the active sites of chains A and C is poor, especially around the adenine ring portions, suggesting that these active sites are either partially occupied by ATP or that the adenine ring portions are flexible. The electron density for ATP in the active site of chain D is much stronger. The stronger electron density for ATP in chain D correlates with a much more complete electron density map for the B domain of that chain indicating that ATP binding holds the B domain in a more rigid closed conformation. The weaker electron density for ATP in chains A and C correlates with a less complete electron density map for the B domains of these chains indicating that some of the tetramers in the crystal have ATP bound in these chains with the B domain in the closed conformation, whereas other tetramers do not have ATP bound in these chains so the B domains are in a more flexible, open conformation.

Comparison of the electron density maps indicates that chain A has the least ATP density, chain D has the most ATP density and chain C has ATP density between that of chain A and chain D (Figure 5.9). The naming of the chains in the tetramer is according to the scheme shown in Figure 5.10; chain D is top left, chain A is top right, chain B is bottom left and chain C is bottom right. An interesting observation is that the chains with strongest ATP electron density (chains D and C) are diagonally related, and so are the chains with weakest or no ATP density (chains A and B). This pattern indicates negative cooperativity of ATP binding; binding of ATP to one chain inhibits ATP binding to adjacent chains. Negative cooperativity of ATP binding has been observed in other enzymes, the most well studied of which is the GroEL chaperonin. GroEL is a large

protein composed of two rings each made up of seven identical subunits. The rings enclose a central cavity in which the denatured protein substrate is bound. During chaperone function large conformational changes occur in each of the two rings. Within the same ring there is positive cooperativity of ATP binding and hydrolysis but between the rings negative cooperativity has been observed [140]. Other examples of enzymes exhibiting negative cooperativity of ATP binding include the ATP-dependent protease HsIU-HsIV from *E.coli* [141], the Na,K-ATPase from pig kidney [142], and the F_1-ATPase of thermophilic bacteria [143].

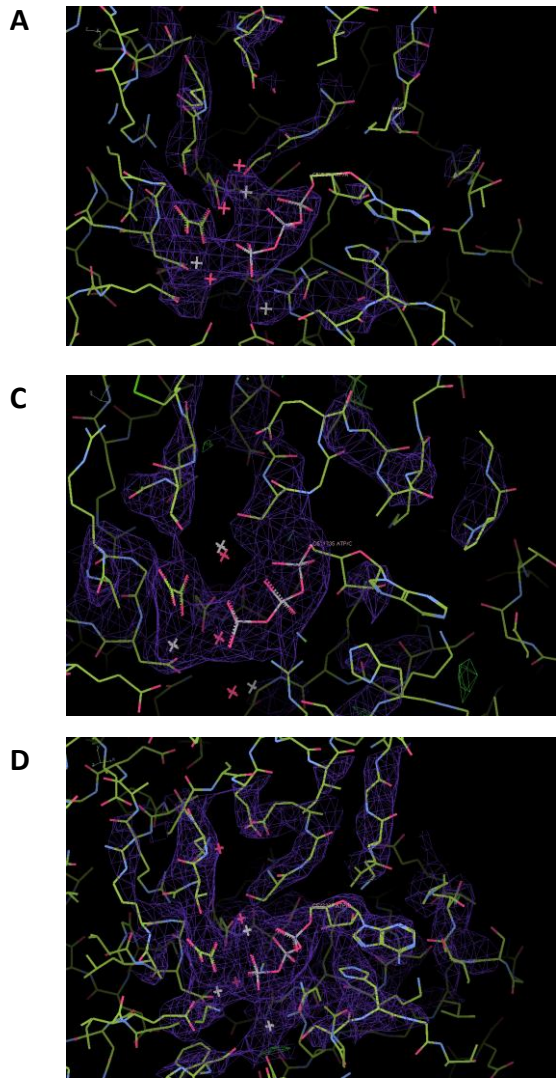

Figure 5.9 Electron density maps of active sites of chains A, C, and D of M2PYK C358S.

The electron density map was calculated from a model of M2PYK WT (PDB code 3SRH). The density maps are all shown using the same map contour level of 0.2583 electrons/Å^3 and illustrate either that chains A and C are only partially occupied by ATP or that the adenine rings portions of the ATP molecules are flexible in these chains. Chain D has good density for the whole ATP molecule and B domain suggesting that the chain D active site is fully occupied and the B domain is more rigid. Chain B is not shown because it has no ligands in active site. Pictures were generated using WinCoot 7.2.1.

5.2.11 Comparison of M2PYK C358S structure to rabbit M1PYK

The pattern of ATP binding and varying B domain flexibility seen in M2PYK C358S is similar to that seen in the rabbit M1PYK structure with ATP bound (PDB ID 1A49)[138]. One of the B domains in the M2PYK C358S structure is disordered and highly flexible with no ligands in the active site, and this B domain corresponds to the same B domain in the rabbit M1PYK tetramer which has been modelled in the open conformation and has no ATP bound in the active site (Figure 5.11). Although the B domain of chain B of M2PYK C358S has been modelled in the closed conformation, the electron density map is very poor so it is likely that this B domain is adopting many different conformations (Figure 5.11). The fact that a similar pattern of ATP binding is seen in both of these muscle PYK structures indicates that it may be a common feature shared between muscle PYKs.

The binding mode of ATP in the active site of M2PYK C358S almost identical to the binding of ATP in rabbit M1PYK [138]. In particular, two of the residues from the B domain move into position to interact with the Mg^{2+}-ATP; Lys206 interacts with the hydroxyls of the ribose moiety, and Arg119 hydrogen bonds to the β phosphate of the ATP molecule [138]. In this way the B domain is held in a closed position when ATP is bound in the active site.

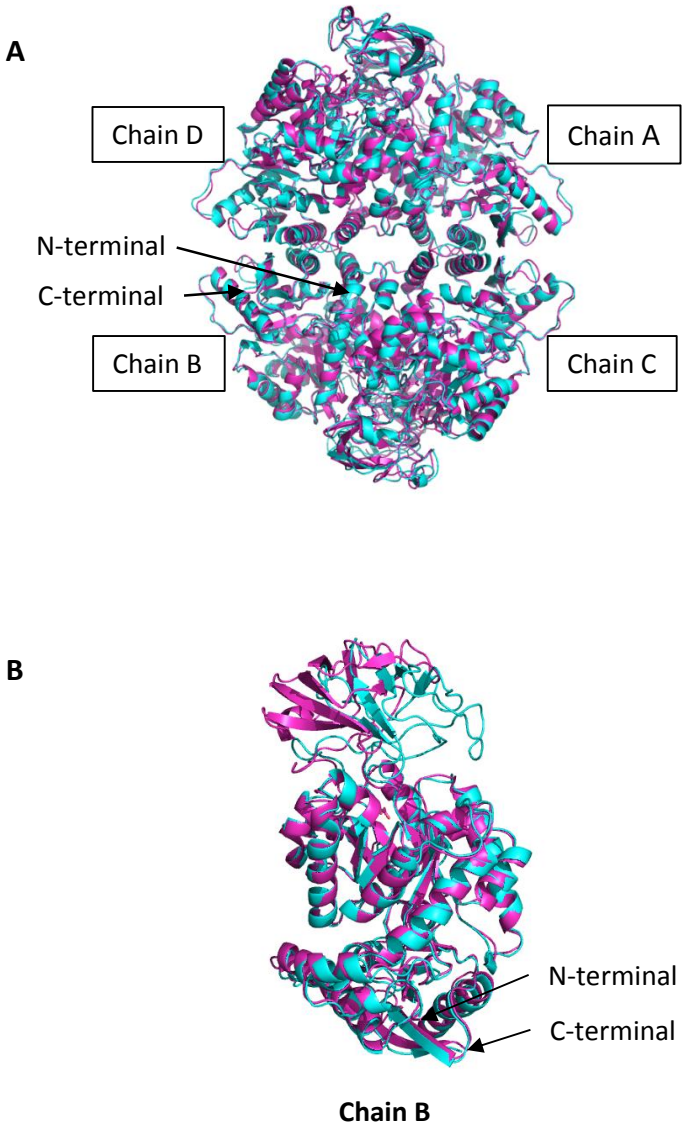

Figure 5.10 Comparison of M2PYK C358S and rabbit M1PYK structures.

A. Rabbit M1PYK (PDB code 1A49) and M2PYK C358S superimposed tetramers; rabbit M1PYK = magenta, M2PYK C358S = cyan. **B.** View of chain B to show orientations of B domains. In M2PYK C358S there a no ligands in the active site, in rabbit muscle PYK (1A49) there is only Mg^{2+}-oxalate. Although the M2PYK C358S B domain has been modelled in a closed conformation, the electron density for this domain is so poor that it is hard to tell what position it is in. The fact that the same pattern of three occupied active sites per tetramer is seen in both of these muscle PYK structures, despite the space group and crystal packing being different, is suggestive of negative cooperativity in nucleotide binding.

5.2.12 M2PYK C358S structure has an unusual B factor distribution

The B factor distribution in the M2PYK C358S tetramer is shown in figure 5.11A in comparison to M2PYK WT (figure 5.11B), M2PYK C424A (figure 5.11C) and rabbit M1PYK (5.11D). It can be seen in figure 5.11A that chain D of the M2PYK C358S tetramer has much lower B factors than the other three chains indicating that this chain is much more rigid than the other three. Chain D is also the chain with the strongest electron density for ATP in the active site and the most complete electron density for the B domain (Figure 5.9). The other two human M2PYK structures in figure 5.11 have a much more symmetrical distribution of B factors. The rabbit M1PYK structure has also been included in figure 5.11 to show the B factor distribution in another MPYK structure that has ATP bound in the active site. The rabbit M1PYK shows quite an even B factor distribution throughout the tetramer suggesting that the B factor distribution seen in the M2PYK C358S structure is a unique feature of this mutant.

An interesting possibility to consider is that the mutation of Cys358 to serine somehow inhibits communication between the chains in the tetramer thereby hindering cooperativity and this could be a possible explanation for the lower activity of this mutant. This characteristic of the M2PYK C358S structure could be further investigated using molecular dynamics which may yield some interesting information about the mechanism of cooperativity in the M2PYK structure.

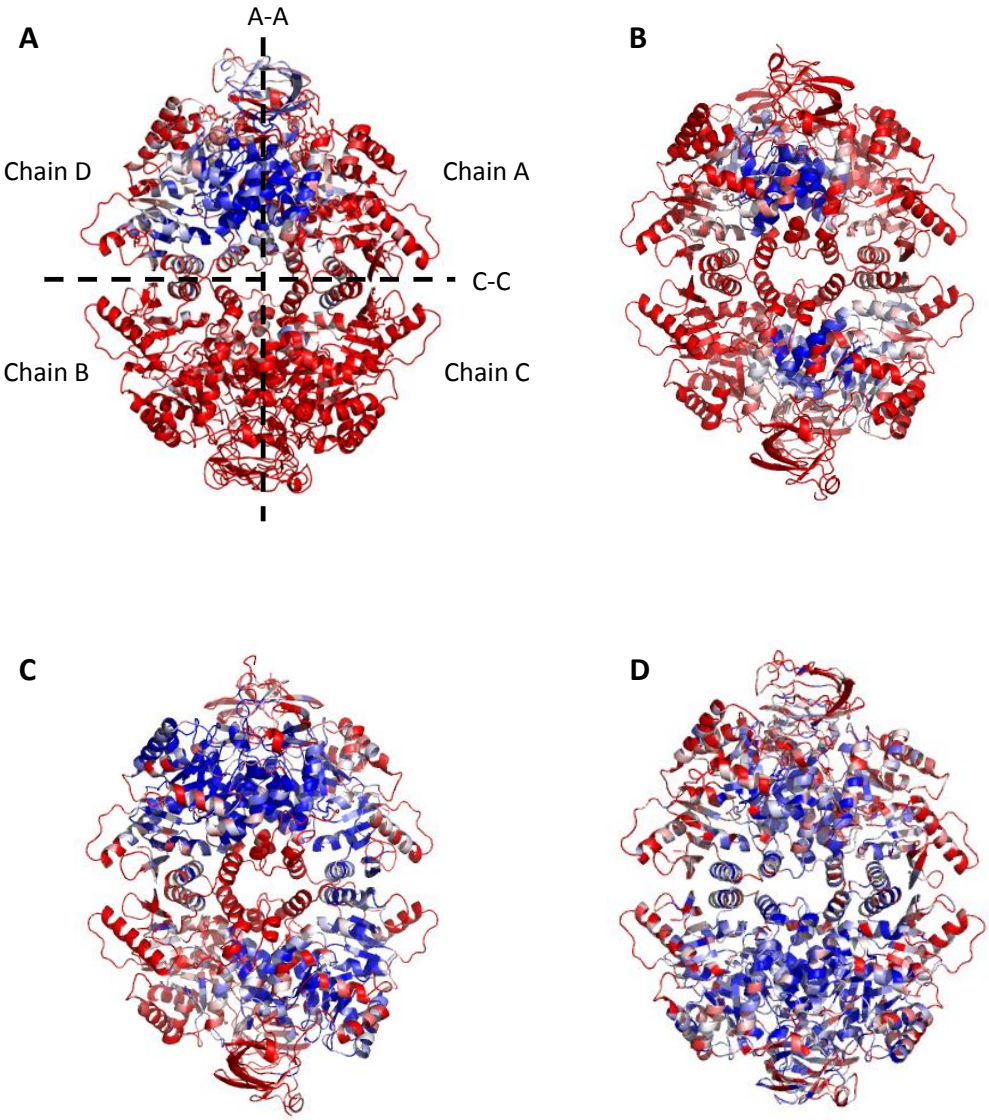

Figure 5.11 B factor distribution in M2PYK C358S tetramer.

Blue = low B factor, Red = high B factor **A.** M2PYK C358S tetramer showing that chain D has very low B factors while all other chains have much higher B factors (B factor range 50-70). **B.** M2PYK WT tetramer (PDB ID: 3SRD) showing a much more symmetrical B factor distribution. (B factor range 50-70). **C.** M2PYK C424A tetramer also shows a more symmetrical distribution of B factors (B factor range 50-70) **D.** Rabbit M1PYK tetramer with ATP in active site (PDB ID: 1A49) has much lower B factors throughout the tetramer (B factor range 15-45)

5.2.13 How do the cysteine point mutations affect stability and activity of M2PYK?

The only difference between the M2PYK point mutants and the wild type enzyme is a change in one amino acid, so it follows that the differences in interactions with amino acids neighouring the one that has been changed must determine the observed differences in activity, melting temperature and tetramer:dimer:monomer equilibrium.

Table 5.7 shows the residues that are in close proximity to residue 358 in both M2PYK WT and M2PYK C358S. The distances between the side-chain sulphur or oxygen atom and closest atom of the neighbouring residue is also shown along with the type of interaction that it likely to occur. Given the hydrophobic nature of cysteine, it could form van der Waals interactions with the hydrophobic side-chains of I48 and L465 which are 3.8Å and 4.7Å away from C358 respectively (Table 5.7). When the cysteine is replaced with serine in M2PYK C358S, these van der Waals interactions would not occur. In M2PYK WT, C358 could also be a hydrogen bond donor to the backbone carbonyl of H464. However, in the mutant, the oxygen of S358 is too far away (6.3Å) from the carbonyl oxygen of H464 for a hydrogen bond to be possible. Another notable difference is that S358 in the mutant structure could be in hydrogen bonding distance to the backbone carbonyl oxygen of V324 (3.5Å), whereas C358 in the WT structure is not (Table 5.7). The changes in interactions between these few residues could lead to slight conformational changes throughout the protein that lead to weaker interactions, and ultimately a less stable, less active protein.

Table 5.7 Closest contacts to M2PYK residue 358 in WT (PDB ID: 3SRD) and C358S structures. When residue 358 is interacting with the side chain of a neighbouring amino acid, the distance to the nearest atom of that side-chain is stated. Carbonyl signifies that the interaction is with the oxygen atom of the backbone carbonyl group of the named residue.

Residue	**Distance from residue 358 side-chain S/O atom (Å)**		**Hydrogen bond interaction**		**Van der Waals interaction**	
	M2PYK WT	**M2PYK C358S**	**WT**	**C358S**	**WT**	**C358S**
I48 Side-chain	3.8	4.0	-	-	Yes	No
V324 Carbonyl	5.0	3.5	No	Maybe	-	-
H464 Carbonyl	3.3	6.3	Yes	No	-	-
L465 Side-chain	4.7	4.2	-	-	Yes	No

There are only two residues that are in close proximity to residue 424 of M2PYK and these are shown in **Table 5.8.** The distances between the side-chain sulphur or carbon atom and closest atom of the neighbouring residue is also shown. These very small differences distances and interactions are consistent with the thermal denaturation results presented in chapter 3 which show that M2PYK C424A has melting behaviour very similar to M2PYK WT (Table 3.3). However, it was also found that M2PYK C424A has reduced activity compared to M2PYK WT (Table 3.2 and Figure 3.17) and this may be due to the much larger distance between A424 and L18 in the mutant, and C424 and L18 in M2PYK WT (Table 5.8). In M2PYK, it may be possible for C424 to interact with L18 by van der Waals forces, however the distance is too large (6.6Å) for A424 and L18 to interact in this way.

Table 5.8 Closest contacts to M2PYK residue 424 in WT (PDB ID: 3SRH) and C424A structures. Both of these interactions are between the side-chains of the residues and the distances are to the nearest atom of the side-chains of the named residues.

Residue	**Distance from residue 424 side-chain S/C atom (Å)**		**Van der Waals interaction**	
	M2PYK WT	**M2PYK C424A**	**M2PYK WT**	**M2PYK C424A**
I404 (adjacent chain)	4.6	4.0	Yes	Yes
L18 (same chain)	4.9	6.6	maybe	No

5.3 Conclusions

Crystals of M2PYK C424A, M2PYK C358A and M2PYK C358S were grown and from these the structures of M2PYK C424A and M2PYK C358S have been solved and refined to 2.87Å and 3.10Å respectively. This resolution was good enough to analyse what affect, if any, the cysteine point mutations had on the overall conformation of the tetramer.

Comparison of the M2PYK C424A structure containing oxalate, Mg^{2+}, and F-1,6-BP to the M2PYK WT holo structure with the same ligands (PDB ID: 3SRD) reveals that there are no significant changes in the overall conformation of the tetramer as a result of the point mutation. A closer look at the region around the mutation at the C-C interface also shows no significant differences that could explain the differences in activity and thermal stability described in Chapter 3. This is surprising given that the activity of M2PYK C424A in the presence of F-1,6-BP is significantly lower than that of M2PYK WT with F-1,6-BP (Figure 3.17). It could be that the changes are too subtle to observe in such a low resolution structure, but it is fascinating that there are apparently no structural changes as a result of a point mutation that has such significant effect on activity.

The M2PYK C358S structure contained oxalate, Mg^{2+}, ATP and F-1,6-BP. The presence of ATP in the active site is an interesting feature in itself due to the fact that there are no other structures of mammalian M2PYK with ATP in the active site, even when ATP was included in the crystallization drop. There is, however, one structure of rabbit M1PYK with ATP in the active site. When the M2PYK C358S structure is compared to M2PYK WT containing oxalate, Mg^{2+} and F-1,6-BP the main difference can be seen in the conformation of the B domain. In the M2PYK C358S structure the B domains are in a

more closed position than in the M2PYK WT structure and this is probably due to the presence of ATP in the M2PYK C358S structure. Another major difference that can be seen between the two structures is in the distribution of B factors within the tetramers. Although the B factors cannot be directly compared between the structures, the difference in the distribution of the low and high B factor regions within each of the tetramers is intriguing and could give some insight into the mechanism of enzyme cooperativity within the M2PYK tetramer (Figure 5.11). It could be that mutating Cys358 to serine somehow inhibits some structural or energetic transmission through the M2PYK tetramer thereby hindering cooperativity. If this is true, then it could be an important contributing factor to the decreased activity and thermal stability of the M2PYK C358S mutant.

A comparison of the M2PYK C358S structure with the only other muscle PYK in the PDB with ATP in the active site, rabbit M1PYK, shows that they share the same pattern of ATP binding. In both structures, only three of the chains have ATP in the active site. Furthermore, in both structures the different B domains of the same structure adopt different conformations. Although this feature cannot be seen in the model of M2PYK C358S, analysis of the electron density of the B domains show that they have very different levels of completeness indicating varying degrees of flexibility. Comparison of the B factor distributions of these two structures, the only two muscle PYK structures with ATP in the active site, shows that the unusual B factor distribution observed in the M2PYK C358S structure could indeed be a unique feature resulting from the point mutation.

Chapter 6: Summary and future work

6.1 Open Questions

- How is M2PYK regulated by oxidation?

- How is M1PYK protected from oxidation?

- What is the effect of M2PYK oxidation *in vivo*?

6.2 Major findings and future work

6.2.1 How is M2PYK regulated by oxidation?

Evidence has been presented in this thesis that shows that oxidation by H_2O_2 decreases M2PYK thermal stability and activity, although none of the cysteine point mutants tested resulted in protection from oxidising effects. This indicates that either there is a different cysteine involved or it is oxidation of a combination of cysteines that regulates M2PYK activity. In order to clarify which cysteines are oxidised in M2PYK it may be possible to identify oxidised cysteines by mass spectrometry, however this is extremely challenging due to the transient nature of cysteine oxidation. Furthermore, special precautions need to be taken throughout sample preparation to ensure that the samples are not exposed to oxidising conditions during processing.

It has also been demonstrated here that M2PYK is modified by S-nitrosylation. However, it is still unclear which cysteine(s) is modified. Although mutation of Cys358 resulted in an almost complete loss of S-nitrosylation, it is likely that this effect is due to the

conformational changes caused by the mutation that result in M2PYK being stabilized in the tetrameric form. Analysis of the protein samples that had undergone S-nitrosylation followed by biotin-switch identified Csy326 as being modified, a cysteine that has been identified in another study as being S-nitrosylated [137]. Interestingly, mutation of Cys326 to serine results in M2PYK that is unable to form tetramers indicating that modification of this cysteine could play an important role in regulation of M2PYK activity.

Following on from this, it would be interesting to find out the effect of oxidation by H_2O_2 and S-nitrosylation on M2PYK oligomeric state using analytical gel filtration. The expected result would be that oxidation causes M2PYK to become more monomeric, thus inactivating the enzyme. This is based on results the results from Cantley's group which show that after cells are treated with oxidizing agent, Flag tagged M2PYK no longer co-precipitated with endogenous M2PYK indicating that M2PYK could not form oligomers in oxidizing conditions [34].

Another form of oxidation that has not been considered in this thesis, but could be involved in the regulation of M2PYK, is S-glutathionylation. S-glutathionylation involves the addition of GSH (γ-glutamylcysteinylglycine) to cysteine residues and acts both to protect and modify protein structure and function. In a proteomic study carried out to identify the glutathionylome of *Plasomodium falciparum*, pyruvate kinase was among the 493 targets of S-glutathionylation identified [144]. It would be interesting to carry out M2PYK activity assays in the presence of GSH and also analyse the effect of GSH on M2PYK oligomeric state. It would also be possible to detect which cysteines are modified using mass spectrometry. M2PYK could also be crystallised in the presence of GSH in order to verify that any affects are due to cysteine modification.

6.2.2 How is M1PYK protected from oxidation?

In this thesis it has been shown that M1PYK thermal stability and activity are mostly unaffected by oxidising conditions, whereas M2PYK stability and activity are significantly decreased (Figure 3.16). Understanding how M1PYK is protected from oxidation could give valuable information about how M2PYK is modified. One major difference between the two isoforms is that M1PYK is constitutively in the active tetrameric T-state, whereas M2PYK shifts between inactive monomer/dimer and tetrameric states in a dynamic equilibrium. Therefore, one possibility is that the tetrameric nature of M1PYK protects those cysteines that are susceptible to oxidation due to their location on the tetramerisation interfaces. In M2PYK these same cysteines would be exposed to the solvent as M2PYK constantly changes its oligomeric state. One way to test this hypothesis would be to add the allosteric activator F-1,6-BP to M2PYK before testing the effect of oxidation on stability and enzyme activity. F-1,6-BP would lock M2PYK in the active tetrameric state and should therefore prevent oxidation of cysteines located on the interfaces.

Another key difference between M1- and M2PYK is that M1PYK lacks one of the cysteines present in M2PYK, C424, and has a leucine in its place. It is conceivable then that this cysteine is the key cysteine that is involved in the regulation of M2PYK by oxidation. However, it has been shown in this study that mutation of this cysteine in M2PYK to the M1PYK equivalent residue, leucine, is not sufficient to protect M2PYK from the oxidative effects of H_2O_2 (Figure 3.16).

6.2.3 What is the effect of M2PYK oxidation/S-nitrosylation *in vivo*?

It is clear from the work presented here together with the work of others that M2PYK is subject to oxidation/S-nitrosylation of at least some of its cysteine residues (Figure 4.5)[34][128][129][130]. An important next step would be to investigate the significance of these modifications *in vivo*. In order to specifically assess the changes caused by M2PYK modifications it is necessary to eliminate any influence that could be attributed to M1PYK. Work is already underway in our laboratory to use CRISPR (Clustered, Regularly Interspaced, Short Palindromic Repeat) technology to knock out the *PKM* gene in a human cancer cell line to allow for selective expression of either M1- or M2PYK [145]. These cell lines can then be treated with oxidising or nitrosylating agents and the effect on cell growth and proliferation measured. The M2PYK cysteine point mutants already developed can also be used to see how these mutants may change the cellular response to oxidising conditions.

References

[1] M. E. Munoz and E. Ponce, "Pyruvate kinase : current status of regulatory and functional properties," *Comp. Biochem. Physiol.*, vol. 135, no. B, pp. 197–218, 2003.

[2] S. Mazurek, "Pyruvate kinase type M2: A key regulator of the metabolic budget system in tumor cells.," *Int. J. Biochem. Cell Biol.*, vol. 43, no. 7, pp. 969–80, Jul. 2011.

[3] S. Allert, I. Ernest, a Poliszczak, F. R. Opperdoes, and P. A. Michels, "Molecular cloning and analysis of two tandemly linked genes for pyruvate kinase of Trypanosoma brucei.," *Eur. J. Biochem.*, vol. 200, no. 1, pp. 19–27, Aug. 1991.

[4] R. Moreno-Sánchez, E. Saavedra, S. Rodríguez-Enríquez, and V. Olín-Sandoval, "Metabolic control analysis: a tool for designing strategies to manipulate metabolic pathways.," *J. Biomed. Biotechnol.*, vol. 2008, p. 597913, Jan. 2008.

[5] J. Heinisch, "Isolation and characterisation of the two structural genes coding for phosphofructokinase in yeast," *Mol. Gen. Genet.*, vol. 202, no. 1, pp. 75–82, 1986.

[6] S. E. C. Davies and K. M. Brindle, "Effects of overexpression of phosphofructokinase on glycolysis in the yeast Saccharomyces cerevisiae," *Biochemistry*, vol. 31, no. 19, pp. 4729–4735, 1992.

[7] J. Hauf, F. K. Zimmermann, and S. Muller, "Simultaneous genomic overexpression of seven glycolytic enzymes in the yeast Saccharomyces cerevisiae," *Enzyme Microb. Technol.*, vol. 26, pp. 688–698, 2000.

[8] I. Schaaf, J. Heinisch, and F. K. Zimmermann, "Overproduction of glycolytic enzymes in yeast," *Yeast*, vol. 5, no. 4, pp. 285–290, 1989.

[9] H. P. Smits, È. Hauf, S. Mu, T. J. Hobley, F. K. Zimmermann, J. Nielsen, and L. Olsson, "Simultaneous overexpression of enzymes of the lower part of glycolysis can enhance the fermentative capacity of Saccharomyces cerevisiae," *Yeast*, vol. 16, no. 14, pp. 1325–1334, 2000.

[10] M. Emmerling, J. E. Bailey, and U. Sauer, "Glucose Catabolism of Escherichia coli Strains with Increased Activity and Altered Regulation of Key Glycolytic Enzymes," *Metab. Eng.*, vol. 1, pp. 117–127, 1999.

[11] M. Emmerling, J. E. Bailey, and U. Sauer, "Altered Regulation of Pyruvate Kinase or Co-Overexpression of Phosphofructokinase Increases Glycolytic Fluxes in Resting Escherichia coli," *Biotechnol. Bioeng.*, vol. 67, no. 5, pp. 623–627, 2000.

[12] C. Solem, B. J. Koebmann, and P. R. Jensen, “Glyceraldehyde-3-Phosphate Dehydrogenase Has No Control over Glycolytic Flux in Lactococcus lactis MG1363,” *J. Bacteriol.*, vol. 185, no. 5, pp. 1564–1571, Mar. 2003.

[13] G. J. . Ruijter, H. Panneman, and J. Visser, “Overexpression of phosphofructokinase and pyruvate kinase in citric acid-producing Aspergillus niger,” *Biochim. Biophys. Acta - Gen. Subj.*, vol. 1334, no. 2–3, pp. 317–326, Mar. 1997.

[14] A. M. Urbano, H. Gillham, Y. Groner, and K. M. Brindle, “Effects of overexpression of the liver subunit of 6-phosphofructo-1-kinase on the metabolism of a cultured mammalian cell line,” *Biochem. J.*, vol. 352, pp. 921–927, 2000.

[15] B. M. Bakker, P. A. M. Michels, F. R. Opperdoes, and H. V. Westerhoff, “What Controls Glycolysis in Bloodstream Form Trypanosoma brucei?,” *J. Biol. Chem.*, vol. 274, no. 21, pp. 14551–14559, May 1999.

[16] M. Domingo, C. Einig, E. Eigenbrodt, and M. Reinacher, “Immunohistological demonstration of pyruvate kinase isoenzyme type L in rat with monoclonal antibodies.,” *J. Histochem. Cytochem.*, vol. 40, no. 5, pp. 665–673, May 1992.

[17] T. Noguchi, K. Yamada, H. Inoue, T. Matsuda, and T. Tanaka, “The L- and R-type isozymes of rat pyruvate kinase are produced from a single gene by use of different promoters.,” *J. Biol. Chem.*, vol. 262, no. 29, pp. 14366–71, Oct. 1987.

[18] T. Noguchi, H. Inoue, and T. Tanaka, “The M1- and M2-type isozymes of rat pyruvate kinase are produced from the same gene by alternative RNA splicing.,” *J. Biol. Chem.*, vol. 261, no. 29, pp. 13807–12, Oct. 1986.

[19] K. Yamada and T. Noguchi, “Nutrient and hormonal regulation of pyruvate kinase gene expression.,” *Biochem. J.*, vol. 337 (Pt 1, pp. 1–11, Jan. 1999.

[20] C. V Clower, D. Chatterjee, Z. Wang, L. C. Cantley, M. G. Vander Heiden, and A. R. Krainer, “The alternative splicing repressors hnRNP A1/A2 and PTB influence pyruvate kinase isoform expression and cell metabolism.,” *Proc. Natl. Acad. Sci. U. S. A.*, vol. 107, no. 5, pp. 1894–9, Feb. 2010.

[21] C. J. David, M. Chen, M. Assanah, P. Canoll, and J. L. Manley, “HnRNP proteins controlled by c-Myc deregulate pyruvate kinase mRNA splicing in cancer.,” *Nature*, vol. 463, no. 7279, pp. 364–8, Jan. 2010.

[22] H. P. Morgan, F. J. O’Reilly, M. A. Wear, J. R. O’Neill, L. A. Fothergill-Gilmore, T. Hupp, and M. D. Walkinshaw, “M2 pyruvate kinase provides a mechanism for nutrient sensing and regulation of cell proliferation.,” *Proc. Natl. Acad. Sci. U. S. A.*, vol. 110, no. 15, pp. 5881–6, Apr. 2013.

[23] S. Ainsworth and N. MacFarlane, “A kinetic study of rabbit muscle pyruvate kinase.,” *Biochem. J.*, vol. 131, no. 2, pp. 223–36, Feb. 1973.

[24] Y. Ikeda, T. Tanaka, and T. Noguchi, “Conversion of non-allosteric pyruvate kinase isozyme into an allosteric enzyme by a single amino acid substitution.,” *J. Biol. Chem.*, vol. 272, no. 33, pp. 20495–501, Aug. 1997.

[25] S. Mazurek, H. C. A. Drexler, J. Troppmair, E. Eigenbrodt, and U. R. Rapp, “Regulation of Pyruvate Kinase Type M2 by A-Raf : A Possible Glycolytic Stop or Go Mechanism,” *Anticancer Res.*, vol. 27, pp. 3963–3971, 2007.

[26] K. Imamura and T. Tanaka, “Pyruvate Kinase Isoenzymes from Rat,” *Methods Enzymol.*, vol. 90, pp. 150–165, 1982.

[27] L. R. Feksa, A. Cornelio, C. S. Dutra-Filho, A. T.D.S. Wyse, M. Wajner, and C. M. D. Wannmacher, “The effects of the interactions between amino acids on pyruvate kinase activity from the brain cortex of young rats.,” *Int. J. Dev. Neurosci.*, vol. 23, no. 6, pp. 509–14, Oct. 2005.

[28] M. Malcovati and H. Kornberg, “Two types of pyruvate kinase in Escherichia coli K12,” *Biochim. Biophys. Acta*, vol. 178, no. 2, pp. 420–423, 1969.

[29] R. Bakszt, A. Wernimont, A. Allali-Hassani, M. W. Mok, T. Hills, R. Hui, and J. C. Pizarro, “The crystal structure of Toxoplasma gondii pyruvate kinase 1.,” *PLoS One*, vol. 5, no. 9, p. e12736, Jan. 2010.

[30] S. Ohta, A. Nishikawa, and K. Imamura, “Molecular cloning and expression of pyruvate kinase from globefish (Fugu rubripes) skeletal muscle,” *Comp. Biochem. Physiol. Part B, Biochem. Mol. Biol.*, vol. 135, no. 2, pp. 397–405, 2003.

[31] L. Lv, D. Li, D. Zhao, R. Lin, Y. Chu, H. Zhang, Z. Zha, Y. Liu, Z. Li, Y. Xu, G. Wang, Y. Huang, Y. Xiong, K.-L. Guan, and Q.-Y. Lei, “Acetylation Targets the M2 Isoform of Pyruvate Kinase for Degradation through Chaperone-Mediated Autophagy and Promotes Tumor Growth,” *Mol. Cell*, vol. 42, no. 6, pp. 719–730, Jun. 2011.

[32] T. Hitosugi, S. Kang, M. G. Vander Heiden, T.-W. Chung, S. Elf, K. Lythgoe, S. Dong, S. Lonial, X. Wang, G. Z. Chen, J. Xie, T.-L. Gu, R. D. Polakiewicz, J. L. Roesel, T. J. Boggon, F. R. Khuri, D. G. Gilliland, L. C. Cantley, J. Kaufman, and J. Chen, “Tyrosine Phosphorylation Inhibits PKM2 to Promote the Warburg Effect and Tumor Growth,” *Sci. Signal.*, vol. 2, no. 97, pp. 1–8, Nov. 2009.

[33] W. Luo, H. Hu, R. Chang, J. Zhong, M. Knabel, R. O’Meally, R. N. Cole, A. Pandey, and G. L. Semenza, “Pyruvate Kinase M2 Is a PHD3-Stimulated Coactivator for Hypoxia-Inducible Factor 1.,” *Cell*, vol. 145, no. 5, pp. 732–44, May 2011.

[34] D. Anastasiou, G. Poulogiannis, J. M. Asara, M. B. Boxer, J. Jiang, M. Shen, G. Bellinger, A. T. Sasaki, J. W. Locasale, D. S. Auld, C. J. Thomas, M. G. Vander Heiden, and L. C. Cantley, "Inhibition of Pyruvate Kinase M2 by Reactive Oxygen Species Contributes to Antioxidant Responses," *Science (80-.).*, vol. 334, no. 6060, pp. 1278–83, 2011.

[35] C. Choudhary, C. Kumar, F. Gnad, M. L. Nielsen, M. Rehman, T. C. Walther, J. V Olsen, and M. Mann, "Lysine acetylation targets protein complexes and co-regulates major cellular functions.," *Science*, vol. 325, no. 5942, pp. 834–40, Aug. 2009.

[36] S. Zhao, W. Xu, W. Jiang, W. Yu, Y. Lin, T. Zhang, J. Yao, L. Zhou, Y. Zeng, H. Li, Y. Li, J. Shi, W. An, S. M. Hancock, F. He, L. Qin, J. Chin, P. Yang, X. Chen, Q. Lei, Y. Xiong, and K.-L. Guan, "Regulation of cellular metabolism by protein lysine acetylation.," *Science*, vol. 327, no. 5968, pp. 1000–4, Feb. 2010.

[37] L. Lv, D. Li, D. Zhao, R. Lin, Y. Chu, H. Zhang, Z. Zha, Y. Liu, Z. Li, Y. Xu, G. Wang, Y. Huang, Y. Xiong, K.-L. Guan, and Q.-Y. Lei, "Acetylation Targets the M2 Isoform of Pyruvate Kinase for Degradation through Chaperone-Mediated Autophagy and Promotes Tumor Growth," *Mol. Cell*, vol. 42, no. 6, pp. 719–730, Jun. 2011.

[38] D. Hanahan and R. Weinberg, "The Hallmarks of Cancer," *Cell*, vol. 100, no. 1, pp. 57–70, 2000.

[39] T. Hitosugi, S. Kang, M. G. Vander Heiden, T.-W. Chung, S. Elf, K. Lythgoe, S. Dong, S. Lonial, X. Wang, G. Z. Chen, J. Xie, T.-L. Gu, R. D. Polakiewicz, J. L. Roesel, T. J. Boggon, F. R. Khuri, D. G. Gilliland, L. C. Cantley, J. Kaufman, and J. Chen, "Tyrosine Phosphorylation Inhibits PKM2 to Promote the Warburg Effect and Tumor Growth," *Sci. Signal.*, vol. 2, no. 97, pp. 1–8, Nov. 2009.

[40] K. L. Gorres and R. T. Raines, "Prolyl 4-hydroxylase.," *Crit. Rev. Biochem. Mol. Biol.*, vol. 45, no. 2, pp. 106–24, Apr. 2010.

[41] R. Berg and D. Prockop, "The thermal transition of a non-hydroxylated form of collagen. Evidence for a role for hydroxyproline in stabilizing the triple-helix of collagen," *Biochem. Biophys. Res. Commun.*, vol. 52, no. 1, pp. 115–120, 1973.

[42] W. Zwerschke, S. Mazurek, P. Massimi, L. Banks, E. Eigenbrodt, and P. Jansen-Dürr, "Modulation of type M2 pyruvate kinase activity by the human papillomavirus type 16 E7 oncoprotein.," *Proc. Natl. Acad. Sci. U. S. A.*, vol. 96, no. 4, pp. 1291–6, Feb. 1999.

[43] A. Steták, R. Veress, J. Ovádi, P. Csermely, G. Kéri, and A. Ullrich, "Nuclear translocation of the tumor marker pyruvate kinase M2 induces programmed cell death.," *Cancer Res.*, vol. 67, no. 4, pp. 1602–8, Feb. 2007.

[44] S. Mazurek, W. Zwerschke, P. Jansen-Dürr, and E. Eigenbrodt, “Effects of the human papilloma virus HPV-16 E7 oncoprotein on glycolysis and glutaminolysis: role of pyruvate kinase type M2 and the glycolytic-enzyme complex.,” *Biochem. J.*, vol. 356, no. Pt 1, p. 247, 2001.

[45] W. W. Wheaton and N. S. Chandel, “Hypoxia . 2 . Hypoxia regulates cellular metabolism,” vol. 2909, 2011.

[46] G. L. Wang, B. H. Jiang, E. A. Rue, and G. L. Semenza, “Hypoxia-inducible factor 1 is a basic-helix-loop-helix-PAS heterodimer regulated by cellular O2 tension.,” *Proc. Natl. Acad. Sci. U. S. A.*, vol. 92, no. 12, pp. 5510–4, Jun. 1995.

[47] V. Gupta, P. Kalaiarasan, M. Faheem, N. Singh, M. A. Iqbal, and R. N. K. Bamezai, “Dominant negative mutations affect oligomerization of human pyruvate kinase M2 isozyme and promote cellular growth and polyploidy.,” *J. Biol. Chem.*, vol. 285, no. 22, pp. 16864–73, May 2010.

[48] K. Akhtar, V. Gupta, A. Koul, N. Alam, R. Bhat, and R. N. K. Bamezai, “Differential behavior of missense mutations in the intersubunit contact domain of the human pyruvate kinase M2 isozyme.,” *J. Biol. Chem.*, vol. 284, no. 18, pp. 11971–81, May 2009.

[49] H. R. Christofk, M. G. Vander Heiden, N. Wu, J. M. Asara, and L. C. Cantley, “Pyruvate kinase M2 is a phosphotyrosine-binding protein.,” *Nature*, vol. 452, no. 7184, pp. 181–6, Mar. 2008.

[50] O. Warburg, “On the Origin of Cancer Cells,” *Science (80-.).*, vol. 123, no. 3191, pp. 309–314, 1956.

[51] H. R. Christofk, M. G. Vander Heiden, M. H. Harris, A. Ramanathan, R. E. Gerszten, R. Wei, M. D. Fleming, S. L. Schreiber, and L. C. Cantley, “The M2 splice isoform of pyruvate kinase is important for cancer metabolism and tumour growth.,” *Nature*, vol. 452, no. 7184, pp. 230–3, Mar. 2008.

[52] B. Altenberg and K. O. Greulich, “Genes of glycolysis are ubiquitously overexpressed in 24 cancer classes.,” *Genomics*, vol. 84, no. 6, pp. 1014–20, Dec. 2004.

[53] S. E. Elf and J. Chen, “Targeting glucose metabolism in patients with cancer.,” *Cancer*, vol. 120, no. 6, pp. 774–80, Mar. 2014.

[54] T. Hitosugi, L. Zhou, S. Elf, J. Fan, H. Kang, J. H. Seo, C. Shan, Q. Dai, L. Zhang, J. Xie, T. Gu, P. Jin, M. Aleckovic, G. LeRoy, Y. Kang, J. A. Sudderth, R. J. DeBerardinis, C. Luan, G. Z. Chen, S. Muller, D. M. Shin, T. K. Owonikoko, S. Lonial, M. L. Arellano, H. J. Khoury, F. R. Khuri, B. H. Lee, K. Ye, T. J. Boggon, S. Kang, C. He, and J. Chen, “Phosphoglycerate mutase 1 coordinates glycolysis

and biosynthesis to promote tumor growth," *Cancer Cell*, vol. 22, no. 5, pp. 585–600, 2013.

[55] M. G. Vander Heiden, L. C. Cantley, and C. B. Thompson, "Understanding the Warburg effect: the metabolic requirements of cell proliferation.," *Science*, vol. 324, no. 5930, pp. 1029–33, May 2009.

[56] N. K. Tonks, "Redox Redux : Revisiting PTPs and the Control of Cell Signaling," *Cell*, vol. 121, pp. 667–670, 2005.

[57] O. Vafa, M. Wade, S. Kern, M. Beeche, T. K. Pandita, G. M. Hampton, G. M. Wahl, and S. Diego, "c-Myc Can Induce DNA Damage , Increase Reactive Oxygen Species , and Mitigate p53 Function : A Mechanism for Oncogene-Induced Genetic Instability," vol. 9, pp. 1031–1044, 2002.

[58] V. Nogueira, Y. Park, C.-C. Chen, P.-Z. Xu, M.-L. Chen, I. Tonic, T. Unterman, and N. Hay, "Akt determines replicative senescence and oxidative or oncogenic premature senescence and sensitizes cells to oxidative apoptosis.," *Cancer Cell*, vol. 14, no. 6, pp. 458–70, Dec. 2008.

[59] A. A. Sablina, A.V. Budanov, G. V Ilyinskaya, L. S. Agapova, J. E. Kravchenko, and P. M. Chumakov, "The antioxidant function of the p53 tumor suppressor.," *Nat. Med.*, vol. 11, no. 12, pp. 1306–13, Dec. 2005.

[60] K. Bensaad, E. C. Cheung, and K. H. Vousden, "Modulation of intracellular ROS levels by TIGAR controls autophagy.," *EMBO J.*, vol. 28, no. 19, pp. 3015–26, Oct. 2009.

[61] W. Hu, C. Zhang, R. Wu, Y. Sun, A. Levine, and Z. Feng, "Glutaminase 2, a novel p53 target gene regulating energy metabolism and antioxidant function.," *Proc. Natl. Acad. Sci. U. S. A.*, vol. 107, no. 16, pp. 7455–60, Apr. 2010.

[62] S. Reuter, S. C. Gupta, M. M. Chaturvedi, and B. B. Aggarwal, "Oxidative stress, inflammation, and cancer: how are they linked?," *Free Radic. Biol. Med.*, vol. 49, no. 11, pp. 1603–16, Dec. 2010.

[63] B. Halliwell, "Oxidative stress and cancer: have we moved forward?," *Biochem. J.*, vol. 401, no. 1, pp. 1–11, Jan. 2007.

[64] Z. T. Schafer, A. R. Grassian, L. Song, Z. Jiang, Z. Gerhart-Hines, H. Y. Irie, S. Gao, P. Puigserver, and J. S. Brugge, "Antioxidant and oncogene rescue of metabolic defects caused by loss of matrix attachment.," *Nature*, vol. 461, no. 7260, pp. 109–13, Sep. 2009.

[65] K. Ishikawa, K. Takenaga, M. Akimoto, N. Koshikawa, A. Yamaguchi, H. Imanishi, K. Nakada, Y. Honma, and J.-I. Hayashi, "ROS-generating

mitochondrial DNA mutations can regulate tumor cell metastasis.," *Science*, vol. 320, no. 5876, pp. 661–4, May 2008.

[66] F. Weinberg, R. Hamanaka, W. W. Wheaton, S. Weinberg, J. Joseph, M. Lopez, B. Kalyanaraman, G. M. Mutlu, G. R. S. Budinger, and N. S. Chandel, "Mitochondrial metabolism and ROS generation are essential for Kras-mediated tumorigenicity.," *Proc. Natl. Acad. Sci. U. S. A.*, vol. 107, no. 19, pp. 8788–93, May 2010.

[67] P. T. Schumacker, "Reactive oxygen species in cancer cells: Live by the sword, die by the sword," *Cancer Cell*, vol. 10, no. 3, pp. 175–176, Sep. 2006.

[68] K. Hirota, M. Murata, H. Nakamura, J. Takeuchi, K. Mori, and J. Yodoi, "Distinct Roles of Thioredoxin in the Cytoplasm and in the Nucleus : a two step mechanism of redox regulation of transcription factor NF- κ B," *J. Biol. Chem.*, vol. 274, pp. 27891–27897, 1999.

[69] B. McDonagh, S. Ogueta, G. Lasarte, C. A. Padilla, and J. A. Bárcena, "Shotgun redox proteomics identifies specifically modified cysteines in key metabolic enzymes under oxidative stress in Saccharomyces cerevisiae," *J. Proteomics*, vol. 72, no. 4, pp. 677–689, May 2009.

[70] P. Maeba and B. D. Sanwal, "The Regulation of Pyruvate Kinase of Escherichia coli by Fructose Biphosphate and Adenylic Acid," *J. Biol. Chem.*, vol. 243, no. 2, pp. 448–450, 1968.

[71] R. C. Cumming, N. L. Andon, P. A. Haynes, M. Park, W. H. Fischer, and D. Schubert, "Protein disulfide bond formation in the cytoplasm during oxidative stress.," *J. Biol. Chem.*, vol. 279, no. 21, pp. 21749–58, May 2004.

[72] S. R. Jaffrey and S. H. Snyder, "The biotin switch method for the detection of S-nitrosylated proteins.," *Sci. STKE*, vol. 2001, no. 86, p. pl1, Jun. 2001.

[73] A. Shevchenko, H. Tomas, J. Havlis, J. V Olsen, and M. Mann, "In-gel digestion for mass spectrometric characterization of proteins and proteomes.," *Nat. Protoc.*, vol. 1, no. 6, pp. 2856–60, Jan. 2006.

[74] A. Vagin and A. Teplyakov, "MOLREP : an Automated Program for Molecular Replacement," *J. Appl. Crystallogr.*, vol. 30, no. 6, pp. 1022–1025, Dec. 1997.

[75] G. N. Murshudov, P. Skubák, A. A. Lebedev, N. S. Pannu, R. a Steiner, R. A. Nicholls, M. D. Winn, F. Long, and A. A. Vagin, "REFMAC5 for the refinement of macromolecular crystal structures.," *Acta Crystallogr. D. Biol. Crystallogr.*, vol. 67, no. Pt 4, pp. 355–67, Apr. 2011.

[76] P. P. Pandolfi, F. Sonati, R. Rivi, P. Mason, F. Grosveld, and L. Luzzatto, "Targeted disruption of the housekeeping gene encoding glucose 6-phosphate

dehydrogenase (G6PD): G6PD is dispensable for pentose synthesis but essential for defense against oxidative stress." pp. 5209–5215, 1995.

[77] R. C. Fahey, J. S. Hunt, and G. C. Windham, "On the cysteine and cystine content of proteins," *J. Mol. Evol.*, vol. 10, no. 2, pp. 155–160, Jun. 1977.

[78] R. Sanchez, M. Riddle, J. Woo, and J. Momand, "Prediction of reversibly oxidized protein cysteine thiols using protein structure properties," *Protein Sci.*, vol. 17, pp. 473–481, 2008.

[79] Y. Ikeda and T. Noguchi, "Allosteric regulation of pyruvate kinase M2 isozyme involves a cysteine residue in the intersubunit contact.," *J. Biol. Chem.*, vol. 273, no. 20, pp. 12227–33, May 1998.

[80] S. R. Stowell, M. Cho, C. L. Feasley, C. M. Arthur, X. Song, J. K. Colucci, S. Karmakar, P. Mehta, M. Dias-Baruffi, R. P. McEver, and R. D. Cummings, "Ligand reduces galectin-1 sensitivity to oxidative inactivation by enhancing dimer formation," *J. Biol. Chem.*, vol. 284, no. 8, pp. 4989–4999, 2009.

[81] L. J. Ignarro, G. M. Buga, K. S. Wood, and R. E. Byrns, "Endothelium-derived relaxing factor produced and released from artery and vein is nitric oxide," *Proc. Natl. Acad. Sci. U. S. A.*, vol. 84, no. December, pp. 9265–9269, 1987.

[82] M. A. Marletta, "Nitric oxide synthase: aspects concerning structure and catalysis.," *Cell*, vol. 78, no. 6, pp. 927–30, Sep. 1994.

[83] W. K. Alderton, C. E. Cooper, and R. G. Knowles, "Nitric oxide synthases: structure, function and inhibition.," *Biochem. J.*, vol. 357, no. Pt 3, pp. 593–615, Aug. 2001.

[84] H. Kleinert, A. Pautz, K. Linker, and P. M. Schwarz, "Regulation of the expression of inducible nitric oxide synthase," *Eur. J. Pharmacol.*, vol. 500, no. 1–3, pp. 255–266, Oct. 2004.

[85] C. Villanueva and C. Giulivi, "Subcellular and cellular locations of nitric oxide synthase isoforms as determinants of health and disease.," *Free Radic. Biol. Med.*, vol. 49, no. 3, pp. 307–16, Aug. 2010.

[86] A. J. Burke, F. J. Sullivan, F. J. Giles, and S. A. Glynn, "The yin and yang of nitric oxide in cancer progression," *Carcinogenesis*, vol. 34, no. 3, pp. 503–512, 2013.

[87] S. Mocellin, V. Bronte, and D. Nitti, "Nitric oxide, a double edged sword in cancer biology: Searching for therapeutic opportunities," *Med. Res. Rev.*, vol. 27, no. 3, pp. 317–352, 2007.

[88] E. Aranda, C. López-Pedrera, J. R. De La Haba-Rodriguez, and A. Rodriguez-Ariza, “Nitric oxide and cancer: the emerging role of S-nitrosylation.,” *Curr. Mol. Med.*, vol. 12, no. 1, pp. 50–67, Jan. 2012.

[89] A. Keszler, Y. Zhang, and N. Hogg, “Reaction between nitric oxide, glutathione, and oxygen in the presence and absence of protein: How are S-nitrosothiols formed?,” *Free Radic. Biol. Med.*, vol. 48, no. 1, pp. 55–64, Jan. 2010.

[90] N. Hogg, “The biochemistry and physiology of S-nitrosothiols,” *Annu. Rev. Pharmacol. Toxicol.*, vol. 42, pp. 585–600, 2002.

[91] J. S. Stamler, E. J. Toone, S. A. Lipton, and N. J. Sucher, “(S)NO signals: translocation, regulation, and a consensus motif.,” *Neuron*, vol. 18, no. 5, pp. 691–6, May 1997.

[92] T. M. Greco, R. Hodara, I. Parastatidis, H. F. G. Heijnen, M. K. Dennehy, D. C. Liebler, and H. Ischiropoulos, “Identification of S-nitrosylation motifs by site-specific mapping of the S-nitrosocysteine proteome in human vascular smooth muscle cells.,” *Proc. Natl. Acad. Sci. U. S. A.*, vol. 103, no. 19, pp. 7420–5, May 2006.

[93] S. F. Kim, D. A. Huri, and S. H. Snyder, “Inducible nitric oxide synthase binds, S-nitrosylates, and activates cyclooxygenase-2.,” *Science*, vol. 310, no. 5756, pp. 1966–70, Dec. 2005.

[94] M. Fang, S. R. Jaffrey, A. Sawa, K. Ye, X. Luo, and S. H. Snyder, “Dexras1: a G protein specifically coupled to neuronal nitric oxide synthase via CAPON.,” *Neuron*, vol. 28, no. 1, pp. 183–93, Oct. 2000.

[95] L. A. Barouch, R. W. Harrison, M. W. Skaf, G. O. Rosas, T. P. Cappola, Z. A. Kobeissi, I. A. Hobai, C. A. Lemmon, A. L. Burnett, B. O’Rourke, E. R. Rodriguez, P. L. Huang, J. A. C. Lima, D. E. Berkowitz, and J. M. Hare, “Nitric oxide regulates the heart by spatial confinement of nitric oxide synthase isoforms.,” *Nature*, vol. 416, no. 6878, pp. 337–9, Mar. 2002.

[96] Y. Iwakiri, A. Satoh, S. Chatterjee, D. K. Toomre, C. M. Chalouni, D. Fulton, R. J. Groszmann, V. H. Shah, and W. C. Sessa, “Nitric oxide synthase generates nitric oxide locally to regulate compartmentalized protein S-nitrosylation and protein trafficking.,” *Proc. Natl. Acad. Sci. U. S. A.*, vol. 103, no. 52, pp. 19777–82, Dec. 2006.

[97] D. A. Mitchell, S. U. Morton, N. B. Fernhoff, and M. A. Marletta, “Thioredoxin is required for S-nitrosation of procaspase-3 and the inhibition of apoptosis in Jurkat cells.,” *Proc. Natl. Acad. Sci. U. S. A.*, vol. 104, no. 28, pp. 11609–14, Jul. 2007.

[98] T. Nakamura, L. Wang, C. C. L. Wong, F. L. Scott, B. P. Eckelman, X. Han, C. Tzitzilonis, F. Meng, Z. Gu, E. A. Holland, A. T. Clemente, S. Okamoto, G. S.

Salvesen, R. Riek, J. R. Yates, and S. A. Lipton, “Transnitrosylation of XIAP regulates caspase-dependent neuronal cell death.,” *Mol. Cell*, vol. 39, no. 2, pp. 184–95, Jul. 2010.

[99] J. S. Stamler and D. T. Hess, “Nascent nitrosylases.,” *Nat. Cell Biol.*, vol. 12, no. 11, pp. 1024–6, Nov. 2010.

[100] C. Porta, P. Larghi, M. Rimoldi, M. G. Totaro, P. Alavana, A. Montovani, and A. Sica, “Cellular and Molecular Pathways Linking Inflammation and Cancer.,” *Immunobiology*, vol. 214, pp. 761–777, 2009.

[101] H. Okayama, M. Saito, N. Oue, J. M. Weiss, J. Stauffer, S. Takenoshita, R. H. Wiltrout, S. P. Hussain, and C. C. Harris, “NOS2 enhances KRAS-induced lung carcinogenesis, inflammation and microRNA-21 expression,” *Int. J. Cancer*, vol. 132, no. 1, pp. 9–18, 2013.

[102] S. Ambs, W. P. Bennett, W. G. Merriam, M. O. Ogunfusika, S. M. Oser, M. A. Khan, R. T. Jones, and C. C. Harris, “Vascular endothelial growth factor and nitric oxide synthase expression in human lung cancer and the relation to p53.,” *Br. J. Cancer*, vol. 78, no. 2, pp. 233–239, 1998.

[103] S. Ambs, W. P. Bennett, W. G. Merriam, M. O. Ogunfusika, S. M. Oser, A. M. Harrington, P. G. Shields, E. Felley-bosco, S. P. Hussain, and C. C. Harris, “Relationship between p53 mutations and inducible nitric oxide synthase expression in human colorectal cancer,” *J. Natl. Cancer Inst.*, vol. 91, no. 1, pp. 86–88, 1999.

[104] S. Ambs, W. G. Merriam, W. P. Bennett, E. Felley-bosco, M. Ogunfusika, S. M. Oser, S. Klein, P. G. Shields, T. R. Billiar, and C. C. Harris, “Frequent Nitric Oxide Synthase-2 Expression in Human Colon Adenomas : Implication for Tumor Angiogenesis and Colon Cancer Progression Frequent Nitric Oxide Synthase-2 Expression in Human Colon Adenomas : Implication for Tumor Angiogenesis and Colon Cancer,” *Cancer Res.*, vol. 58, no. 2, pp. 334–341, 1998.

[105] E. A. Grimm, “Constitutive Intracellular Production of iNOS and NO in Human Melanoma; Possible role in Regulaton of Growth and Resistance to Apoptosis,” *Nitric Oxide*, vol. 19, no. 2, pp. 133–137, 2009.

[106] S. A. Glynn, B. J. Boersma, T. H. Dorsey, M. Yi, H. G. Yfantis, L. A. Ridnour, D. N. Martin, C. H. Switzer, R. S. Hudson, D. A. Wink, D. H. Lee, R. M. Stephens, and S. Ambs, “Increased NOS2 predicts poor survival in estrogen receptor – negative breast cancer patients,” *J. Clin. Invest.*, vol. 120, no. 11, pp. 3843–3854, 2010.

[107] L. L. Thomsen, D. W. Miles, L. Happerfield, L. G. Bobrow, R. G. Knowles, and S. Moncada, “Nitric oxide synthase activity in human breast cancer.,” *Br. J. Cancer*, vol. 72, no. 1, pp. 41–44, 1995.

[108] A. S. Bulut, E. Erden, S. D. Sak, H. Doruk, N. Kursun, and D. Dincol, "Significance of inducible nitric oxide synthase expression in benign and malignant breast epithelium: An immunohistochemical study of 151 cases," *Virchows Arch.*, vol. 447, no. 1, pp. 24–30, 2005.

[109] J. K. Kundu and Y. J. Surh, "Inflammation: gearing the journey to cancer," *Rev. Mutat. Res.*, vol. 659, pp. 15–30, 2008.

[110] J. K. Kundu and Y. J. Surh, "Emerging avenues linking inflammation and cancer," *Free Radic. Biol. Med.*, vol. 52, no. 2012, pp. 2013–2037, 2012.

[111] H. Ohshima, T. Sawa, and T. Akaike, "8-Nitroguanine,a product of nitrative DNA damage caused by reactive nitrogen species: formation, occurrence, and implications in inflammation and carcinogenesis," *Antioxid. Redox Signal.*, vol. 8, pp. 1033–1045, 2006.

[112] V. Yermilov, J. Rubio, M. Becchi, M. D. Friesen, B. Pignatelli, and H. Ohshima, "Formation of 8-Nitroguanine by the reaction of guanine with peroxynitrite in vitro," *Carcinogenesis*, vol. 16, pp. 2045–2050, 1995.

[113] S. Kawanishi and Y. Hiraku, "Oxidative and nitrative DNA damage as a biomarker for carcinogenesis with special reference to inflammation," *Antioxid. Redox Signal.*, vol. 8, pp. 1047–1058, 2006.

[114] L. Hofseth, "Nitric oxide in cancer and chemoprevention," *Free Radic. Biol. Med.*, vol. 34, no. 8, pp. 955–968, Apr. 2003.

[115] J. A. Crowell, V. E. Steele, C. C. Sigman, and J. R. Fay, "Is Inducible Nitric Oxide Synthase a Target for Chemoprevention?," *Mol. Cancer Ther.*, vol. 2, pp. 815–823, 2003.

[116] D. Fukumura, S. Kashiwagi, and R. K. Jain, "The role of nitric oxide in tumour progression.," *Nat. Rev. Cancer*, vol. 6, no. 7, pp. 521–34, Jul. 2006.

[117] A. Orucevic, J. Bechberger, A. M. Green, R. A. Shapiro, T. R. Billiar, and P. K. Lala, "Nitric-oxide Production by Murine Mammary Adenocarcinoma Cells Promotes Tumor-cell Invasiveness," *Int. J. Cancer*, vol. 81, no. 6, pp. 889–896, 1999.

[118] A. Siegert, C. Rosenberg, W. D. Schmitt, C. Denkert, and S. Hauptmann, "Nitric oxide of human colorectal adenocarcinoma cell lines promotes tumour cell invasion," *Br. J. Cancer*, vol. 86, no. 8, pp. 1310–1315, 2002.

[119] L. C. Jadeski, C. Chakraborty, and P. K. Lala, "Nitric oxide-mediated promotion of mammary tumour cell migration requires sequential activation of nitric oxide synthase, guanylate cyclase and mitogen-activated protein kinase.," *Int. J. cancer.*, vol. 106, no. 4, pp. 496–504, Sep. 2003.

[120] L. M. Barreiro Arcos, G. Gorelik, A. Klecha, N. Goren, C. Cerquetti, and G. A. Cremaschi, “Inducible nitric oxide synthase-mediated proliferation of a T lymphoma cell line,” *Nitric Oxide*, vol. 8, no. 2, pp. 111–118, Mar. 2003.

[121] X. M. Zhang and Q. Xu, “Metastatic melanoma cells escape from immunosurveillance through the novel mechanism of releasing nitric oxide to induce dysfunction of immunocytes,” *Melanoma Res.*, vol. 11, no. 6, pp. 559–567, Dec. 2001.

[122] S. Ambs, W. G. Merriam, M. O. Ogunfusika, W. P. Bennett, N. Ishibe, S. P. Hussain, E. E. Tzeng, D. A. Geller, T. R. Billiar, and C. C. Harris, “p53 and vascular endothelial growth factor regulate tumor growth of NOS2-expressing human carcinoma cells.,” *Nat. Med.*, vol. 4, no. 12, pp. 1371–6, Dec. 1998.

[123] D. C. Jenkins, I. G. Charles, L. L. Thomsen, D. W. Moss, L. S. Holmes, S. A. Baylis, P. Rhodes, K. Westmore, P. C. Emson, and S. Moncada, “Roles of nitric oxide in tumor growth,” *Proc. Natl. Acad. Sci. U. S. A.*, vol. 92, no. 10, pp. 4392–4396, 1995.

[124] D. Fukumura, S. Kashiwagi, and R. K. Jain, “The role of Nitric Oxide in tumour cell progression. Supplemental Table S1,” *Nat. Rev. Cancer*, 2006.

[125] P. A. Brennan, M. Palacios-Callender, T. Umar, D. Hughes, A. V Spedding, G. A. Zaki, and J. D. Langdon, “Correlation between type II nitric oxide synthase and p53 expression in oral squamous cell carcinoma.,” *Br. J. Oral Maxillofac. Surg.*, vol. 38, no. 6, pp. 627–632, Dec. 2000.

[126] W. Tschugguel, C. Schneeberger, G. Unfried, K. Czerwenka, W. Weninger, M. Mildner, D. M. Gruber, M. O. Sator, T. Waldhör, and J. C. Huber, “Expression of inducible nitric oxide synthase in human breast cancer depends on tumor grade,” *Breast Cancer Res. Treat.*, vol. 56, no. 2, pp. 143–149, Jul. 1999.

[127] C. Gao, H. Guo, J. Wei, Z. Mi, P. Y. Wai, and P. C. Kuo, “Identification of S-nitrosylated proteins in endotoxin-stimulated RAW264.7 murine macrophages.,” *Nitric Oxide*, vol. 12, no. 2, pp. 121–6, Mar. 2005.

[128] X. Zhou, P. Han, J. Li, X. Zhang, B. Huang, H.-Q. Ruan, and C. Chen, “ESNOQ, proteomic quantification of endogenous S-nitrosation.,” *PLoS One*, vol. 5, no. 4, p. e10015, Jan. 2010.

[129] P.-T. Doulias, M. Tenopoulou, J. L. Greene, K. Raju, and H. Ischiropoulos, “Nitric oxide regulates mitochondrial fatty acid metabolism through reversible protein S-nitrosylation.,” *Sci. Signal.*, vol. 6, no. 256, p. rs1, Jan. 2013.

[130] J. S. Paige, G. Xu, B. Stancevic, and S. R. Jaffrey, “Nitrosothiol reactivity profiling identifies S-nitrosylated proteins with unexpected stability.,” *Chem. Biol.*, vol. 15, no. 12, pp. 1307–16, Dec. 2008.

[131] M. R. Hara, N. Agrawal, S. F. Kim, M. B. Cascio, M. Fujimuro, Y. Ozeki, M. Takahashi, J. H. Cheah, S. K. Tankou, L. D. Hester, C. D. Ferris, S. D. Hayward, S. H. Snyder, and A. Sawa, "S-nitrosylated GAPDH initiates apoptotic cell death by nuclear translocation following Siah1 binding," *Nat. Cell Biol.*, vol. 7, pp. 665–674, 2005.

[132] G. A. Spoden, D. Morandell, D. Ehehalt, M. Fiedler, P. Jansen-Dürr, M. Hermann, and W. Zwerschke, "The SUMO-E3 ligase PIAS3 targets pyruvate kinase M2," *J. Cell. Biochem.*, vol. 107, no. February, pp. 293–302, 2009.

[133] J. Ignacak and M. B. Stachurska, "The dual activity of pyruvate kinase type M2 from chromatin extracts of neoplastic cells," *Comp. Biochem. Physiol. - B Biochem. Mol. Biol.*, vol. 134, no. 02, pp. 425–433, 2003.

[134] J. Lee, H. K. Kim, Y. M. Han, and J. Kim, "Pyruvate kinase isozyme type M2 (PKM2) interacts and cooperates with Oct-4 in regulating transcription," *Int. J. Biochem. Cell Biol.*, vol. 40, pp. 1043–1054, 2008.

[135] A. Hoshino, J. A. Hirst, and H. Fujii, "Regulation of cell proliferation by interleukin-3-induced nuclear translocation of pyruvate kinase.," *J. Biol. Chem.*, vol. 282, pp. 17706–17711, 2007.

[136] P.-T. Doulias, J. L. Greene, T. M. Greco, M. Tenopoulou, S. H. Seeholzer, R. L. Dunbrack, and H. Ischiropoulos, "Structural profiling of endogenous S-nitrosocysteine residues reveals unique features that accommodate diverse mechanisms for protein S-nitrosylation.," *Proc. Natl. Acad. Sci. U. S. A.*, vol. 107, no. 39, pp. 16958–63, Sep. 2010.

[137] J. S. Paige, G. Xu, B. Stancevic, and S. R. Jaffrey, "Nitrosothiol reactivity profiles identifies S-nitrosylated proteins with unexpected stability," *Chem. Biol.*, vol. 15, no. 12, pp. 1307–1316, 2008.

[138] T. M. Larsen, M. M. Benning, I. Rayment, and G. H. Reed, "Structure of the bis(Mg2+)-ATP-oxalate complex of the rabbit muscle pyruvate kinase at 2.1 A resolution: ATP binding over a barrel.," *Biochemistry*, vol. 37, no. 18, pp. 6247–55, May 1998.

[139] J. D. Dombrauckas, B. D. Santarsiero, and A. D. Mesecar, "Structural basis for tumor pyruvate kinase M2 allosteric regulation and catalysis.," *Biochemistry*, vol. 44, no. 27, pp. 9417–29, Jul. 2005.

[140] A. M. Roseman, S. Chen, H. White, K. Braig, and H. R. Saibil, "The chaperonin ATPase cycle: Mechanism of allosteric switching and movements of substrate-binding domains in GroEL," *Cell*, vol. 87, pp. 241–251, 1996.

[141] M. Bochtler, C. Hartmann, H. K. Song, G. P. Bourenkov, H. D. Bartunik, and R. Huber, "The structures of HslU and the ATP- dependent protease HslU – HslV," *Nature*, vol. 403, no. February, pp. 13091–13096, 2000.

[142] D. G. Ward and J. D. Cavieres, "Solubilized alpha beta Na,K-ATPase remains protomeric during turnover yet shows apparent negative cooperativity toward ATP.," *Proc. Natl. Acad. Sci. U. S. A.*, vol. 90, no. June, pp. 5332–5336, 1993.

[143] S. Ono, K. Y. Hara, J. Hirao, T. Matsui, H. Noji, M. Yoshida, and E. Muneyuki, "Origin of apparent negative cooperativity of F1-ATPase," *Biochim. Biophys. Acta - Bioenerg.*, vol. 1607, pp. 35–44, 2003.

[144] S. Kehr, E. Jortzik, C. Delahunty, J. R. Yates, S. Rahlfs, and K. Becker, "Protein S-glutathionylation in malaria parasites.," *Antioxid. Redox Signal.*, vol. 15, no. 11, pp. 2855–65, Dec. 2011.

[145] J. D. Sander and J. K. Joung, "CRISPR-Cas systems for editing, regulating and targeting genomes.," *Nat. Biotechnol.*, vol. 32, no. 4, pp. 347–55, Apr. 2014.